DYNAMIC PROPERTIES OF SOME POLYMERIC SYSTEMS

J. L. DEN OTTER

Prof Stuart

DYNAMIC PROPERTIES OF SOME POLYMERIC SYSTEMS

PROEFSCHRIFT

TER VERKRIJGING VAN DE GRAAD VAN DOCTOR IN DE WISKUNDE EN NATUURWETENSCHAPPEN AAN DE RIJKSUNIVERSITEIT TE LEIDEN, OP GEZAG VAN DE RECTOR MAGNIFICUS DR P. MUNTENDAM, HOOGLERAAR IN DE FACULTEIT DER GENEESKUNDE TEN OVERSTAAN VAN EEN COMMISSIE UIT DE SENAAT TE VERDEDIGEN OP WOENSDAG 29 NOVEMBER 1967 TE 14 UUR

DOOR

JOHAN LEONARD DEN OTTER

GEBOREN TE 'S-GRAVENHAGE IN 1932

DRUCO DRUKKERIJBEDRIJVEN N.V. – LEIDEN

PROMOTOR: PROF. DR. A. J. STAVERMAN

Aan de nagedachtenis van mijn vader
aan mijn moeder

CONTENTS

I INTRODUCTION

On deformation of what are commonly called simple liquids, such as water, the shear stresses become zero nearly instantaneously after ending the deformation. On the other hand the stresses on deformation of a solid, such as a crosslinked rubber, will, to a first approximation, be a function of the deformation with respect to a certain reference state. The stresses will only become zero again, when this "undeformed" reference state has been reached.

The mechanical behaviour of many polymer solutions and melts lies in between these two extremes. An intuitive definition for these materials can be given by assuming, that the shear stresses in the liquid become zero after waiting for a sufficiently long period after ending the deformation. The influence of a preceding deformation is the smaller, the longer ago the deformation took place. These kinds of liquids can be described as liquids with limited memory.

Polymeric solutions and melts show some unusual properties during flow. An example is the so-called Weissenberg-effect[1]. When a cylinder is being rotated in a polymer solution or melt, the liquid will climb the walls of this cylinder. Another example is that, on flowing through a capillary, the extrudate shows die swell, the diameter of the extrudate may be up to five times that of the capillary diameter[2] This sometimes very large effect can only be explained by the relaxation of the stresses induced by the flow. Another characteristic property of polymer melts and some concentrated solutions is melt fracture[3]. The extrudate from a capillary becomes distorted as soon as the shear stress at the wall exceeds a critical value.

Polymeric solutions and melts show in general a viscosity very large compared to that of the pure solvent or the monomer. For example a 5 % solution of a very high molecular weight polyisobutene in a low viscosity solvent has a viscosity about 10^5 times greater than that of the solvent (Chapter 6). Polymer melts used in industrial processing have viscosities up to 10^7 poise.

All these effects are probably connected and very interesting in themselves. Because in industry the use and processing of these materials is increasingly common and often gives rise to difficulties, a study of these properties is of great practical interest.

In the following, laminar shear flow will be considered exclusively. If the flow of the liquid takes place between two parallel plates, the coordinate system is taken so that the flow lines are in the 1-direction, parallel to the plates, the

direction perpendicular to the plates is the 2-direction.

The third direction is chosen so that a right handed coordinate system results. With shear flow the cartesian components of the flow velocity $\underline{v}$ are:

$$v_1 = qx_2 \qquad v_2 = v_3 = 0 \tag{I. 1}$$

$$\text{here } q = \frac{dv_1}{dx_2} \tag{I. 2}$$

is the rate of shear.

The nomenclature of the stress tensor is explained in Fig. 1[4)5)]:

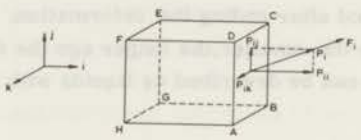

Fig. 1

If a plane in the liquid perpendicular to the i-direction is chosen, a traction say F_i will act on it. On dividing the force by the area of the surface ABCD, a stress P_i is obtained, of which the components in the i, j and k direction are P_{ii}, P_{ij} and P_{ik}. For planes perpendicular to the j-direction (say DCEF) and to the k-direction (say ADFH) the same can be done. In this way nine components of the stress tensor are defined. The stress tensor will be indicated by P_{ik}, which means

$$\begin{matrix} P_{11} & P_{12} & P_{13} \\ P_{21} & P_{22} & P_{23} \\ P_{31} & P_{32} & P_{33} \end{matrix}$$

The components with mixed indices P_{12}, P_{21}, P_{13}, P_{23} and P_{32} are called shear stresses, because they try to change the shape of the body ABCDEFGH. The components with equal indices P_{11}, P_{22}, and P_{33} are called normal stresses.

The study of shear stresses in liquids is rather old, and is known as viscometry. Only a short time ago, about twenty years, it was first realized[1)] that the three normal stresses at the same point in a liquid can be different

from each other. The study of all components of the stress tensor is sometimes called rheogoniometry.

The way in which normal stress differences occur in polymer solutions or melts can be easily connected with the definition of the stress tensor given above. The end-to-end distances of polymer molecules in the plane ABCD can be represented by the vectors $\underline{\ell}$. These will either point through or lie in the plane ABCD. In the undeformed liquid the orientation and the lengths of these vectors will have a random distribution in space.

In that case, the sum of all forces due to the polymer molecules in the plane ABCD or any other plane will be zero. However, if a velocity field is generated in the liquid, the polymer molecules will be on the average both oriented and stretched. Both the orientation and the stretching result in forces in the liquid, because both increase the free energy. The relation between the stretching of the molecules and the resulting forces is given by the theory of rubber elasticity (see for example [4] and [6]), which shows that the tensile force in a molecule is proportional to its length and has the same direction as the end-to-end vector. The vectorial sum of all the forces due to the molecules in the plane will result in a force F_i, which can be resolved into its components as has been shown before. This will be treated in greater detail in Chapter II. At the same time the liquid will in general show optical anisotropy. If the polarizability of a molecule is proportional to the end-to-end vector and has the same direction[7], as is usually assumed for polymers, the flow birefringence in the liquid can be calculated in a manner similar to that for components of the stress tensor. The molecular theories predict as a result a close connection between the index of refraction ellipsoid and the stress tensor. Experiments to investigate this connection are reported in Chapter VII. Flow birefringence during laminar shear flow can be defined by Δn, the difference between the main axes of the index-of-refraction ellipse in the 1-2 plane, and by the sharp angle χ between the 1-direction (the flow lines), and one of the main axes of the index of refraction ellipse[7].

It is also clear from the foregoing, that the stress tensor is a macroscopic quantity. Although, on the one hand, the surface ABCD must be small enough to have a uniform stress, on the other hand it must be large enough to permit calculating contributions of the molecules by a statistical treatment. The same is valid for flow birefringence.

A type of deformation which is often used to investigate mechanical behaviour of viscoelastic materials is sinusoidal shear flow. In this case the displacement in the 1-direction is $\gamma = \gamma_o x_2 \sin \omega t$, where $\gamma_o x_2$ is the amplitude of

the displacement, and ω the angular frequency. It is now possible to write the shear stress p_{12} as[4)8)]

$$p_{12} = \gamma_o(G' \sin \omega t + G'' \cos \omega t) \qquad (I.3)$$

where G' and G'' are the storage and loss part of the shear modulus, and the deformation is linear. This will be described in greater detail in Chapter IV. The results are compared with normal stress differences and flow birefringence measurements, on the same materials, in Chapter VIII.

It can be shown (see[7)]) that for an incompressible fluid during laminar shear flow, only three functions of the components of the stress tensor, p_{12}, $(p_{11} - p_{22})$ and $(p_{22} - p_{33})$ are of interest. In the literature very few measurements of $(p_{11} - p_{22})$ and even less of $(p_{22} - p_{33})$ as a function of shear rate q have been published. Up till now no Newtonian liquids, defined so that the viscosity $\eta = p_{12}/q$ is constant with changing q, have been found for which $(p_{11} - p_{22})$ or $(p_{22} - p_{33})$ are different from zero in steady shear flow. Up till now, all investigated liquids showing measurable normal stress differences were found to show also a non-Newtonian behaviour and elastic properties, $G'(\omega) \neq 0$.

As has been pointed out before (Ref.[5)] page 184) it is, in general, impossible to measure any normal stress component except p_{22} during shear flow without disturbing the flow. For this reason it is necessary to perform all experiments with curvilinear shear flow, and measure p_{22} as a function of the radius. From the equations for the equilibrium of forces (Chapter II) the normal stress differences $(p_{22} - p_{33})$ and $(p_{11} - p_{22})$ can then be calculated[5)]. This is the reason why all evidence of the existence of normal stress differences are indirect, so that as late as 1959[9)] in a publication the existence of normal stress differences in steady shear flow could be ascribed to experimental errors. The first phenomenon for which the existence of normal stress differences was postulated was the Weissenberg-effect described before[1)].

A peculiar thing about the measurements of normal stress differences is that so few experiments have been performed. The number of publications with theories to explain normal stress differences is a multiple of the number of publications describing experiments. It is clear that this is not a healthy state of affairs, because different experimenters do not agree with each other on some important points. Especially there is no agreement about the magnitude of $(p_{22} - p_{33})$ during steady shear flow (see Chapter VIII). The number of investigations on this point is very small and the opinions are divided. As a result of experimental and theoretical considerations all normal stress meas-

urements have been done in three types of apparatus: parallel plate, cone-and-plate and concentric cylinder viscometers (Chapter V).

Some investigators[10] have tried to measure normal stress differences from capillary measurements, either by post-extrusion swell or by the recoil caused by the liquid leaving the capillary. The experimental and theoretical difficulties are considerable, however, so that the interpretation of the results is uncertain. Another method[11] is to determine $p_{11} - p_{22}$ (assuming $p_{22} = p_{33}$) from the entrance correction in capillary measurements. It is often found that a considerable pressure is needed to let a polymer solution or melt flow through an orifice, the entrance correction. Part of this pressure is used to build up normal stress differences. This method does not yet rest on a firm mathematical basis, the interpretation of the results is very difficult and has not yet been done successfully.

Very few attempts have, as yet, been published to compare normal stress measurements and other viscoelastic properties as determined by dynamic measurements, although a connection would be expected intuitively. A theoretical foundation for this connection was first given in a recent phenomenological theory by Coleman and Markovitz[12], moreover, the existing molecular theories give on inspection the same result (see Chapter II).

For all theories, and for the interpretation of the measurements, the liquid has been supposed incompressible. This is a necessary simplification, the mathematical difficulties are very considerable otherwise. With moderately concentrated polymer solutions this assumption is probably justified, because the forces are rather small. With polymer melts, however, the volume may change easily 5 % under experimental conditions, on account of the very high pressures used. Under the influence of these very large forces the spectrum of relaxation times will change. One of the reasons for the different results, obtained by different experimenters, for the influence of hydrostatic pressure on the viscosity of polymer melts may be, that by compression the $\eta - q$ curve shifts not only along the η-axis, but also along the q-axis. This can lead to wrong conclusions in the interpretation of the results, unless the complete $\eta - q$ curve is measured.

In general, inertial forces are omitted in the rheological equations of state. This is not permissable with many experiments, so that for instance the contribution of centrifugal forces in normal stress experiments must be deducted from the measured stresses (compare the Hagenbach correction in capillary viscometry). Where necessary, this and similar corrections have been applied for the determination of normal stress differences (see Chapter V).

All investigations described in this thesis were performed on synthetic polymers, both in solution and in the molten state. The word polymer, as used here, means that one molecule consists of a large number of repeating units, the monomer. Synthetic polymers consist of molecules of varying molecular weight.

Two different molecular weight averages will be used, the number average molecular weight, M_n, and the weight average molecular weight, M_w. If the polymer contains, per unit weight, n_i molecules of molecular weight M_i, the two averages can be defined as:

$$M_n = \frac{\Sigma n_i M_i}{\Sigma n_i} \tag{I. 4}$$

$$M_w = \frac{\Sigma n_i M_i^2}{\Sigma n_i M_i} \tag{I. 5}$$

An often used measure of the width of the molecular weight distribution of a polymer is given by the ratio M_w/M_n

Most of the polymers investigated as regards their viscoelastic properties, were also characterized as regards the width of the molecular weight distribution. The results are given in Chapter III.

The mechanical behaviour of polymer solutions is the result partly of movements within one molecule, and partly of interactions between neighbouring molecules. An experimental method to separate the two effects is to dilute the solution, so that the molecules become separated from one another by the solvent. This effect can be expressed in the intrinsic viscosity, $[\eta]$. If the viscosity of the solution is given by η, and the viscosity of the solvent is η_s, the intrinsic viscosity is defined by the limit:

$$[\eta] = \lim_{c \to 0} \frac{\eta - \eta_s}{c\eta_s} \tag{I. 6}$$

where c is the concentration in g/cm^3.

At sufficiently low concentrations the contributions of individual molecules to the viscoelastic behaviour can be added, so that $(\eta - \eta_s)$ is directly proportional to the concentration.

On the other hand, for polymer melts, interactions between molecules dominate the mechanical behaviour completely.

The molecular theories, which will be given in Chapter II, describe either

exclusively the behaviour of isolated molecules (the dumbbell model, the Rouse and Zimm theories),or exclusively interactions (the network theory and the extension of the theory of Rouse).

It is interesting,that the two sets of theories give identical results for the viscoelastic functions,as expressed in the relaxation spectrum.

Implicit in the interpretation of all viscoelastic measurements in the following chapters is the assumption, that the liquid adheres to the wall, and that the flow consists of steady shear flow. These assumptions can be investigated directly by measuring the velocity profile. This has been done for polymer melts flowing through capillaries and rectangular slits. Good agreement was found between measured velocity profiles and those calculated from the flow curves[13].

Another method of investigating sources of systematic errors consists of repeating measurements with apparatuses of different geometry. For this reason, several different methods of measuring normal stress differences (Chapters V and VII),or viscosity (Chapters IV and VI),were used. Different types of apparatus also had to be used in many cases, because different materials require different measuring techniques. For instance, an apparatus suitable for dilute polymer solutions would,in general,be of little use for measurements on polymer melts.

In Chapter VIII normal stress differences,determined with different experimental techniques,are compared with each other and with predictions of the theories discussed in Chapter II.

Literature

1) K. Weissenberg, Proceed., 1st Intern. Congr. on Rheology, I 29, North Holland, Amsterdam 1949.

2) E.B. Bagley, S.H. Storey, D.C. West, J. Appl. Polymer Sci., 7, 1661 (1963).

3) R.S. Spencer, R.E. Dillon, J. Colloid Sci., 4, 241 (1949).

4) A.J. Staverman, F. Schwarzl, in H.A. Stuart, ed., Physik der Hochpolymeren, Vol. IV, Springer, Berlin 1956.

5) A.S. Lodge, Elastic liquids, Academic Press, London 1964.

6) A.J. Staverman, Thermodynamics of polymers, Vol. XIII Handbuch der Physik, Springer, Berlin 1962.

7) A. Peterlin, H.A. Stuart, Chapter XII in H.A. Stuart, ed., Physik der Hochpolymeren, Vol. III, Springer, Berlin 1953.

8) J.D. Ferry, Viscoelastic properties of polymers, Wiley, New York 1961.

9) S. Peter, W. Noetzel, Z. Phys. Chemie (Frankfurt), 21, 422 (1959).

10) J. Gavis, S. Middleman, J. Appl. Polymer Sci., 7, 493 (1963).

11) W. Philippoff, Trans. Soc. Rheol., 2, 263 (1958).

12) B.D. Coleman, H. Markovitz, J. Appl. Phys., 35, 1 (1964).

13) J.L. den Otter, J.L.S. Wales, J. Schijf, Rheologica Acta 6, 205 (1967).

II THEORY

A. Phenomenological theories

The number of theories in the literature giving rheological equations of state that predict the existence of normal stress differences is very large. The possible number of formulations is even infinite. For this reason, a completely general equation of state is of little value to experimenters, because the more general a theory is, the less information is provided by it[1)2)3)].

Lately, a new development in continuum mechanics has been the classification of possible formulations of equations of state. This would give the possibility of classifying the rheological behaviour of a particular material on the basis of a few experiments[1)2)].

For the formulation of the equations in part B.5., the nomenclature of Lodge[1)] will be used, it is essentially the same as that used by Oldroyd[4)]. These authors use a convecting coordinate system, for which the Greek alphabet will be used, in which each material particle has three coordinates ξ^i remaining constant during an arbitrary deformation. What does change are the metric tensors $\gamma_{ij}(\xi, t)$ and $\gamma^{ij}(\xi, t)$, which will depend, in general, both on the coordinates ξ^i, and on time t. The metric tensors can be defined in the usual tensor notation by:

$$(ds)^2 = \sum_{ij} \gamma_{ij}(\xi, t)\, d\xi^i d\xi^j = \Sigma_{ij} g_{ij} dx^i dx^j \qquad \text{(II. 1)}$$

in which ds is the distance between two neighbouring material points, g_{ij} is the metric tensor in a fixed (space) coordinate system. The formulation in the convecting coordinate system has certain advantages, as the equation of state can sometimes be formulated in a more compact way than by using a fixed coordinate system. A formula similar to (II. 1), but using the contravariant metric tensor $\gamma^{ij}(\xi, t)$, describes the distance between neighbouring planes[1)]. From (II. 1) it can be seen that an often used measure of deformation, defined as the change in distance between neighbouring points in the material, during the time interval from t' to t, is given by:

$$(ds)^2(\xi, t) - (ds)^2(\xi, t') = \Sigma_{ij} [\gamma_{ij}(\xi, t) - \gamma_{ij}(\xi, t')]\, d\xi^i d\xi^j \qquad \text{(II. 2)}$$

In a rather complicated manner[1)4)], a convecting time derivative can be defined. With the convecting time derivative, indicated by $\frac{D}{Dt}$, the same material particle is observed, so that during differentiation the space coordinates of the particle change. It is clear that this derivative is particularly useful to

describe memory effects. With many materials the flow history of particles of the liquid influences the present state of stress. Then it is necessary to add contributions to the stress tensor due to preceding deformations. The adding of tensor components in different coordinate systems (the space coordinates change during deformation) gives some peculiar difficulties, which were discussed by Oldroyd[4]. A formulation of an equation of state in convecting coordinates is often simpler than the corresponding equation in space coordinates.

If the stress tensor for an incompressible liquid is described, it is customary to split the stress tensor P^{ij} into two parts[1)2)]:

$$P^{ij} = -\bar{p}g^{ij} + p^{ij} \qquad \text{(II. 3)}$$

The pressure $\bar{p}$ is the "hydrostatic pressure", p^{ij} will be called the stress tensor from now on, only incompressible liquids will be considered.

In a cylindrical coordinate system, with coordinates r, θ, z, the dynamic equation in r-direction is[1)2)]:

$$-\frac{\partial \bar{p}}{\partial r} + \frac{\partial p_{rr}}{\partial r} + \frac{1}{r}\frac{\partial p_{r\theta}}{\partial \theta} + \frac{\partial p_{rz}}{\partial z} + \frac{p_{rr} - p_{\theta\theta}}{r} + F_r = 0 \qquad \text{(II. 4a)}$$

and in z-direction:

$$-\frac{\partial \bar{p}}{\partial z} + \frac{\partial p_{rz}}{\partial r} + \frac{1}{r}\frac{\partial p_{\theta z}}{\partial \theta} + \frac{\partial p_{zz}}{\partial z} + \frac{1}{r}p_{rz} + F_z = 0 \qquad \text{(II. 4b)}$$

In spherical polar coordinates, with coordinates r, φ and ϑ, the dynamic equation in r-direction becomes[1)2)]:

$$-\frac{\partial \bar{p}}{\partial r} + \frac{\partial p_{rr}}{\partial r} + \frac{1}{r \sin \vartheta}\frac{\partial p_{r\varphi}}{\partial \varphi} + \frac{1}{r}\frac{\partial p_{r\vartheta}}{\partial \vartheta} + \frac{2p_{rr} - p_{\varphi\varphi} - p_{\vartheta\vartheta} + p_{r\vartheta}\cot\vartheta}{r} + F_r = 0 \qquad \text{(II. 5)}$$

The continuity equations become:

$$\text{Div } \underline{v} = 0 \qquad \text{(II. 6)}$$

The coordinates in the above equations have their usual meaning[1)2)]:

F_r and F_z are r or z components of the volume forces

$\underline{v}$ is velocity

p_{rr}, $p_{r\theta}$ ..... are physical components of the stress tensor.

It will also be assumed that the liquid cannot transfer torques, the stress tensor will then be symmetric:

$$p^{ik} = p^{ki} \tag{II. 7}$$

When using convecting coordinates ξ^i, it is often necessary to convert them at a certain stage in the calculations into space coordinates. With liquids there is no unique reference state, as for example the "undeformed state" in a cross-linked rubber. For this reason, the rheological equation of state for a liquid is in general given the simplest form, if the deformation at present time t is taken as the reference system.

For a very wide range of equations of state, it is possible to express the components of the stress tensor during steady shear flow as[2)5)6)]:

$$\begin{aligned} p_{11} - p_{22} &= F_1 q^2 & \qquad p_{22} - p_{33} &= F_2 q^2 \\ p_{12} = p_{21} &= F_3 q & \qquad p_{13} = p_{31} = p_{23} = p_{32} &= 0 \end{aligned} \tag{II. 8}$$

F_1, F_2, F_3 are in general functions of shear rate q, and p_{11}, p_{12} ..... are physical components of the stress tensor.

Ericksen has shown[3)] that, unless certain relations between F_1, F_2 and F_3 are complied with, it is impossible to maintain steady shear flow through pipes of non-circular cross-section, or in cone-and-plate or cone-and-cone viscometers. Otherwise secondary flow, superimposed on the assumed shear flow, will occur under these conditions. Qualitative experimental agreement with calculated secondary flow patterns has been obtained by Giesekus and co-workers[5)].

A recent phenomenological theory[6)] gives a connection between components of the stress tensor and the dynamic shear moduli. The authors investigate the behaviour of a "second order fluid", defined by a constitutive equation giving a correction for viscoelastic effects complete up to terms of the order larger than two in the time scale. From this treatment values of $(p_{11} - p_{22})$ and $(p_{22} - p_{33})$, in general both different from zero, were obtained. Moreover, at low shear rates or frequencies:

$$\lim_{\omega \to 0} \frac{G''}{\omega} = \lim_{q \to 0} \frac{p_{12}}{q} \tag{II. 9}$$

$$2 \lim_{\omega \to 0} \frac{G'}{\omega^2} = \lim_{q \to 0} \frac{(p_{11} - p_{22})}{q^2} \tag{II. 10}$$

Equations (II. 9) and (II. 10) give the required connection between the dynamic moduli and components of the stress tensor during steady shear flow.

Another recent theory of Ericksen[7] with a possible use for polymer solutions or melts investigates liquids, in which an orientation is induced by flow. As a result, the flowing liquid is anisotropic. Unfortunately, the resulting equations for the stress tensor are, even in stationary shear flow, very complicated, so that an interpretation is difficult.

A completely different approach was made by Yamamoto, who defines an inner deformation tensor, because the deformation of individual polymer molecules is presumably different from the macroscopic deformation[8]. While this is probably true, the theory is rather complicated and difficult to interpret.

Finally, a difficulty for any molecular or phenomenological theory is caused by the relatively large size of polymer molecules. During steady shear flow molecules are rotating around the 3-axis, according to the convention described in Chapter I, so that two neighbouring segments, belonging to different molecules, may be moving in opposite directions. The same effect is present with low molecular weight liquids, but it will become more serious for larger molecules. This may be quite important in concentrated solutions or polymer melts at high shear rates, because this effect will introduce discontinuities in the deformation.

B. Molecular theories

B. 1. Introduction

Polymeric solutions and melts have viscoelastic and optical properties which have been described with considerable success by a number of molecular theories. In the following sections some of these will be compared; i. e. the dumbbell model[9], the theories of Rouse and Zimm for dilute solutions[10][11][12], the extension of the theory of Rouse[13] and the network theory of Lodge[14] for concentrated solutions and melts. The last two theories describe mostly or exclusively (Lodge) interactions between molecules.

The molecular theories describe viscoelastic properties and flow birefringence. It has been shown that they all predict a simple relationship between the stress tensor and the index of refraction ellipsoid, if the average polarizability of a polymeric segment is equal to that of the solvent[14][15]. This means that the orientation angle χ of the main axes of the index of refraction ellipse in the 1-2 plane, is equal to the orientation of the main axes of the stress tensor χ', during laminar shear flow:

$$\tan 2\chi = \tan 2\chi' = \frac{2 p_{12}}{p_{11} - p_{22}} \qquad \text{(II. 11)}$$

B. 2. The dumbbell model

The oldest and simplest molecular model is the dumbbell model of Kuhn. This model has, in principle, all the features of the more sophisticated theories of Rouse and Zimm, which will be discussed in the next section.

The polymer molecule is represented by two spheres connected by a spring. All hydrodynamic interaction is concentrated in the spheres, interactions between different molecules are neglected, so that it is a dilute solution theory. A very clear calculation has been given by Hermans[9], the main points of the calculation will be repeated here.

The number of molecules per cm^3 is n, and $\psi(\underline{\ell})dV$ is the fraction of molecules having an end-to-end distance $\underline{\ell}$, with one endpoint in the volume element dV, if the other is in the origin. The magnitude of $\underline{\ell}$ is ℓ, and the Cartesian coordinates are ℓ_1, ℓ_2 and ℓ_3. A plane of unit area, perpendicular to the i-direction (i = 1, 2, 3), is crossed by $n \psi \ell_i$ of these molecules. If the force on each molecule is $\underline{K}$, with magnitude K and the same direction as $\underline{\ell}$, the components of $\underline{K}$ in the 1, 2 and 3 direction are:

$$K\frac{\ell_1}{\ell}, \quad K\frac{\ell_2}{\ell} \quad \text{and} \quad K\frac{\ell_3}{\ell}.$$

From the definition of the stress tensor given in Chapter 1, we get, averaging over all configurations:

$$p_{ij} = \int_0^V n \psi(\underline{\ell}) \ell_i K \frac{\ell_j}{\ell} dV = n \int_0^V \psi(\underline{\ell}) . K \frac{\ell_i \ell_j}{\ell} dV \qquad \text{(II. 12)}$$

A more exact derivation of this equation has been given by Kramers[16]. Here only p_{12} was explicitly given, but without any change the derivation is valid for other components of the stress tensor. Very recently, a very similar relation has been derived by Fixman[17]. The relation between $\underline{K}$ and $\underline{\ell}$ is here not specified, it is only assumed that they are parallel. According to the theory of rubber elasticity, the force in a chain with length $\underline{\ell}$ is[9]:

$$\underline{K} = -kT \operatorname{grad} (\ln \psi) - \frac{3\,kT}{\ell_o^2} \underline{\ell} \qquad \text{(II. 13)}$$

taking the diffusion of the endpoints into account, and assuming that the distribution of undisturbed lengths of the dumbbell $\psi_o(\ell)$ is:

$$\psi_o(\ell) = \left(\frac{3}{2\pi\ell_o^2}\right)^{3/2} \exp\left(\frac{3}{2}\frac{\ell^2}{\ell_o^2}\right) \qquad \text{(II. 14)}$$

From these fundamental equations, and from the continuity equation, all components of the stress tensor during laminar flow with shear rate q, can be expressed in one another. From the definition of the intrinsic viscosity $[\eta]$, Eq. (I. 6), the shear stress is:

$$p_{12} = c[\eta]\eta_s q \qquad \text{(II. 15)}$$

The other relations become:

$$p_{11} - p_{22} = \frac{2\,c[\eta]^2\eta_s^2 M q^2}{RT} \qquad \text{(II. 16)}$$

$$\tan 2\chi' = \frac{RT}{M[\eta]\eta_s q} \qquad \text{(II. 17)}$$

$$p_{22} = p_{33} \qquad \text{(II. 18)}$$

η_s solvent viscosity; M molecular weight; c concentration; T absolute temperature; R gas constant.

If it is, moreover, assumed that the contribution to components of the polarizability tensor α_{ik} of a chain with length $\underline{\ell}$ and anisotropy $\alpha_1 - \alpha_2$ is given by[9]:

$$\alpha_{ik} = \alpha_o \delta_{ik} + \frac{3(\alpha_1 - \alpha_2)}{5\ell_o^2} \ell_i \ell_k \qquad \text{(II. 19)}$$

$$\text{Then } \Delta n = n_I - n_{II} = \frac{2\,Cc[\eta]\eta_s q}{RT} \{M^2[\eta]^2 q^2 \eta_s^2 + R^2T^2\}^{\frac{1}{2}} \qquad \text{(II. 20)}$$

$$\tan 2\chi = \frac{RT}{M[\eta]\eta_s q} = \tan 2\chi' \qquad \text{(II. 21)}$$

Here n_I and n_{II} are the main axes of the index of refraction ellipse in a plane perpendicular to the 3-axis. Obviously, a close connection exists between components of the stress tensor and deviatoric components of the index of refraction ellipse, with a proportionality factor C:

$$C = \frac{2\pi}{45\,kT} \frac{(n_s^2 + 2)^2}{n_s} (\alpha_1 - \alpha_2) \qquad \text{(II. 22)}$$

n_s is the index of refraction of the solvent, k is the Boltzmann constant. As has been shown before by Janeschitz-Kriegl , Eq. (II. 22) is the consequence of the use of the theory of rubber elasticity[15]. In the literature on flow birefringence, not C but 2 C is usually called the stress-optical coefficient.

A suspension of rigid ellipsoids will also show normal stress differences, the optical properties, however, have in general no simple relationship with the stress tensor in this case[5].

B. 3. The theories of Rouse and Zimm

The linear viscoelastic behaviour of dilute polymer solutions was first described by Rouse[10] and Bueche[11], using the submolecule model. With the normal-coordinate method they were able to give a good description of the behaviour found experimentally in dynamic measurements. A few years later, Zimm[12] extended the theory to include hydrodynamic interaction with the Kirkwood-Riseman[18] approximation. The Zimm treatment gives the Rouse theory as the special case of zero hydrodynamic interaction, the free-draining case. What is usually called the Zimm theory, is the special case of strong hydrodynamic interaction, the non-free-draining case. As it is rather simple to get normal stress differences from the paper of Zimm, this calculation will be used in the following.
The model consists of a chain of N identical segments, submolecules, joining N + 1 identical beads, with complete flexibility at each bead. The chain is suspended in a viscous liquid, with which it is supposed to interact through the beads only. The forces working on any bead consist of the force due to the liquid, the statistical force in the submolecules, and the Brownian motion. The effect of a force on the motion of the liquid is supposed to be the Kirkwood-Riseman approximation of the Oseen-interaction tensor[18].

The conformation of the polymer molecule is represented by a column vector $\underline{L}$, defined as:

$$\underline{L} = \{ \underline{\varrho}^{(0)}, \underline{\varrho}^{(1)}, \underline{\varrho}^{(2)} \ldots \underline{\varrho}^{(N)} \} \qquad \text{(II. 23)}$$

$\underline{\varrho}^{(i)}$ is the end-to-end vector of the i-th submolecule, with an undisturbed distribution of lengths $\psi_o^{(i)}$ given by Eq. (II. 14). The undisturbed distribution of end-points of the polymer molecule with its N submolecules, each with end-to-end vector $\underline{\varrho}^{(i)}$, i = 0 ... N, can be given by Ψ:

$$\Psi = \prod_{i=1}^{N} \psi_o^{(i)} \qquad \text{(II. 24)}$$

According to Kirkwood and Riseman, the local velocity of the liquid $\dot{\underline{L}}^*$ is given by:

$$\dot{\underline{L}}^* = \dot{\underline{L}}^o + \underline{T}\,\underline{K} \qquad \text{(II. 25)}$$

where $\dot{\underline{L}}^o$ is the velocity of the liquid in the absence of polymer molecules, dots indicate time derivatives, $\underline{T}$ is the Kirkwood-Riseman approximation of the Oseen-tensor and $\underline{K}$ the force on the molecule. The sum of all forces working on the molecule must be zero, on the average:

$$-f(\dot{\underline{L}} - \dot{\underline{L}}^*) + \underline{K} = 0 \qquad \text{(II. 26)}$$

f is a friction factor.

$\underline{K}$ is a column vector given by:

$$\underline{K} = -kT \operatorname{grad}(\ln \Psi) - \frac{3\,kT}{\ell_o^2}\,\underline{A}\,\underline{L} \qquad \text{(II. 27)}$$

$\underline{A}$ is a matrix of order N + 1, with elements defined by:

$$\begin{aligned} A_{ii} &= 2 \quad i \neq 1 \text{ or } i \neq N+1 \\ A_{11} &= A_{N+1\,N+1} = 1 \\ A_{i\,i+1} &= A_{i-1\,i} = -1 \end{aligned} \qquad \text{(II. 28)}$$

A restriction on the movement of the molecule is given by the continuity equation:

$$\frac{\partial \Psi}{\partial t} = -\operatorname{div}(\Psi\,\dot{\underline{L}}) \qquad \text{(II. 29)}$$

Inserting (II. 26) and (II. 27) into (II. 29), we get:

$$\frac{\partial \Psi}{\partial t} = -\operatorname{div}\Psi\left[\dot{\underline{L}}^o_{\ell} - \frac{kT}{f}(f\underline{T} + \underline{I})\operatorname{grad}(\ln\Psi) - \frac{3\,kT}{f\,\ell_o^2}(f\underline{T} + \underline{I})\,\underline{A}\,\underline{L}\right] \qquad \text{(II. 30)}$$

where $\underline{I}$ is the unit matrix. The problem can be solved by using the normal coordinate transformation of Rouse and Bueche, by means of which the matrices $(f\,\underline{T} + \underline{I})$ and $(f\,\underline{T} + \underline{I})\,\underline{A}$ are diagonalized. The diagonal elements of the matrix obtained after diagonalization of $(f\,\underline{T} + \underline{I})$ were called ν_i by Zimm, and those obtained from $(f\,\underline{T} + \underline{I})\underline{A}$ were called λ_i. If the hydrodynamic interaction is zero, the case considered by Rouse and Bueche, only diagonalisation of $\underline{A}$ is

needed, the resulting diagonal elements are called μ_i. Zimm showed that:

$$\nu_i = \frac{\lambda_i}{\mu_i} \qquad i = 0 \ldots\ldots N \qquad \text{(II. 31)}$$

The components of the stress tensor can be calculated, using Eqs (II. 12), (II. 27) and (II. 30):

$$p_{ik} = - kT \langle x^i \frac{\partial}{\partial x^k} (\ln \Psi) \rangle \quad - \frac{3\ kT}{\ell_o^2} \langle x^i \underline{A} x^k \rangle \qquad \text{(II. 32)}$$

where $\langle\ \rangle$ indicates taking the average over all configurations.
On averaging, the first term on the right of (II. 32) is found to be zero or independent of deformation, so that:

$$p_{ik} = - \frac{3\ kT}{\ell_o^2} \langle x^i \underline{A} x^k \rangle \qquad \text{(II. 33)}$$

Eq. (II. 33) shows that the stress tensor is symmetric:

$$p_{ik} = p_{ki} \qquad \text{(II. 34)}$$

After transformation to normal coordinates, Zimm[12] obtained expressions for the average chain configurations in Eq. (II. 33), his Eqs 46 to 49. From these relations it is easy to obtain the components of the stress tensor. It is found that the components $p_{13} = p_{31}$ and $p_{23} = p_{32}$ are zero. Eq. 47 in [12] is not correct, as was first pointed out by Williams [19] (in this paper Eq. 5 contains trivial printing error, so that τ_ℓ must be replaced by τ_ℓ^2 in the numerator of the first right hand term).

If the shear rate is given by:

$$q = q_o \cos \omega t = \frac{d\gamma}{dt} = \omega \gamma_o \cos\ \omega t \qquad \text{(II. 35)}$$

and the deformation $\gamma = \gamma_o \sin\ \omega t$, Eq. (II. 33) gives results that can be expressed in relaxation times τ_p.

For the Rouse theory:

$$\tau_p = \frac{6\ M\ \eta_s[\eta]}{\pi^2\ RT\ p^2} = \frac{\tau_1}{p^2} \qquad p = 1 \ldots\ldots N \qquad \text{(II. 36)}$$

and for the Zimm theory:

$$\tau_p = \frac{M\ \eta_s[\eta]}{0.586\ RT\ \lambda_p} \qquad p = 1 \ldots\ldots N \qquad \text{(II. 37)}$$

Here M is the molecular weight, η_s the viscosity of the solvent, $[\eta]$ is given

by Eq. (I. 6), R is the gas constant, T the absolute temperature, and λ_p in (II. 37) is given in the paper by Zimm, Roe and Epstein[20] (see also [21]). Both theories give identical results, if expressed in the relaxation times given by (II. 36) or (II. 37):

$$p_{12} = \frac{cRT}{M} q \sum_{p=1}^{N} \tau_p = c[\eta]\eta_s q \tag{II. 38}$$

$$p_{22} - p_{33} = 0 \tag{II. 39}$$

$$p_{11} - p_{22} = 2 q^2 \frac{cRT}{M} \sum_{p=1}^{N} \tau_p^2 = F_1 q^2 \tag{II. 40}$$

$$\Delta n = 2 Cq[(\sum_{p=1}^{N} \tau_p)^2 + q^2 (\sum_{p=1}^{N} \tau_p^2)^2]^{\frac{1}{2}} \tag{II. 41}$$

$$\tan 2\chi = \frac{\sum_p \tau_p}{q \sum_p \tau_p^2} = \tan 2\chi' \tag{II. 42}$$

during steady shear flow. During sinusoidal shear $\gamma = \gamma_o \sin \omega t$:

$$G' = \frac{cRT}{M} \sum_p \frac{\omega^2 \tau_p^2}{1 + \omega^2 \tau_p^2} \tag{II. 43}$$

$$G'' = \frac{cRT}{M} \sum_p \frac{\omega \tau_p}{1 + \omega^2 \tau_p^2} + \omega \eta_s \tag{II. 44}$$

$$p_{11} - p_{22} = \frac{c \gamma_o^2 RT}{M} \sum_p \left\{ \frac{\omega^2 \tau_p^2}{1 + \omega^2 \tau_p^2} + \sin 2\omega t \frac{3 \omega^3 \tau_p^3}{(1 + \omega^2 \tau_p^2)(1 + 4 \omega^2 \tau_p^2)} + \right.$$

$$\left. + \cos 2\omega t \frac{\omega^2 \tau_p^2 - 2 \omega^4 \tau_p^4}{(1 + \omega^2 \tau_p^2)(1 + 4 \omega^2 \tau_p^2)} \right\} \tag{II. 45}$$

n, χ and C were defined in Sec. B. 2.

It is easily seen that in the limit $\omega \to 0$ (II. 40) and (II. 45) become identical. Moreover, the two molecular theories give also in the limit $\omega \to 0$ Eqs (II. 9) and (II. 10). The viscosity η, as defined by (II. 38), is found to be independent of shear rate, the normal stress difference $p_{11} - p_{22}$ is proportional to q^2. Obviously, the last two properties are connected, they can also be described by saying that the relaxation times τ_p are independent of shear rate or deformation.

An extension of the model of Zimm, including a dynamic rigidity of the polymer chain, has been given by Cerf[22]. This theory also predicts normal stress differences, but the equations cannot be solved in closed form.

Extensions of the Zimm model have been given recently by several authors [23)24)21)]. These calculations give no difference in the case of zero hydrodynamic interaction, so that the theory of Rouse is not affected. The difference appears in the case of strong hydrodynamic interaction, where the numerical factors λ_p in Eq. (II. 37) are somewhat different. Eqs (II. 38) to (II. 45) remain unchanged, at least in the first two papers. Tschoegl[24] showed, that dilute solutions in theta solvents are well described by the Zimm theory. With increasing solvent power, the viscoelastic behaviour approaches the Rouse theory more and more.

B. 4. Extension of the theory of Rouse to concentrated solutions or melts

In order to adapt the dilute solution theories for solutions of higher concentrations, invariably the theory of Rouse is chosen[13]. The reasons for this are the experimentally found similarity, for concentrated solutions, between the shape of the dynamic moduli, as a function of ω, with those predicted by the Rouse theory, and mathematical difficulties in adapting the Zimm theory. It is assumed that the relation

$$\tau_p = \frac{\tau_1}{p^2}$$

from Eq. (II. 36), and Eq. (II. 38) remain valid. The relaxation times can then be obtained from the zero-shear viscosity η_o:

$$\tau_p = \frac{\tau_1}{p^2} = \frac{6(\eta_o - \eta_s) M}{\pi^2 cRTp^2} \qquad \text{(II. 46)}$$

It is, moreover, assumed that Eq. (II. 39) to Eq. (II. 45) remain valid; all viscoelastic functions can then be calculated. Eq. (II. 46) is only valid for a monodisperse polymer, for polydisperse polymers Peticolas[34] has derived:

$$\tau_{p,i} = \frac{6(\eta_o - \eta_s) M_i^2}{\pi^2 cRTM_w p^2} = \frac{\tau_{1,i}}{p^2} \qquad \text{(II. 47)}$$

$\tau_{p,i}$ is the p-th relaxation time for a polymer molecule with molecular weight M_i, if M_w is the weight average molecular weight, as defined by (I. 5). Eqs (II. 46) and (II. 47) are also valid for dilute solutions.

For the calculation of viscoelastic functions it is necessary to know the mo-

lecular weight distribution.

With polymers of high molecular weight, an entanglement structure is formed in concentrated solutions or melts. In order to explain the viscoelastic behaviour in this case, it must be assumed that the friction factor f is very much higher for movements of parts of the polymer chain longer than M_e, the molecular weight between two successive entanglements along the chain, than for movements of parts of the chain having a molecular weight lower than M_e. Moreover, to explain the experimentally found molecular weight dependence of the zero shear viscosity, it must be assumed that f in that case is proportional to $M_w^{2.4}$. The friction factor for movements of parts of the chain shorter than the length between two successive entanglements, is supposed to be unchanged. This gives:

$$\tau_{p,i} = \frac{\tau_{1,i}}{p^2} \left(\frac{M_e}{M_i}\right)^{2.4} \qquad p > p_e = \frac{M_i}{M_e} \qquad \text{(II. 48)}$$

In Eq. (II. 48) M_e is used (see discussion in Ref. [30]), and not 2 M_e, as originally proposed [13].

If the polymer consists of i fractions, each of n_i molecules per cm^3 with molecular weight M_i, the dynamic moduli will be [31][32]:

$$G' = kT \sum_i \sum_p \frac{n_i \omega^2 \tau_{p,i}^2}{1 + \omega^2 \tau_{p,i}^2} \qquad \text{(II. 49)}$$

$$G'' = kT \sum_i \sum_p \frac{n_i \omega \tau_{p,i}}{1 + \omega^2 \tau_{p,i}^2} \qquad \text{(II. 50)}$$

where $\tau_{p,i}$ is given by Eqs (II. 47) and (II. 48). This model, with minor variations, has been used by a number of authors [13][25][34][26][27][28][29].

In Chapter IV. 6, experimental and calculated values of the dynamic moduli are compared for a dilute solution and for a polymer melt. For the calculation the polymer was divided into a number of fractions, the moduli were then calculated by means of Eqs (II. 49) and (II. 50). This procedure differs from that used by Barlow, Harrison and Lamb [28], who used an average value of p_e, and a continuous function for the molecular weight distribution. Their method tends to underestimate the contribution of high molecular weight material, however.

B. 5. The network theory

An entirely different approach to the calculation of the viscoelastic behaviour of moderately to highly concentrated polymer solutions and melts, is that of Lodge[1)14)]. A similar model was independently used by Yamamoto[8)]. In these theories it is assumed that the molecules form a network consisting of temporary crosslinks, which are continually being broken and newly formed. If the liquid is deformed, the structure can be assumed to consist of a number of substructures, each consisting of a number of temporary crosslinks with the same age. It is evident, that the deformation of every substructure depends on the age of its crosslinks. If contributions of these substructures to the viscoelastic properties can be obtained by adding them, and if, moreover, the theory of rubber elasticity can be used, it is possible to describe the behaviour of the liquid during deformation. It will also be assumed, that the deformation does not effect the rate of formation or breaking of the crosslinks. These assumptions are obviously not realistic. During a continuous deformation crosslinks, which have been deformed, will tend to break earlier than in the undeformed liquid. Several attempts have been made[8)29)] to account for this effect, the results do not seem to be in agreement with experiment, however. Yamamoto reports[8)], that the influence of shear rate on the viscoelastic functions depends on the model used, so that the procedure becomes arbitrary.

Another assumption is, that the deformation of a substructure is equal to that of the liquid. This assumption is probably not realistic either, but an estimate of the error, introduced this way, is very difficult (see Chapter VIII).

According to the theory of rubber elasticity, the relation between components of the stress tensor π^{ij} and components of the contravariant metric tensor γ^{ij}, both in a convecting coordinate system, so that Greek letters are used, is given by[1)]:

$$\pi^{ij} + \bar{p}\,\gamma^{ij}(t) = kTs_n N_o \gamma^{ij}(t_o) \qquad \text{(II. 51)}$$

where N_o is the number of crosslinks and s_n is a numerical factor depending on the network structure, $\bar{p}$ is the hydrostatic pressure. If it can be assumed that this is the contribution of every substructure, and with the assumptions listed above, we get for an incompressible liquid:

$$\pi^{ij}(t) + \bar{p}\,\gamma^{ij}(t) = kTs_n \int_{t'=-\infty}^{t} N(t-t')\gamma^{ij}(t')dt' \qquad \text{(II. 52)}$$

Here $N(t - t')dt'$ is the number of crosslinks in the substructure formed at the time t', and still existing at the time t. For a laminar shear flow, $\gamma^{ij}(t)$ and $\gamma^{ij}(t')$ are given by[1]:

$$\gamma^{ij}(t) = \begin{matrix} 1 & 0 & 0 \\ 0 & 1 & 0 \\ 0 & 0 & 1 \end{matrix} \qquad \gamma^{ij}(t') = \begin{matrix} 1+\gamma^2 & \gamma & 0 \\ \gamma & 1 & 0 \\ 0 & 0 & 1 \end{matrix} \qquad \text{(II. 53)}$$

γ is the shear in the material as defined in Chapter I.

If the deformation in the liquid can be given as the sum of a laminar flow with shear rate q, and a periodic shear $\gamma_o \sin \omega t$, the deformation of a substructure with an age of $\tau = (t - t')$ seconds is:

$$\gamma = q\tau + \gamma_o \{ \sin \omega t (1 - \cos \omega\tau) + \cos \omega t \sin \omega\tau \} \qquad \text{(II. 54)}$$

(Eq. (6. 40) in [1] is not correct)

If (II. 53) and (II. 54) are inserted into (II. 52) we get for laminar flow:

$$p_{12} = q s_n kT N_1 \qquad \text{(II. 55)}$$

$$p_{11} - p_{22} = q^2 s_n kT N_2 \qquad \text{(II. 56)}$$

$$\text{with } N_r = \int_o^\infty N(\tau)\, \tau^r d\tau \qquad \text{(II. 57)}$$

$$p_{22} - p_{33} = 0 \qquad \text{(II. 58)}$$

$$\Delta n = 2 s_n kT N_1 qC \left\{ 1 + \frac{q^2 N_2^2}{4N_1^2} \right\}^{\frac{1}{2}} \qquad \text{(II. 59)}$$

C is given in (II. 22)

$$\tan 2\chi = \frac{2N_1}{qN_2} = \tan 2\chi' \qquad \text{(II. 60)}$$

and for a periodic shear $\gamma = \gamma_o \sin \omega t$:

$$G' = s_n kT \int_o^\infty N(\tau)\, (1 - \cos \omega\tau)\, d\tau \qquad \text{(II. 61)}$$

$$G'' = s_n kT \int_o^\infty N(\tau) \sin \omega\tau\, d\tau \qquad \text{(II. 62)}$$

$$p_{11} - p_{22} = \gamma_o^2 s_n kT \int_o^\infty N(\tau) \{ (1 - \cos \omega\tau) + \cos 2\omega t \cos \omega\tau\, (1 - \cos \omega\tau) + \sin 2\omega t \sin \omega\tau (1 - \cos \omega\tau)\, d\tau \qquad \text{(II. 63)}$$

The cos and the sin terms in (II. 61) and (II. 62) can be developed into a series in the limit $\omega \to 0$ this gives results equivalent with (II. 9) and (II. 10), as was also found for the Zimm and Rouse models.

Following Lodge[1], the very general assumption is now made, that $N(\tau)$ can be represented by a sum of exponentials, so that:

$$N(\tau) = \sum_i a_i' \, e^{-\tau/\tau_i} = \sum_i \frac{a_i}{\tau_i} e^{-\tau/\tau_i} \qquad a_i \geq 0 \quad \tau_i \geq 0 \tag{II. 64}$$

If this is inserted in Eqs (II. 55) to (II. 63), the following results are obtained:

$$p_{12} = s_n kTq \sum_i a_i \tau_i \tag{II. 65}$$

$$p_{11} - p_{22} = s_n kTq^2 \, 2 \sum a_i \tau_i^2 \tag{II. 66}$$

$$\Delta n = 2 s_n Cq \left(\sum a_i \tau_i \right) \left\{ 1 + \frac{q^2 \left(\sum a_i \tau_i^2 \right)^2}{\left(\sum a_i \tau_i \right)^2} \right\}^{\frac{1}{2}} \tag{II. 67}$$

$$\tan 2\chi = \frac{\sum a_i \tau_i}{q \sum a_i \tau_i^2} = \tan 2\chi' \tag{II. 68}$$

$$G' = s_n kT \sum \frac{a_i \omega^2 \tau_i^2}{1 + \omega^2 \tau_i^2} \tag{II. 69}$$

$$G'' = s_n kT \sum \frac{a_i \omega \tau_i}{1 + \omega^2 \tau_i^2} + \omega \eta_s \tag{II. 70}$$

$$p_{11} - p_{22} = s_n \gamma_o^2 kT \sum a_i \left\{ \frac{\omega^2 \tau_i^2}{1 + \omega^2 \tau_i^2} + \cos 2\omega t \, \frac{\omega^2 \tau_i^2 - 2\omega^4 \tau_i^4}{(1 + \omega^2 \tau_i^2)(1 + 4\omega^2 \tau_i^2)} + \right.$$
$$\left. + \sin 2\omega t \, \frac{3 \omega^3 \tau_i^3}{(1 + \omega^2 \tau_i^2)(1 + 4\omega^2 \tau_i^2)} \right. \tag{II. 71}$$

If the factors $s_n a_i kT$ are interpreted as the contributions of relaxation times τ_i to the viscoelastic functions, Eqs (II. 64) to (II. 71) become formally identical with the results of the Zimm and Rouse models. This is a surprising result, because the two sets of equations have been derived in a very different manner. In both theories results from the theory of rubber elasticity are used, which has been put forward to explain this similarity[15].

B. 6. Comparison of molecular theories

Comparing the preceding sections, it becomes possible to combine the molecular theories in a generalized three-dimensional Maxwell model, that also describes normal stress differences and flow birefringence. The relaxation spectrum is described by a function $H(\tau)$, defined so that the contribution to the moduli by relaxation times lying between $\ln\tau$ and $\ln\tau + d(\ln\tau)$ is given by $H(\tau)\, d(\ln\tau)$[31)32)]. This gives:

$$G' = \int_{-\infty}^{\infty} \frac{H(\tau)\ \omega^2\tau^2 d(\ln\tau)}{1+\omega^2\tau^2} \tag{II. 72}$$

$$G'' = \int_{-\infty}^{\infty} \frac{H(\tau)\,\omega\,\tau\, d(\ln\tau)}{1+\omega^2\tau^2} \tag{II. 73}$$

In the same way equations for the other viscoelastic functions are obtained.

$$\eta = \frac{p_{12}}{q} = \int_{-\infty}^{\infty} H(\tau)\,\tau\, d(\ln\tau) = \lim_{\omega\to 0}\frac{G''}{\omega} \tag{II. 74}$$

$$p_{11} - p_{22} = 2q^2 \int_{-\infty}^{\infty} H(\tau)\tau^2 d(\ln\tau) = 2q^2 \lim_{\omega\to 0}\frac{G'}{\omega^2} \tag{II. 75}$$

$$p_{22} - p_{33} = 0 \tag{II. 76}$$

$$\Delta n = 2Cq\left\{\left[\int_{-\infty}^{\infty} H(\tau)\,\tau\, d(\ln\tau)\right]^2 + q^2\left[\int_{-\infty}^{\infty} H(\tau)\tau^2 d(\ln\tau)\right]^2\right\}^{\frac{1}{2}} \tag{II. 77}$$

$$\tan 2\chi = \frac{\int_{-\infty}^{\infty} H(\tau)\,\tau\, d(\ln\tau)}{q\int_{-\infty}^{\infty} H(\tau)\tau^2 d(\ln\tau)} = \tan 2\chi' \tag{II. 78}$$

and during sinusoidal shear:

$$p_{11} - p_{22} = \gamma_o^2 \int_{-\infty}^{\infty} H(\tau)\left[\frac{\omega^2\tau^2}{1+\omega^2\tau^2} + \cos 2\omega t\,\frac{\omega^2\tau^2 - 2\omega^4\tau^4}{(1+\omega^2\tau^2)(1+4\omega^2\tau^2)} + \right.$$

$$\left. + \sin 2\omega t\,\frac{3\omega^3\tau^3}{(1+\omega^2\tau^2)(1+4\omega^2\tau^2)}\right] d(\ln\tau) \tag{II. 79}$$

The difference between the theories is in the relaxation spectra, which are given in the Rouse and Zimm theories, but not by the network theory. As the theories of Rouse and Zimm are valid for dilute solutions, and the theory of Lodge for concentrated solutions and melts, Eqs (II. 72) to (II. 79) would ap-

pear to be valid over the complete concentration range. The agreement between theory and experiment will be discussed in Chapter VIII.

All three molecular theories predict that the normal stress difference $p_{22}-p_{33}$ is zero, and that a simple relationship exists between G' and $p_{11} - p_{22}$, and between G'' and p_{12}, at low shear rates or frequencies.

Moreover, they predict that G' and G'' are proportional to γ_o, that $p_{11}-p_{22}$ is proportional to q^2 or γ_o^2 and that η is independent of q. All these properties are related, and will be called second order behaviour of the material.

It is interesting to apply Eqs (II. 74) and (II. 75) to a simple monomeric liquid of molecular weight M. If each molecule has one relaxation time τ giving a contribution kT to the viscoelastic functions, Eq. (II. 74) gives:

$$\tau = \frac{\eta M}{cRT} \qquad \text{(II. 80)}$$

where c is the concentration in g/cm^3 Inserting this value for τ into Eq. (II. 75), we get:

$$p_{11} - p_{22} = \frac{2\, M\, \eta^2 q^2}{cRT} \qquad \text{(II. 81)}$$

The last equation gives for the reasonable values M = 100, $\eta = 10^{-2}$ poise, c = 0.8 g/cm^3 and T = 298 °K: $p_{11} - p_{22} = 10^{-12} q^2$, so that $p_{11} - p_{22}$ is 10 dyne/cm^2 (the experimental scatter of p_{22} in Chapter V) at shear rates above 10^6 sec^{-1}.

According to this view, there is no fundamental difference in rheological behaviour between simple monomeric liquids and polymer solutions or melts. Eq. (II. 81) shows that for constant viscosity, $p_{11} - p_{22}$ increases with molecular weight. This explains, why noticeable normal stress differences are so much associated with polymeric solutions and melts, which have high molecular weights, and also high viscosities in most cases.

As it would appear that there is no fundamental difference in viscoelastic behaviour between liquids of low molecular weight and polymer solutions or melts, it seems useful to separate the viscoelastic behaviour of any liquid into three regions:

(a) first order behaviour: shear independent viscosity η_o, no perceptible normal stress differences; G' = 0; G'' = $\omega \eta_o$.

(b) second order behaviour: constant viscosity, normal stress differences proportional to the square of the shear rate, so that the normal stress functions F_1 and F_2 of Eq. (II. 8) are constants; G' $\neq$ 0 = $\frac{1}{2} F_1 q^2$ ($\omega = q$).

(c) third order behaviour: viscosity and normal stress functions diminishing with increasing shear rate; $\eta(q) < \eta_o$; $\frac{G'}{\omega^2} \neq \frac{1}{2} F_1 (\omega = q)$.

B. 7. Third order effects

With the network theory it is easy to visualize a reason for third order behaviour, and its consequences for the relaxation spectrum. During laminar flow with shear rate q, the deformation of a polymer chain will be proportional to $q\tau$, τ being the lifetime of the crosslink. During a periodic oscillation the deformation will be proportional to γ_o. From this reasoning it follows that the shear rate where the viscosity becomes shear rate dependent, and the amplitude of deformation where the dynamic moduli become dependent upon γ_o, should be connected. It seems reasonable to assume, as a first approximation, that in the non-linear case the Eqs (II. 72) to (II. 79) remain valid, but that the relaxation spectrum changes.

As a first approximation it can be assumed[33], that all relaxation times change by the same factor a_q, which is supposed to be a function of q only. From Eq. (II. 74) this gives:

$$a_q = \frac{\eta(q) - \eta_s}{\eta_o - \eta_s} = \frac{\tau_p(q)}{\tau_p(q=0)} \qquad \text{(II. 82)}$$

where η_o is zero shear viscosity, η_s solvent viscosity and $\eta(q)$ the viscosity at shear rate q. Then from (II. 75), (II. 77) and (II. 78), the other viscoelastic functions during laminar shear can be expressed in the ratio of $\eta(q)$ and η_o, so that the shape of the curves giving Δn, $p_{11} - p_{22}$, and χ as a function of q can be predicted from the $\eta(q)$ - q curve.

Eq. (II. 82) can only be a first approximation, because one would expect the longer relaxation times to be more effected than the shorter ones. This would give values of a_q dependent upon τ, $a(q, \tau)$.

Measurements of third order effects will be given in Chapter VIII. 3.

Literature

1) A. S. Lodge, Elastic liquids, Academic Press, London 1964.
2) B. D. Coleman, H. Markovitz, W. Noll, Viscometric flows of non-Newtonian fluids, Springer, Berlin 1966.
3) J. L. Ericksen in Viscoelasticity ed. J. T. Bergen, Academic Press, New York 1960.
4) J. G. Oldroyd, Proceed. Roy. Soc. (London) A 200, 523 (1950).
5) H. Giesekus, Rheologica Acta 1, 395 (1961).
6) B. D. Coleman, H. Markovitz, J. Appl. Phys. 35, 1 (1964).

7) J. L. Ericksen, Trans. Soc. Rheology 6, 275 (1962).
8) M. Yamamoto, J. Phys. Soc. Japan, 18, 413 (1956); 12, 1148 (1957); 13, 1200 (1958).
9) J. J. Hermans, Physica 10, 777 (1943).
10) P. E. Rouse, J. Chem. Phys. 21, 1272 (1953).
11) F. Bueche, J. Chem. Phys. 22, 603 (1954).
12) B. H. Zimm, J. Chem. Phys. 24, 269 (1956).
13) J. D. Ferry, R. F. Landel, M. L. Williams, J. Appl. Phys. 26, 359 (1955).
14) A. S. Lodge, Trans. Faraday Soc. 52, 120 (1956).
15) H. Janeschitz-Kriegl, Makromol. Chem. 40, 140 (1960).
16) H. A. Kramers, Physica 11, 1 (1944).
17) M. Fixman, J. Chem. Phys. 42, 3831 (1965).
18) J. G. Kirkwood, J. Riseman, J. Chem. Phys. 16, 565 (1948).
19) M. C. Williams, J. Chem. Phys. 42, 2988 (1965).
20) B. H. Zimm, G. M. Roe, L. F. Epstein, J. Chem. Phys. 24, 279 (1956).
21) C. W. Pyun and M. Fixman, J. Chem. Phys. 42, 3831 (1965).
22) R. Cerf, Fortschritte Hochpol. Forschung 1, 382 (1959).
23) J. E. Hearst, J. Chem. Phys. 37, 2547 (1962).
24) N. W. Tschoegl, J. Chem. Phys. 39, 149 (1963).
25) F. Bueche, J. Chem. Phys. 24, 903 (1956).
26) J. A. Duiser, Thesis Leiden 1965.
27) A. J. Chömpff, Thesis Delft 1965.
28) A. J. Barlow, G. Harrison, J. Lamb, Proceed. Roy. Soc. (London) A 282, 228 (1964).
29) S. Hayashi, J. Phys. Soc. Japan 18, 131 (1963); 18, 249 (1963).
30) H. Markovitz, T. G. Fox, J. D. Ferry, J. Phys. Chem. 66 1567 (1962).
31) A. J. Staverman and F. Schwarzl, in H. A. Stuart, Die Physik der Hochpolymeren, Vol. 4, Chapter I, Springer Verlag, Berlin 1956.
32) J. D. Ferry, Viscoelastic properties of polymers, John Wiley & Sons, New York, 1961.
33) A. J. de Vries, J. Tochon, J. Appl. Polymer Sci. 7, 315 (1963).
34) W. L. Peticolas, Rubber Chem. and Tech. 36, 1422 (1963).

III MATERIALS

1. Materials used

All measurements described in the following chapters were performed on solutions of polyisobutene (B 100 and B 200) and a polystyrene (PS III), and melts of a polyisobutene (Oppanol B 1), a polydimethyl siloxane (PDMS-RS), two polystyrenes (S 111 and B 8), two high density polyethylenes (HDPE-NMWD and HDPE-BMWD) and two low density polyethylenes (LDPE-NMWD and LDPE-BMWD). With the last three pairs of polymers the first had a fairly narrow, the second a much broader molecular weight distribution.

The solutions ranged in concentration from dilute (0.2 volume %) to concentrated (about 25 volume %). Cetane (hexadecane) and a low molecular weight polyisobutene, Oppanol B 1 (a Newtonian oil with a viscosity of 0.236 poise at 25 ^{o}C), were used as solvents for polyisobutene. Polystyrene (PS III) was dissolved in bromobenzene.

Polystyrenes B 8 and S 111 and the two high density polyethylenes were kindly supplied by Dow Chemical Corporation, Midland, Michigan, U.S.A. The two low density polyethylenes were supplied by Monsanto Chemicals Ltd., Newport, Mon., Great Britain.

Polyisobutenes Oppanol B 1, B 100 and B 200, and polystyrene PSIII are commercial polymers of BASF, Ludwigshafen a/R., Germany.

Polydimethyl siloxane, PDMS RS, is a commercial polymer supplied by Bayer, Leverkusen, Germany.

Analar bromobenzene was supplied by Merck (density 1.488 g/cm^3, viscosity 0.0106 poise at 25 ^{o}C). Cetane was supplied by Fluka, it was stated to be better than 99 % pure, and free of olefins (density 0.7664 g/cm^3, viscosity 0.0272 poise at 30 ^{o}C).

A list of all liquids investigated, together with some physical data, is given in Table III.1. In this table a list of the experiments performed is also indicated.

Table III. 1

Dilute solutions

conc.		polymer	solvent	temp. °C	density g/cm^3	$\frac{dn}{dc}$ cm^3/g	measurements
0.2	wt %	PIB B 200	B 1	25	0.8167	0.02	1, 2, 3, 4
0.4	"	"	"	"	(0.817)	"	1
1.03	"	"	"	"	(0.817)	"	1, 2, 3, 4
2	"	"	"	"	(0.817)	"	1, 2, 3, 4

Intermediate range concentrations

5	wt %	PIB B 200	B 1	25	(0.817)	"	1
5	"	"	cetane	30	(0.7728)	0.0805	1
3.90	"	PIB B 100	"	"	0.7711	"	1, 2
5.39	"	"	"	"	0.7734	"	1, 2
6.86	"	"	"	"	0.7760	"	1, 2
8.54	"	"	"	"	(0.779)	"	1, 2
7	g/100 ml	PS III	bromo-benzene	25	1.465	0.0455	1, 3, 4
15	"	"	"	"	1.435	"	1, 2, 3, 4
25	"	"	"	"	1.402	"	1, 3, 4

Melts

100	wt %	PDMS RS	-	25	0.98	-	1, 3, 4, 5
"	"	PS S111	-	190	0.979	-	1, 3, 4
"	"	PS B 8	-	"	"	-	1, 3, 4
"	"	HDPE-NMWD	-	"	0.756	-	1, 3, 4
"	"	HDPE-BMWD	-	"	"	-	1, 3, 4
"	"	LDPE-NMWD	-	"	"	-	1, 3, 4
"	"	LDPE-BMWD	-	"	"	-	1, 3, 4
"	"	PIB B1	-	25	0.8167	-	1, 2, 3, 4

concentration: wt % means weight percentage of polymer.
polymer : PIB = polyisobutene; PS = polystyrene; PDMS = polydimethyl siloxane; HDPE = high density polyethylene; LDPE = low density polyethylene; NMWD = narrow molecular weight distribution; BMWD = broad molecular weight distribution.

Density values in brackets are extrapolated values. For the solutions in B 1 or cetane it was assumed that densities at other temperatures were proportional to that of the solvent.
Densities of polymer melts were taken from the literature[1].
$\frac{dn}{dc}$ is the index of refraction increment (see Chapter VII).

Measurements performed:
1 = dynamic shear modulus, Chapter IV
2 = normal stress gradient, Chapter V
3 = viscosity, Chapter VI
4 = flow birefringence, Chapter VII
5 = recovery after steady shear flow, Chapter V

Normal stress gradient measurements on solutions of B 100 in cetane were taken from the literature[2].

2. Molecular weights

For the interpretation of viscoelastic measurements on polymeric liquids it is desirable to have information about the molecular weight distribution. For a few polymers (PIB B 100 and B 200, and PDMS-RS) this was obtained by precipitation into 5 to 8 fractions. The molecular weight of each fraction was estimated from the intrinsic viscosity in a suitable solvent[3)4)]. Two molecular weight averages, M_w and M_n, were then calculated by means of Eqs (I. 5) and (I. 4).

Molecular weights of most of the other polymers were obtained from the suppliers[5)6)], those for PS III were kindly supplied by Dr. Th. G. Scholte, Dutch State Mines, Limburg, Netherlands[7)]. All results are summarized in Tables III. 2 and III. 3, for explanation of polymer names, see Table III. 1.

Table III. 2

		M_n	M_w	M_w/M_n	
PIB	B 1	430	-	-	6)
	B 100	6.0×10^5	1.18×10^6	2	
	B 200	2.22×10^6	4.52×10^6	2	
PDMS	RS	-	5.36×10^5	-	
PS	S 111	2.14×10^5	2.24×10^5	1.05	5)
	B 8	1.13×10^5	2.79×10^5	2.5	5)
HDPE-NMWD*)		-	4.2×10^4	-	5)
HDPE-BMWD*)		-	9.2×10^4	-	5)
LDPE-NMWD		2×10^4	10^5	about 5	5)
LDPE-BMWD		2×10^4	4.2×10^5	about 20	5)
PS	III	0.82×10^5	4.1×10^5	5.0	7)

*) HDPE-BMWD was stated by the supplier to have a much broader molecular weight distribution than HDPE-NMWD.

Table III. 3

Oppanol B 200

fraction	weight	molecular weight of fraction
1	0.0711	77×10^5
2	0.4065	70×10^5
3	0.1842	32×10^5
4	0.1396	23×10^5
5	0.1791	7×10^5

Polystyrene S 111

fraction	weight	molecular weight of fraction
1	0.055	1.25×10^5
2	0.095	1.625×10^5
3	0.170	1.875×10^5
4	0.233	2.125×10^5
5	0.225	2.375×10^5
6	0.145	2.625×10^5
7	0.060	2.875×10^5
8	0.025	3.125×10^5
9	0.015	3.5×10^5

3. Preparation of solutions

Solutions of polystyrene in bromobenzene and a solution of 5 % by weight of Oppanol B 200 in cetane were prepared by standing at room temperature, during periods of several months in the dark.

Solutions of Oppanol B 200 in Oppanol B 1, all solutions of Oppanol B 100, and a 5 % solution (the same as above) of Oppanol B 200 in cetane were dissolved first in hexane (May and Baker, the non-volatile residue was given as less than 0.01 %) at room temperature in the dark. Afterwards, the required amount of solvent (B 1 or cetane) was added, and the solution was left until the mixture was found homogeneous by visual inspection. Finally, the hexane was removed by a vacuum destillation at about 40 - 50 ^{o}C, with oxygen free nitrogen bubbling through. It was possible, by weighing, to check how much of the hexane had been removed. The process was stopped when the weight remained constant; the resulting solution contained less than 0.2 % by weight of hexane. The solutions were completely clear and homogeneous on visual

inspection. The control solutions of 5 % by weight of Oppanol B 200 in cetane, prepared by the two methods, gave dynamic results in excellent agreement (see Chapter IV). This rather involved procedure was necessary, because it was noticed that the molecules in solutions prepared by stirring at elevated temperatures during a rather long period (several days to a week) were broken down, as shown by a slight discoloration and a viscosity diminishing with increasing time of stirring.

4. Reasons for the choice of materials

The molecular theories discussed in Chapter II, should be valid over the complete concentration range, going from dilute solutions to concentrated systems. For this reason, the range of concentrations was taken as wide as possible. In our case concentrations ranged from 0.2 to 100 volume per cent.

With the available experimental equipment it was not feasible to investigate dilute solutions and melts of the same polymer. In order to measure very dilute solutions it was necessary to choose polymers of very high molecular weight, otherwise the effects to be measured would have been too small. In the molten state, polymers of such high molecular weight are very difficult to handle, in fact measurements at similar shear rates as those at which measurements were done on solutions were not possible, on account of mechanical degradation or viscous heating during flow. For this reason a rather wide range of polymers had to be chosen. This was no disadvantage, however, as it was desirable to compare the viscoelastic behaviour of different polymers.

Because the molecular theories given in Chapter II will probably not be valid for polyelectrolytes, these were not investigated. It is quite possible that the viscoelastic behaviour of polyelectrolyte solutions will differ in certain respects from that of the materials described here.

As fairly large amounts of polymer were needed for the complete program, only commercially available polymers could be used for the solutions.

For the different types of measurements, the requirements for the liquids are also different. For measurement of the dynamic shear moduli, as described in Chapter IV, the requirements are:

(a) the liquid must be non-volatile;
(b) shear moduli must be in the range of about 10 dyne/cm^2 to 10^7 dyne/cm^2 in the angular frequency range from about 10^{-3} to 300 rad/sec;
(c) the liquid must be chemically stable, otherwise its properties will change during the experiment.

For normal stress measurements, described in Chapter V, a requirement, in addition to (a), (b) and (c) above, is:

(d) a viscosity lower than about 10^3 poise.

The viscosity measurements, given in Chapter VI, caused no additional requirements, but for flow birefringence measurements, described in Chapter VII, two additional requirements are:

(e) no form-birefringence. This means that the average index of refraction of the polymer must be equal to the index of refraction of the solvent.

(f) the polarizability of a segment of the polymer chain must be different in the directions parallel and perpendicular to the chain.

Because an object of the investigation was to compare the behaviour of polymer solutions with those of melts, an additional requirement was:

(g) the solvent must be chemically similar to the polymer.

As a result of requirements (b), (c) and (f) for the low concentrations (0.2 to 2 volume %) a very high molecular weight polyisobutene, Oppanol B 200, was chosen. As solvent for these solutions, with requirements (a), (b), (c), (e) and (g), a low molecular weight polyisobutene, Oppanol B 1, was used.

For the intermediate concentration range, from 5 to about 25 volume %, solutions were chosen of the lower molecular weight polyisobutene, Oppanol B 100, and of polystyrene III. As solvent for polyisobutene solutions cetane was taken, bromobenzene was chosen as solvent for polystyrene (requirements (a), (c), (d), (e) and (g)).

The lower molecular weight of the polymers, and the lower viscosity of the solvents, were necessary because otherwise the viscosities of the solutions would have been too high (requirement (d)).

On B 100 solutions in cetane a large number of normal stress measurements had been performed by Dr. H. Markovitz[2], who kindly supplied the polymer. On solutions of polystyrene III, Dr. H. Janeschitz-Kriegl at our institute had performed a large number of flow birefringence experiments[8].

The highest concentrations investigated were polymer melts, 100 volume per cent. A number of polymers, all with weight average molecular weights in the range from about 10^5 to 5.10^5, were investigated. Normal stress gradients could not be measured on melts of these polymers, because the viscosities were too high (requirement (d)). Most of the experiments on melts were performed as part of an investigation on behalf of the International Union of Pure and Applied Chemistry (IUPAC)[5]. These results were used because they gave an obvious extension of the experimental program.

References

1. J.M. McKelvey, Polymer Processing, Wiley, New York 1962.
E.C. Bernhardt, Ed., Processing of thermoplastic materials, Reinhold, New York 1959.
2. H. Markovitz, D.R. Brown, Trans. Soc. Rheology 7, 137 (1963).
3. E.W. Merrill, J. Polymer Sci. 38, 531 (1959).
4. V. Crescendi, P.J. Flory, J. Am. Chem. Soc. 86, 141 (1964).
5. IUPAC Report, to be published.
6. J. Meiszner, Personal communication.
7. Th.G. Scholte, Personal communication.
8. H. Janeschitz-Kriegl, Makromolekulare Chemie 33, 55 (1959).

IV DYNAMIC MEASUREMENTS

1. Apparatus

The linear viscoelastic behaviour of a number of polymer solutions and melts was investigated with a concentric cylinder viscometer, in the angular frequency range from about 10^{-3} to about 300 rad/sec. The apparatus was developed from a very similar apparatus, which has been described in detail by Duiser [1)2)] Only the principles will be repeated here.

The polymer solution or melt is held between two concentric cylinders. The inner cylinder is suspended by a torsion wire from a driving axis, executing a sinusoidal oscillation around the common axis of the system. In the stationary state, the inner cylinder will also execute a sinusoidal motion, so that the material between the stationary outer cylinder and the oscillating inner cylinder will undergo sinusoidal shear. In general, the viscoelastic properties of the material, the inertia of the system and the torsional stiffness of the wire will give rise to a difference in phase and amplitude between the motion of the driving axis, and that of the inner cylinder. By an optical system the amplitude of the driving axis ε_{ao}, of the inner cylinder ε_{co}, and the phase angle φ between the two are measured. Together with the torsional stiffness of the torsion wire, and with the geometry of the cylinders, the shear moduli of the material can be calculated. By changing the angular frequency ω of the oscillation, it is possible to investigate the part of the shear modulus in phase with the oscillation, G', and the part out of phase, G'', as a function of ω.

If the deformation is sufficiently small, so that the behaviour of the material is in the linear region, the shear moduli are given by:

$$G' = \frac{D_1}{D_2}\left(\frac{\varepsilon_{ao}}{\varepsilon_{co}}\cos\varphi - 1\right) + \frac{I}{D_2}\omega^2 \qquad \text{(IV. 1)}$$

$$G'' = \frac{D_1}{D_2}\frac{\varepsilon_{ao}}{\varepsilon_{co}}\sin\varphi \qquad \text{(IV. 2)}$$

where D_1 torsional stiffness of the wire

D_2 geometric constant for the two cylinders

$$D_2 = \frac{4\pi h}{R_i^{-2} - R_u^{-2}} \qquad \text{(IV. 3)}$$

R_i diameter of the inner cylinder

R_u diameter of the outer cylinder; h length of the cylinders

For the interpretation of the measurements only D_1/D_2 and I/D_2 are required, these were obtained by measurements with a non-elastic liquid of known viscosity. Another method was a direct measurement of D_1 and calculation of D_2 from Eq. (IV. 3). The two methods agreed within a few per cent. The diameter of the outer cylinder was 0. 900 cm, it was made of glass in order to enable inspection of the sample. The diameters of the inner cylinders were 0. 500 and 0. 700 cm, the lengths were 5. 0 cm. The wires used had diameters of 0. 10, 0. 07, 0. 05, 0. 03, 0. 02 and 0. 01 cm. The constants D_1 and D_2 are given in Table IV. 1. The values of I were calculated from the resonance frequency of the system[1], the values are also given in Table IV. 1.

Table IV. 1

nominal diameter wire	D_1	diameter cylinder	D_2	I/D_2
cm	dynecm/rad	cm	cm^3	g/cm
0. 01	142	0. 500	5. 68	0. 0746
0. 02	2172	0. 700	19. 45	0. 0516
0. 03	1.34×10^4			
0. 05	1.04×10^5			
0. 07	4.21×10^5			
0. 10	1.59×10^6			

The measurements of ε_{ao}, ε_{co} and $\varepsilon_{ao} \sin \varphi$ were accurate to 1.4×10^{-4} radian, the lowest values actually measured were at least about 0. 008 rad., and in most cases considerably larger (0. 05 to 0. 2 rad.). This gives as the minimal accuracy about 2 %. The accuracy of G' and G'' can then be estimated in each case from Eqs (IV. 1) and (IV. 2). The estimated overall accuracy was about 5 %.

The inner cylinder was centered either by a magnet at the bottom (for solutions) or by a second torsion wire at the bottom (for melts). The second torsion wire gives a contribution to G' only, as this contribution was considerably less than 1 % for all measurements, this effect was neglected.

2. Reduction of measurements

In order to compare measurements performed at different temperatures, a temperature reduction scheme was proposed empirically by Ferry and coworkers[4]. This was later theoretically justified by the molecular theories discussed in Chapter II. Eqs (II. 72) and (II. 73) give a connection between the

relaxation times and the shear moduli.

A change of temperature has three different effects on the moduli:

(a) each relaxation mechanism has a contribution to the moduli proportional to kT, according to the molecular theories;

(b) the density ρ of the material changes with temperature, so that the number of relaxation mechanisms per unit volume changes;

(c) the relaxation times are temperature dependent.

In order to account for the changes in the moduli due to effects (a) and (b), the moduli are divided by a factor ρT:

$$G'_r = \frac{G'}{\rho T} \qquad G''_r = \frac{G'' - \omega \eta_s}{\rho T} \qquad \text{(IV. 4)}$$

η_s is the solvent viscosity, for a melt $\eta_s = 0$.

If all relaxation times change by the same factor $a(T, T_o)$ when the temperature is changed from an arbitrary reference temperature T_o to T, we get:

$$a(T, T_o) = a_T = \frac{\tau_p(T)}{\tau_p(T_o)} \qquad \text{(IV. 5)}$$

The simple index T can be used, because T_o will be indicated in each case. Since a_T is assumed to be the same for all relaxation times, all functions of the relaxation times will change by simple functions of a_T. Modulus measurements at different temperatures will be expressed in the following by the reduced moduli given in Eq. (IV. 4) as a function of ωa_T, with a_T defined by Eq. (IV. 5).

Experimentally, $\log a_T$ was determined by measuring the distance along the $\log \omega$-axis, between curves giving $\log G'_r$ or $\log G''_r$ as a function of $\log \omega$, at the two temperatures T and T_o. A check on the consistency of the results is, that a_T as determined from G'_r and G''_r should be equal, and that a_T should be constant along the curve at different values of ω. A typical example of such a reduction scheme is given in Figs 1 and 2 for the molten high density polyethylene HDPE-NMWD. The measurements can be reduced very well, within experimental accuracy the temperature shift is equal for G'_r and G''_r, and independent of ω. Over a sufficiently small temperature range it can sometimes be assumed[3], that the relaxation times have a temperature dependence of the type:

$$\tau_p(T) = \tau_p(T_o) e^{\frac{H_a}{RT}} \qquad \text{(IV. 6)}$$

H_a is called the apparent flow activation energy, R is the gas constant.

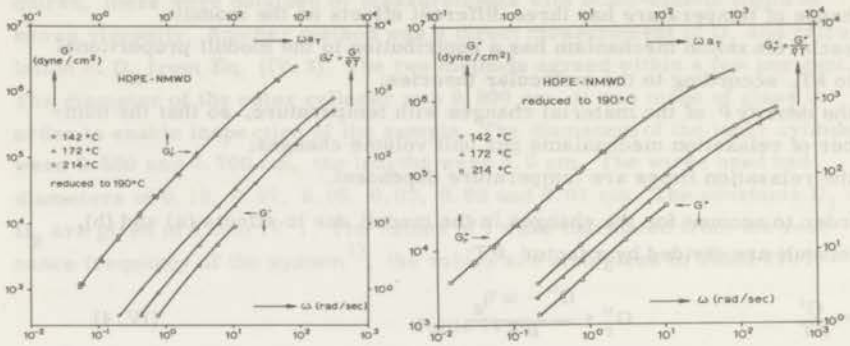

Fig. 1.

As the temperature dependence of all relaxation times was found to be the same, a plot of a_T as a function of 1/T will yield H_a. In Fig. 2, log a_T as a function of 1/T is given for the polymer of Fig. 1. Values of a_T obtained from G''_r, the circles, are in good agreement with those obtained from G'_r, the triangles. From the slope of the plot through the experimental points, H_a can be determined from the equation[3)4)]:

$$H_a = 2.303\, R \frac{d(\log a_T)}{d(1/T)} \qquad \text{(IV. 7)}$$

The reduction given above is only feasible, if the deformation is in the linear region

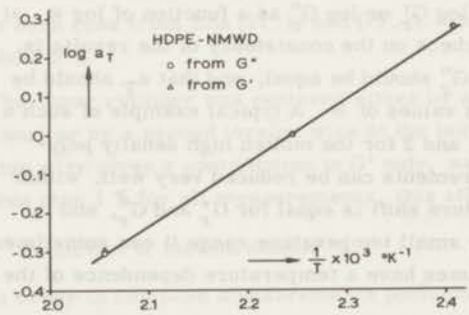

Fig. 2.

The maximum shear during the dynamic measurements is about 0.05 to 0.2. The moduli were measured as a function of deformation at several frequencies, in order to investigate, whether the material was still in the linear region during this deformation. Fig. 3 gives G' and G'', as a function of the maximum deformation γ_o, for a polydimethylsiloxane with a zero shear viscosity η_o of 10^5 poise at 25 °C. This material was chosen for its chemical stability. It is clear that within the accuracy of the experiment, G' and G'' are independent of γ_o, so that the material is indeed in the linear region.

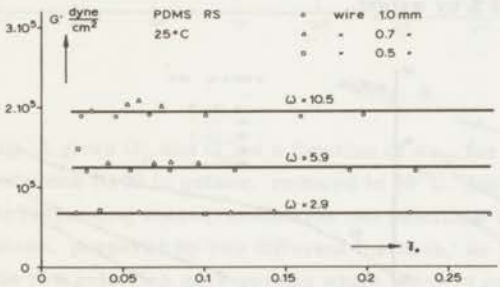

Fig. 3.

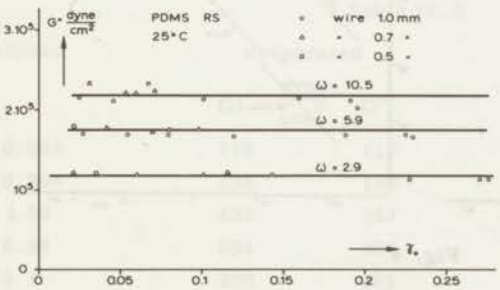

3. Measurements

Measurements were performed both on polymer solutions and on melts. Measurements on solutions were all performed with magnetic centering of the inner cylinder. Measurements on melts were all performed with the inner cylinder kept centered by means of the lower torsion wire. All measurements have been reduced as indicated in Section 2, except those for solutions of polystyrene III in bromobenzene, where all dynamic measurements were performed at 25 °C only.

Fig. 4 gives G'_r and G''_r, reduced to 25 °C, as a function of ωa_T for a series of solutions of polyisobutene B 200 in the low molecular weight polyisobutene B 1, at concentrations from 0.2 to 5.0 % by weight.

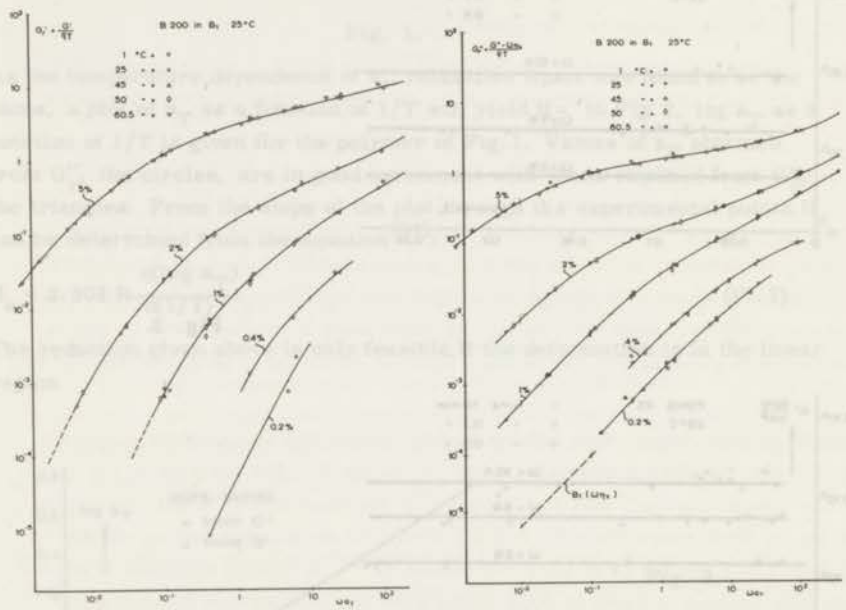

Fig. 4.

H_a determined from Eq. (IV.7) varied from 8 to 10 kcal/mol, the values at the two lowest concentrations are the least accurate. This can be compared with a value of about 16 kcal/mol for bulk high molecular weight polyisobutene, also at 25 °C[3)4)].

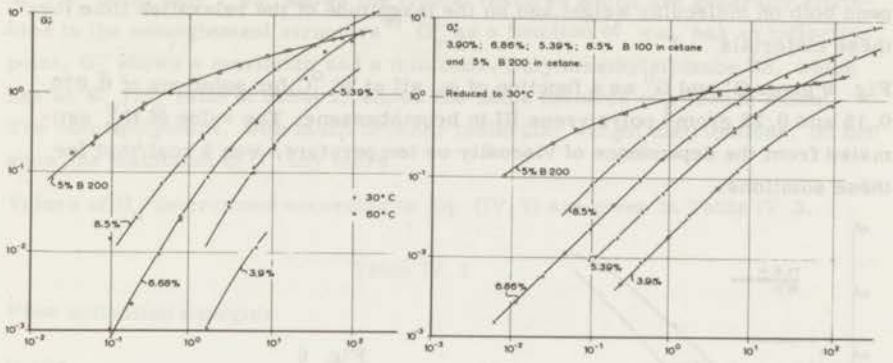

Fig. 5

Fig. 5 gives G'_r and G''_r, as a function of ωa_T, for a series of solutions of polyisobutene B100 in cetane, reduced to 30°C. Included in these graphs are the corresponding measurements on two solutions of 5 % polyisobutene B200 in cetane, prepared by two different methods, as indicated in Chapter III. 3. The two solutions gave results which were in good agreement. Table IV. 2 gives G' and G'' at a number of frequencies for the solution prepared by evaporation of a dilute solution (evaporated), and for the solution prepared by standing at room temperature (room temperature).

Table IV. 2

rad/sec	evaporated		room temperature	
	G' $\frac{\text{dyne}}{\text{cm}^2}$	G''	G' $\frac{\text{dyne}}{\text{cm}^2}$	G''
0.099	116	116	103	115
0.396	235	186	236	189
1.58	433	247	437	251
6.28	684	307	677	300
25.1	980	365	971	357
95	1370	456	1358	414

Comparing these measurements with those performed on B100, it is clear that a reduction scheme, based on a single shift factor $a(M_1, M_2)$, cannot shift the 5 % B200 solution along either of the axes to get an overlap with a solution of B100 of the same concentration. For this reason, no reduction with respect to molecular weight was attempted. In terms of the spectrum of re-

laxation times this means, that the necessary shift factor $a(M_1, M_2)$ would depend both on molecular weight, and on the magnitude of the relaxation time for these materials

Fig. 6 gives G' and G'' as a function of ω, all at 25 °C, for solutions of 0.070, 0,15 and 0.25 g/cm^3 polystyrene III in bromobenzene. The value of H_a, estimated from the dependence of viscosity on temperature, was 5 kcal/mol for these solutions.

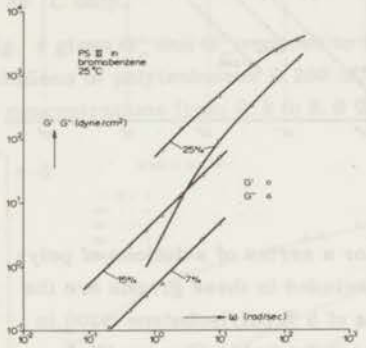

Fig. 6

Fig. 7 gives G'_r and G''_r as a function of ωa_T for polydimethylsiloxane RS, reduced to 25 °C; Figs 8 and 9 the same for the polystyrenes S 111 and B 8, and Fig 10 for polyethylene melts, HDPE-NMWD, HDPE-BMWD, LDPE-NMWD and LDPE-BMWD, all reduced to 190 °C. The molecular parameters of the polymers are given in Chapter III. The polymer melt experiments will be published elsewhere[17)18)]

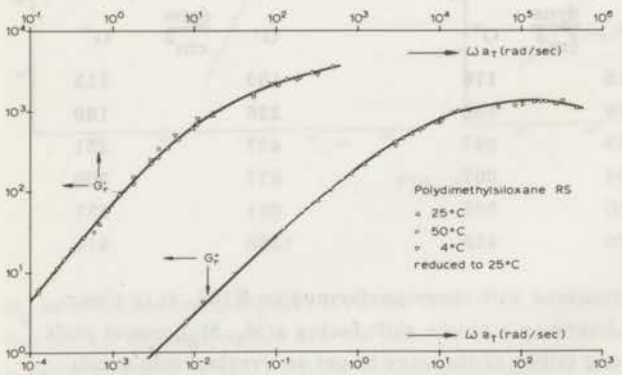

Fig. 7

Polystyrene S 111, which has a very narrow molecular weight distribution, M_w/M_n being only 1.05, shows the typical features which are generally attributed to the entanglement structure[4]: G'_r as a function of ωa_T has an inflection point, G''_r shows a maximum and a minimum. Polydimethylsiloxane RS, which has an M_w/M_n ratio of about 2, shows the same features to a lesser extent. The other polymers, with much broader molecular weight distributions, do not show the maximum in G''_r any more.

Values of H_a determined according to Eq. (IV.7) are given in Table IV.3.

Table IV.3

Flow activation energies

liquid	temp. °C	H_a in kcal/mol
PIB B 200 in B_1 0.2 %	25	8.1
PIB B 200 in B_1 0.4 %	25	8.3
PIB B 200 in B_1 1.03 %	25	9.8
PIB B 200 in B_1 2 %	25	9.3
PIB B 200 in B_1 5 %	25	9.5
PIB B 100 in cetane 3.90 %	30	
PIB B 100 in cetane 5.39 %	30	about 4.5
PIB B 100 in cetane 6.86 %	30	
PIB B 100 in cetane 8.54 %	30	
PS III in bromobenzene 7 to 25 %	25	5.0
PDMS RS	25	3.9
PS S 111	190	37.6
PS B 8	190	38
HDPE-NMWD	190	7.5
HDPE-BMWD	190	7.6
LDPE-NMWD	190	13.6
LDPE-BMWD	190	13.8

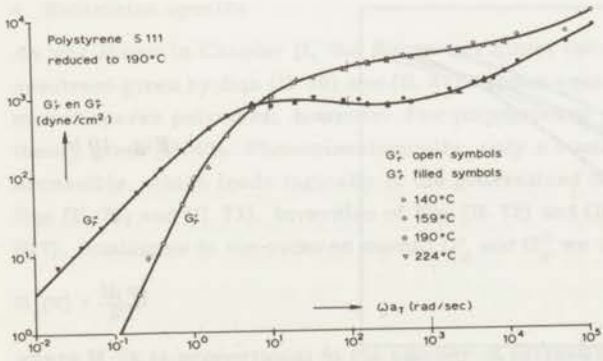

Fig. 8

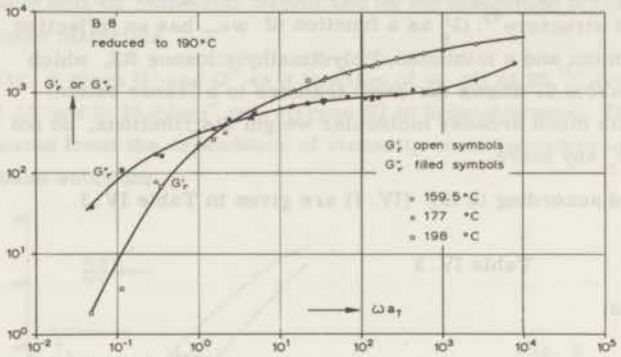

Fig. 9

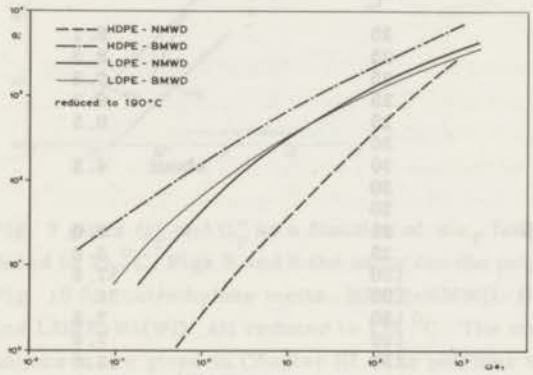

Fig. 10 a

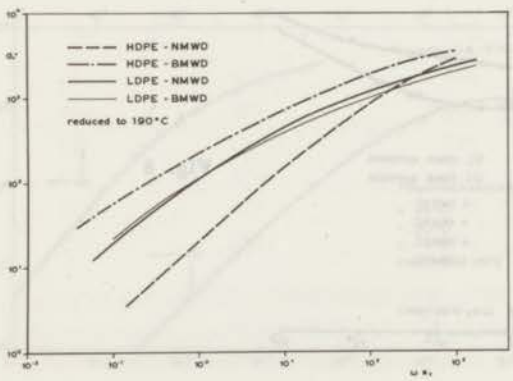

Fig. 10 b

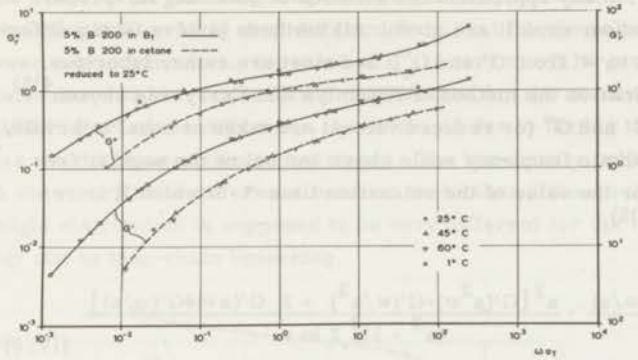

Fig. 11

In Fig. 11, G'_r and G''_r as a function of ωa_T, reduced to 25 °C, are given for 5 % solutions of polyisobutene B200 in cetane and in polyisobutene B1. According to Eq. (II. 36) and (II. 37) the ratio of the relaxation times for the two solutions should be the ratio of the two solvent viscosities η_s. As the viscosity of cetane at 25°C is 0. 0309 poise, and that of B1 0. 236 poise, the ratio is 7. 6. The shift factor along the ωa_T axis, necessary in Fig. 11 to bring the curves for the two solutions to coverage, is about 7. 4. This value agrees within about 5% with the ratio of the solvent viscosities. Because the original measurements, before reduc tion, were performed over temperatures ranging from 1°C to 60°C, the actual change in viscosity was by a factor of about 70. The two solvents are very similar chemically. For these reasons this result would seem to exclude any appreciable influence of internal viscosity for polyisobutene (see Chapter VIII. 4).

4. Relaxation spectra

As was shown in Chapter II, the Rouse and Zimm theories predict a line spectrum given by Eqs (II. 36) and (II. 37). These equations are only valid for monodisperse polymers, however. For polydisperse polymers, the Rouse theory gives (II. 47). Phenomenologically, only a continuous spectrum is accessible, which leads logically to the generalized Maxwell model given in Eqs (II. 72) and (II. 73). Inversion of Eqs (II. 72) and (II. 73) gives, in principle, $H(\tau)$. Analogous to the reduced moduli G'_r and G''_r we define:

$$H_r(\tau) = \frac{H(\tau)}{\rho T} \qquad \text{(IV. 8)}$$

where H_r/k is proportional to the number of relaxation mechanisms, each with a contribution kT, per gram of material.

In the literature[3)4)], many approximation methods of obtaining $H(\tau)$ from measured dynamic shear moduli are given. All methods involve taking differentials with respect to ω from G' and G'', and most are rather laborious. For ease of determination the method of Ninomiya and Ferry was chosen[4)5)]. With this method, G' and G'' (or reduced values) are taken at equal intervals, log a, on the logarithmic frequency scale above and below the angular frequency $\omega = 1/\tau$ for the value of the relaxation time τ at which H is required. This gives[4)5)]:

$$H(\tau) = \frac{G'(a\omega) - G'(\omega/a)}{2 \ln a} - \frac{a^2 [G'(a^2\omega) - G'(\omega/a^2) - 2\, G'(a\omega) + G'(\omega/a)]}{(a^2 - 1)^2\, 2 \ln a} \qquad \omega = 1/\tau \qquad \text{(IV. 9)}$$

$$H(\tau) = \frac{2\, G''(\omega)}{\pi} - \frac{2a}{\pi (a-1)^2} [G''(a\omega) + G''(\omega/a) - 2\, G''(\omega)] \qquad \omega = 1/\tau \qquad \text{(IV. 10)}$$

As pointed out in[5)], Eq. (IV. 9) in the limit $a \to 1$ corresponds to the fourth approximation method of Fujita[6)]. Eq. (IV. 10) corresponds in the limit $a \to 1$ to the third approximation method of Schwarzl and Staverman[7)].

As proposed by Ninomiya and Ferry, a value for log a of 0. 2 was chosen.

Fig. 12 gives H_r as a function of log τ, reduced to 25 °C, for solutions of polyisobutene B 200 in B 1. Although at large values of τ the curves for different concentrations are very different, at smaller τ-values H_r is very nearly proportional to the concentration. Values of H_r for the different concentrations, calculated from the experimental value at 1 % at the small τ-end of the spectrum, assuming them to be proportional to the concentration, are indicated in Fig. 12 by dashed lines. The agreement is reasonable.

The longest relaxation times increase very rapidly with increasing concentration. The 5 % solution has relaxation times well in excess of 10^3 sec. These are very long relaxation times, not normally associated with a liquid.

Fig. 13 gives the relaxation spectrum for solutions of polyisobutene in cetane, reduced to 30 °C. Fig. 14 gives the relaxation spectrum for polydimethylsiloxane RS, reduced to 25 °C, and Fig. 15 gives relaxation spectra for the other polymer melts, all reduced to 190 °C[18)]. The narrow fraction S 111 shows a maximum in H_r at τ = 0. 1 sec, and a minimum at τ = 0. 0015 sec. These two features, which can be attributed to the entanglement network[4)11)], have nearly disappeared in B 8, which has a broader molecular weight distribution.

The shape of the curves giving the relaxation spectra of the high density polyethylenes in Fig. 15 is very different from that for the polystyrenes. At the lower relaxation times, the value of H_r is very much larger for the broad molecular weight fraction HDPE-BMWD than for the narrow fraction HDPE-NMWD. Part of the difference, however, is due to the big difference in molecular weight between the two polymers. The low density polyethylenes in Fig. 15 show very little difference between each other, although the molecular weight distribution is supposed to be very different for the two. This is probably due to long-chain branching.

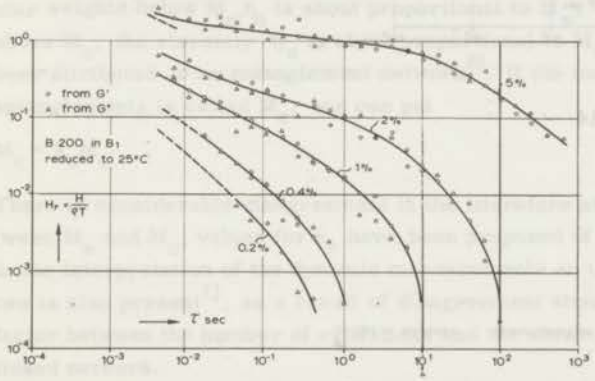

Fig. 12

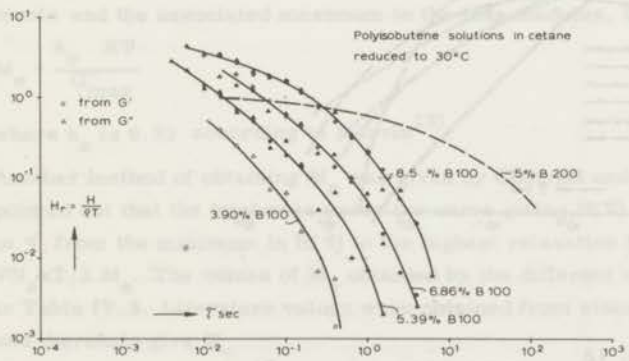

Fig. 13

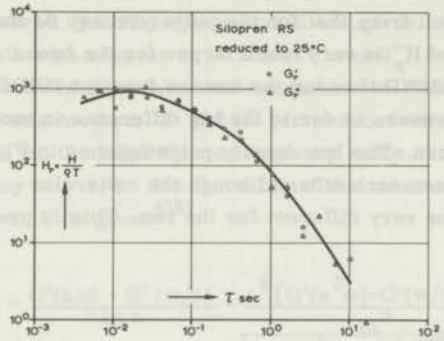
Silopren RS
reduced to 25°C
• G'
▲ G''
$H_r = \frac{H}{\partial T}$
τ sec

Fig. 14

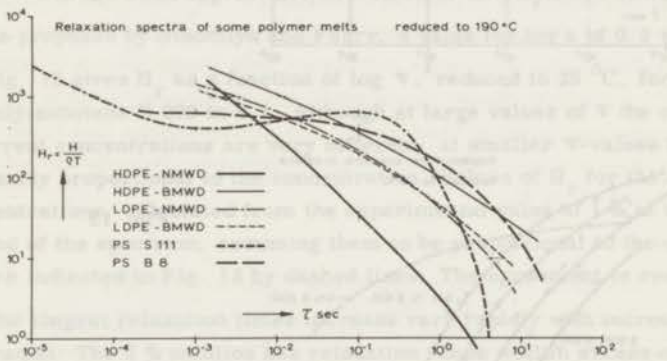
Relaxation spectra of some polymer melts reduced to 190 °C
$H_r = \frac{H}{\partial T}$
HDPE - NMWD
HDPE - BMWD
LDPE - NMWD
LDPE - BMWD
PS S 111
PS B 8
τ sec

Fig. 15

5. The entanglement network

In order to explain the very large increase in viscosity and elasticity with increasing concentration and molecular weight of polymer solutions and melts, an entanglement network has been postulated[4)8)]. This probably means for non-polar polymers, that molecules lie in long range contour loops around each other, which impedes their movement[4)8)].

The zero shear viscosity η_o of polymer melts, when plotted on a log-log scale as a function of the weight average molecular weight M_w, as defined by Eq. (I. 5), shows a discontinuity at a certain molecular weight M_c. At molecular weights below M_c, η_o is about proportional to M_w, at molecular weights above M_c, the viscosity η_o is about proportional to $M_w^{3.4}$ [3)4)8)20)]. This has been attributed to an entanglement network[8)]. If the molecular weight between entanglements is called M_e, one can put

$$M_c = k_c M_e \qquad \text{(IV. 11)}$$

There is considerable disagreement in the literature about the relation between M_e and M_c; values for k_c have been proposed of 2 [8)], 1.5 [9)], or 1 [10)]. In the interpretation of the dynamic measurements an uncertainty of a factor two is also present[1)], as a result of disagreement about the proportionality factor between the number of crosslinks and the shear modulus in a crosslinked network.

By a number of authors the following relation between the number of entanglements and the associated maximum in the loss modulus, G''_{max} was proposed

$$M_e = \frac{k_e \, RT}{G''_{max}} \qquad \text{(IV. 12)}$$

where k_e is 0.32 according to Marvin[13)].

Another method of obtaining M_e was given by Chömpff and Duiser[11)], who pointed out that the total area under the curve giving $H(\tau)$ as a function of $\ln \tau$, from the minimum in $H(\tau)$ to the highest relaxation time, is equal to $\rho N_a kT/2\, M_e$. The values of M_e obtained by the different methods are given in Table IV. 3. Literature values were obtained from viscosity measurements, and therefore give M_c.

Table IV. 3

polymer	M_e from G''_{max} (Marvin[13)])	M_e (Chömpff and Duiser[11)])	lit.[16)]
PS S 111	29600	12700	32000
PS B 8	38800	-	
PDMS RS	30000	-	29000

6. Discussion of results

As discussed in Chapter II, the dynamic viscosity $\eta'(\omega)$ and storage modulus $G'(\omega)$ are related to the viscosity and normal stress difference $p_{11} - p_{22}$ during steady shear flow (Eqs (II. 9) and (II. 10)). The two viscosities will be compared in Chapter VI; $G'(\omega)$ and $p_{11} - p_{22}$ will be compared in Chapter VIII.

Another comparison between (molecular) theory and experiment is possible, if the molecular weight distribution of the polymer is known. Experimental values of $G'_r(\omega)$ and $G''_r(\omega)$ are compared with calculated ones in Figs 16 and 17. Fig. 16 gives a dilute solution, 0.2 % B 200 in B 1. The symbols have the same meaning as in Fig. 4, the dashed lines were calculated from Eqs (II. 47), (II. 43) and (II. 44), using the molecular weight distribution given in Chapter III. 2.

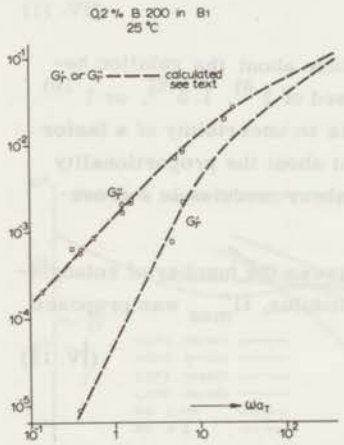

Fig. 16

The same comparison is given in Fig. 17 for the melt PS S 111, with experimental points as in Fig. 8, the dashed lines were calculated from Eq. (II. 47), (II. 49) and (II. 50), with the molecular weight distribution from Chapter III. 2. The agreement between calculated and experimental results is satisfactory.

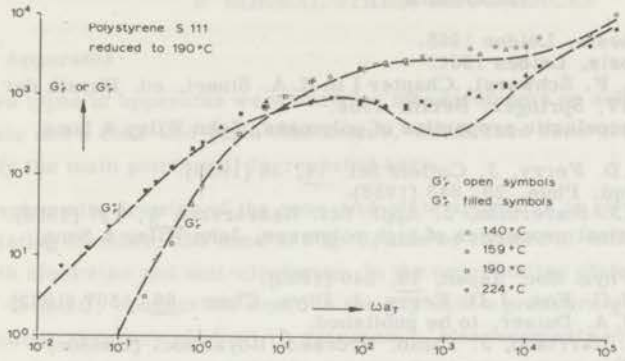

Fig. 17. G'_r and G''_r calculated from Eqs (II. 47) - (II. 50), with M_e=30.000.

According to the extension of the Rouse theory movements of a polymer chain, in concentrated solutions or melts, can be described by an enhanced friction factor. This would mean, that for a number of solutions of the same polymer, to a first approximation the maximum relaxation time τ_m will be proportional to the total viscosity (zero shear viscosity) of the solution. In Fig. 18 log τ_m is plotted as a function of log η_o (zero shear viscosity). The experimental points are in fair agreement with a line of slope 1.

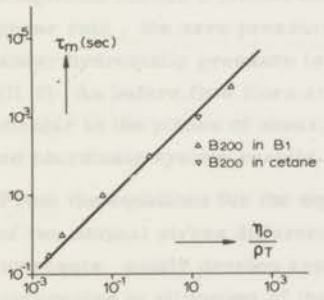

Fig. 18

Literature

1. J.A. Duiser, Thesis, Leiden 1965.
2. P. Dekking, Thesis, Leiden 1961.
3. A.J. Staverman, F. Schwarzl, Chapter I in H.A. Stuart, ed. Physik der Hochpolymeren IV, Springer, Berlin 1956.
4. J.D. Ferry, Viscoelastic properties of polymers, John Wiley & Sons, New York 1961.
5. K. Ninomiya, J.D. Ferry, J. Colloid Sci. 14, 36 (1959).
6. H. Fujita, J. Appl. Phys. 29, 943 (1958).
7. F. Schwarzl, A.J. Staverman, J. Appl. Sci. Research A 4, 127 (1953).
8. F. Bueche, Physical properties of high polymers, John Wiley & Sons, New York 1962.
9. S. Hayashi, J. Phys. Soc. Japan, 18, 249 (1963).
10. H. Markovitz, T.G. Fox, J.D. Ferry, J. Phys. Chem. 66, 1567 (1962).
11. A.J. Chömpff, J.A. Duiser, to be published.
12. A.J. Barlow, G. Harrison, J. Lamb, Proceed. Royal Soc. (London) A 282, 228 (1964).
13. R.S. Marvin, in J.T. Bergen, ed., Viscoelasticity, Academic Press, New York 1960, page 109.
14. W.L. Peticolas, Rubber Chem. and Tech. 36, 1422 (1963).
15. V.R. Allen, T.G. Fox, J. Chem. Phys. 41, 337 (1964).
16. R.S. Porter, J.F. Johnson, Chem. Reviews 66, 1 (1966).
17. J.L. den Otter, J.L.S. Wales, TNO-Reports CL/65/57 and CL/66/11.
18. J.L. den Otter, TNO-Report CL/66/25.
19. W. Philippoff, Chapter 7 in Physical Acoustics, Vol. 2 B, Academic Press, New York 1965.
20. T.G. Fox, P.J. Flory, J. Phys. Chem. 55, 221 (1951).

V NORMAL STRESS DIFFERENCES

1. Apparatus

Two types of apparatus were used for measurements on solutions: a parallel plate and a cone-and-plate viscometer, which have been described before[1], only the main points will be repeated here.

A schematic drawing of the cone-and-plate apparatus is given in Fig. 1. The rotating member, the cone in Fig. 1, can be rotated at different speeds, both clockwise and anti-clockwise. In the non-rotating plate three small holes, A, B and C, connect the liquid in the gap with a pressure gauge, with an estimated accuracy of about 10 dynes/cm^2. Measurements at different positions in the gap are possible by moving the bottom plate in Fig. 1, as indicated by arrows.

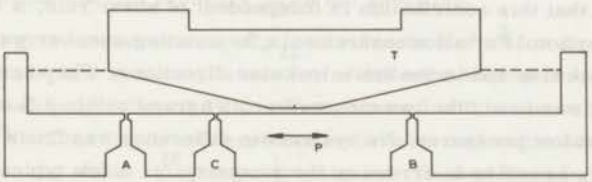

Fig. 1

Pressures are measured by balancing them against a gas pressure of known magnitude across a membrane[1]. Before and after the experiment, at zero shear rate, the zero pressure is checked. This means, in effect, that the zero shear hydrostatic pressure is subtracted, so that p_{22} is measured (see Eq. (II. 3). As before, flow lines are in the 1-direction, the 2-direction is perpendicular to the planes of shear, the 3-direction is chosen so that a right-handed coordinate system results.

From the equations for the equilibrium of forces (see Chapter II), functions of two normal stress differences can be obtained[1)2)3)]. Normal stress measurements easily develop systematic errors, for instance as a result of inaccuracies in alignment of the apparatus[1)3)]. A few other sources of systematic errors were also investigated in Sections 2 and 3.

Most measurements described in this chapter were performed with an apparatus kindly made available by Dr. A. S. Lodge, at the University of Man-

chester, College of Science and Technology. With this apparatus measurements are performed at temperatures near room temperature, on liquids having viscosities not exceeding 10^3 poise and with low volatility. The resulting choice of experimental liquids has been explained in Chapter III. Five liquids were investigated: three solutions of polyisobutene B 200 in B 1 with concentrations of 0.2, 1.03 and 2 volume per cent.; a solution of 15 g/100 ml of polystyrene III in bromobenzene; and a Newtonian oil, polyisobutene B 1.

The hydrostatic pressure $\bar{p}$ depends partly on the surface tension of the liquid. According to calculations of Slattery[5], the contribution of surface tension to $\bar{p}$ will be about $2\sigma/R_{cp}$ for a cone-and-plate apparatus, and σ/R_{pp} for a parallel plate apparatus. R_{cp} or R_{pp} is here the radius of the apparatus, σ is the surface tension of the liquid. For a 0.2 % solution of B200 in B1, a value of about σ = 30 dynes/cm was estimated by a capillary rise method. This would give a contribution to $\bar{p}$ of 14 dyne/cm^2 for the cone-and-plate, and 7 dyne/cm^2 for the parallel plate apparatus, a small effect. Moreover, it is only assumed that this contribution is independent of shear rate, a very reasonable assumption. For all measurements, the rotating member was rotated both in the clockwise and in the anti-clockwise directions. The average of the two pressures was used, the two measurements agreed within 3 % or within 10 dyne/cm^2 at low pressures. No systematic difference was found (this difference is very sensitive to errors in the geometry[3]). A few typical results will be given in Sections 4 and 5.

Before each set of measurements the apparatus was lined up, so that the gap angle in the cone-and-plate system was constant within $\pm$ 0.001 radians, or about 1 %. The distance between plates in the parallel plate system was constant during rotation to within better than 1 %.

The temperature was kept at 25 °C $\pm$ 0.1 °C by means of a thermostat, the room temperature was 25 °C $\pm$ 1 °C.

The radii R_{cp} and R_{pp} were both 4.40 cm, the gap angles of the cones used were 0.0565 and 0.0912 radians.

In later sections, the index pp refers to parallel plate measurements, cp refers to cone-and-plate measurements.

In addition to measurements on solutions, a few recovery experiments on the polymer melt pdms RS are given in Section 5.

2. Inertial forces

The effect of inertial forces on pressures in the parallel plate system has been calculated by Greensmith and Rivlin[3], who get the approximate formula:

$$p'(r) = \frac{1}{6}\,\omega^2\,\rho(r^2 - R_{pp}^2) + p_R \qquad (V.1)$$

$p'(r)$ is the pressure change due to inertial forces

ρ is the density of the liquid

ω is the speed of rotation in rad/sec

r is the distance from the axis of rotation.

By a more exact calculation, Kaye[4] obtained the result:

$$p'(r) = \frac{3}{20}\,\rho\,\omega^2(r^2 - R^2) + p_R \qquad (V.2)$$

Eq. (V. 2) is valid for both the cone-and-plate and the parallel plate system. In both equations the rim pressure p_R is not specified.

Figs 2 and 3 give measurements of p_{22} as a function of r^2 for a parallel plate and a cone-and-plate system at a number of different values of ω. The material chosen was polyisobutene B 1, a Newtonian oil with a viscosity of 0. 236 poise at 25 °C. This liquid was expected to have no noticeable normal stress differences in the shear rate range investigated. Dashed lines in Figs 2 and 3 give pressures calculated from Eq. (V. 2). The agreement between experimental and calculated values in reasonable. At higher speeds, $\omega > 10$ rad/sec, p_R is no longer equal to zero, probably as a result of radial flow in the gap. At lower speeds, $\omega < 10$ rad/sec, p_R is zero.

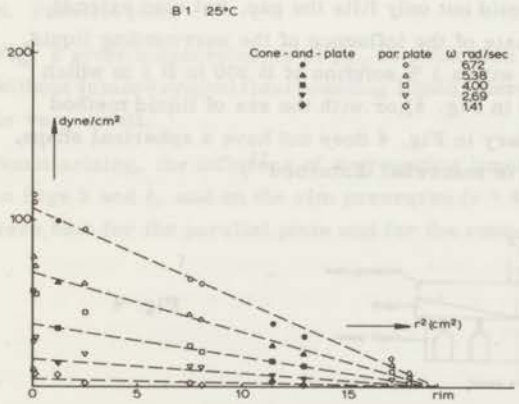

Fig. 2

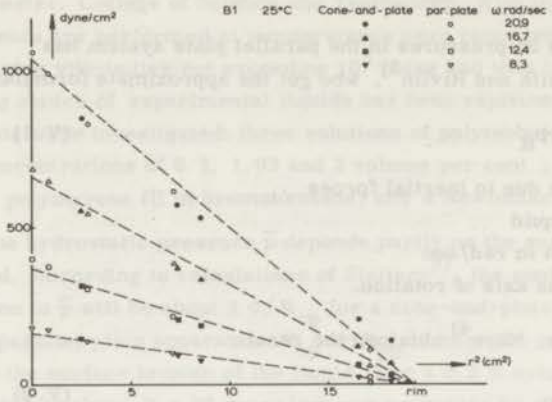

Fig. 3

In the following sections, corrections for inertial forces were applied in those cases, where the correction would be larger than 1 %. This meant, that in the experimental shear rate range, no corrections were necessary for the 1.03 % and 2 % solutions. For the 0.2 % and 15 % solutions the corrections were fairly large. As the procedure for inertial corrections is only justified if the correction is small, the measurements on the last two solutions will be less accurate than those on the 1.03 % and 2 % solutions.

For all measurements p_R was assumed to be zero ($\omega < 10$ rad/sec).

3. Influence of surrounding liquid.

All measurements in Sections 4 and 5 were done with the sea of liquid method, as shown in Fig. 1. Here the liquid not only fills the gap, but also extends beyond the gap. To get an estimate of the influence of the surrounding liquid, some measurements were done with a 1 % solution of B 200 in B 1 in which the liquid filled the gap only (as in Fig. 4),or with the sea of liquid method (as in Fig. 1). The liquid boundary in Fig. 4 does not have a spherical shape, so that the flow at the boundary is somewhat disturbed[1)].

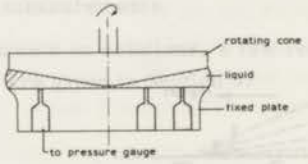

Fig. 4

A. Cone-and-plate

Fig. 5 gives p_{22} as a function of log r both with (open symbols)and without (filled symbols) surrounding liquid for the indicated rates of shear. It is usual to plot p_{22} as a function of log r, this is advantageous because as a result of the constant shear rate in the cone-and-plate apparatus a straight line can be expected (see Sec. 5). This is not the case with parallel plate measurements, because here the shear rate in the gap is not constant (see Sec. 4). The agreement between the two sets of measurements is quite good, which indicates that surrounding liquid has very little influence on p_{22} in this case. Moreover, adding small amounts of liquid,which changes the shape of the liquid-air boundary slightly, had no influence on pressures measured near the rim.

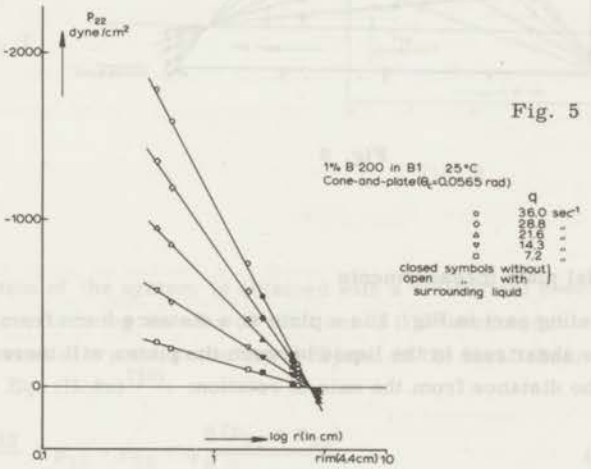

Fig. 5

B. Parallel plate

Fig. 6 gives measurements of p_{22} as a function of r with (open symbols) or without (closed symbols)surrounding liquid. Here also,the difference is zero or very small.

Summarizing, the influence of surrounding liquid on the slopes of the lines in Figs 5 and 6, and on the rim pressures (r = 4.4 cm), is very small or zero,both for the parallel plate and for the cone-and-plate systems.

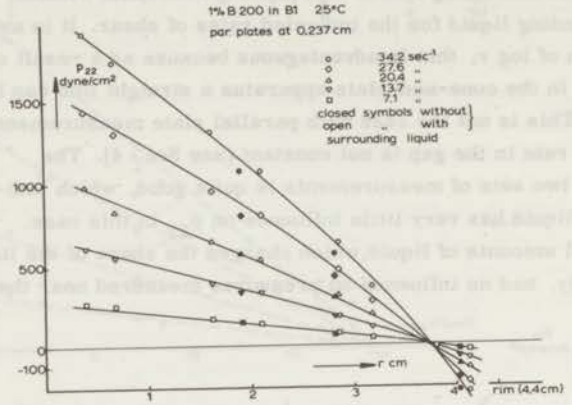

Fig. 6

4. Parallel plate measurements

If the rotating part in Fig. 1 is a plate at a distance h cm from the lower plate, the shear rate in the liquid between the plates will increase linearly with r, the distance from the axis of rotation:

$$q = \frac{\omega r}{h} \qquad (V.3)$$

ω is the speed of rotation of the upper plate.

The alignment of the apparatus was checked by rotating the upper plate clockwise and anti-clockwise. Two typical sets of measurements, given in Fig. 7 (O clockwise: Δ anti-clockwise), are in very good agreement.

In Figs 7 and 8 (for the 2 % solution of B 200 in B 1, values of $p_{22}(r)$ are plotted as a function of r. The relationship is non-linear in all cases. The lines giving $p_{22}(r)$ as a function of r at different values of ω, all concur at one point, at a value of p_{22} of about zero, and at r is about 3.9 cm. Values of p_{22} at the rim, r = 4.4 cm, are all positive. According to the results in the preceding sections, this cannot be attributed to the surrounding liquid or to inertial effects.

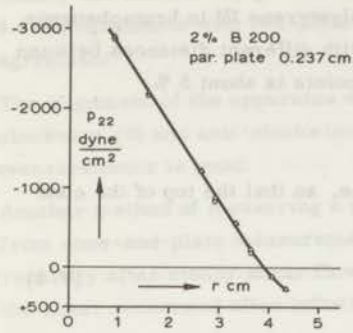

Fig. 7

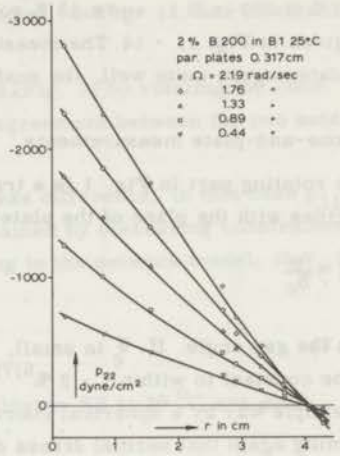

Fig. 8

A simple description of the system is obtained with a cylindrical coordinate system, the z-axis being the axis of rotation. If it is assumed that normal stress differences at a point in the liquid depend on the local shear rate only, we get from Eq. (II. 4a)[7)9)]:

$$\Delta_{pp} = r \frac{\partial p_{22}}{\partial r} = p_{11} - p_{33} + q \frac{\partial (p_{22} - p_{33})}{\partial q} \qquad (V.4)$$

From the slopes of the lines in Figs 7 and 8 the combination of normal stresses ,given in Eq. (V. 4),can be determined at the local shear rate given by Eq. (V. 3). As measuring slopes is not very accurate in principle, an alternative determination of Δ_{pp} due to Markovitz and Brown[2)] was also used. These authors use the relation:

$$\Delta_{pp}(r) = [p_{22}(r) - p_{22}(0)] \frac{\partial [\log p_{22}(r) - p_{22}(0)]}{\partial (\log q)} \qquad (V.5)$$

where $p_{22}(0)$ is de value of p_{22} at the axis of rotation. Using Eq. (V. 5), values of Δ_{pp} as a function of q were obtained, which were in excellent agreement(within 2 %) with those obtained from Eq. (V. 4).

The parallel plate results of Δ_{pp} for the solutions investigated, 0.2, 1.03 and 2 % B 200 in B 1, and a 15 % solution of polystyrene III in bromobenzene, are given in Figs 11 - 14. The measurements with different distances between the plates agree quite well, the scatter of the points is about 5 %.

5. Cone-and-plate measurements

If the rotating part in Fig. 1 is a truncated cone, so that the top of the cone coincides with the plane of the plate, q will be:

$$q = \frac{\omega}{\theta_c} \qquad (V.6)$$

θ_c is the gap angle. If θ_c is small, as in this case, the shear rate in the gap will be constant to within 1 - 2 %[6)7)]. The forces in the liquid can be described in a simple way by a spherical coordinate system. Eq. (II.5) gives then, assuming again that normal stress differences at a point depend on the local shear rate only[7)9)]:

$$\Delta_{cp} = \frac{\partial\ p_{22}}{\partial \ln r} = p_{11} + p_{22} - 2\,p_{33} \qquad (V.7)$$

According to Eq. (V.7), $p_{22}(r)$ plotted as a function of log r, will give a straight line for cone-and-plate measurements, because q is constant in the gap. In Figs 9 and 10 this is done for the 2 % solution of B 200 in B 1.

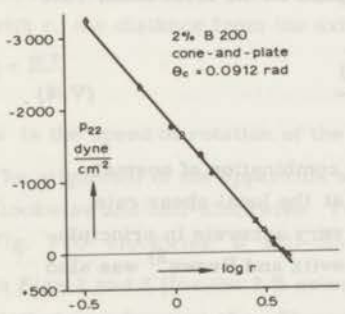

Fig. 9

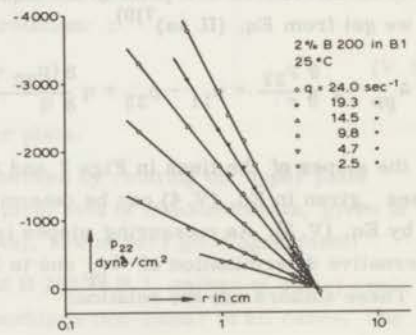

Fig. 10

It is clear that the lines are straight down to the lowest values of r (0.25 cm). Also it appears that the lines for different shear rates cross at a value of r = 3.9 cm and p_{22} about zero. Using Eqs (V.6) and (V.7), Δ_{cp} can be deter-

mined, the results are given in Figs 11 to 14 for the same solutions as in Sec. 4. Measurements with two different cone angles, in Fig. 12, are in excellent agreement.

The alignment of the apparatus was checked (Fig. 9) by rotating the cone clockwise (0) and anti-clockwise (Δ). The agreement between the two sets of measurements is good.

Another method of measuring a normal stress difference, in this case $p_{11}-p_{22}$, from cone-and-plate measurements, is obtained by measuring constrained recovery after steady shear flow. According to the network model, if γ_r is the shear recovered after infinite time[7]:

$$p_{11} - p_{22} = 2\, p_{12}\, \gamma_r \qquad (V.8)$$

In Table V.1 the results for polydimethylsiloxane RS at 20 °C are given.

Table V.1.

Constrained recovery of PDMS-RS after steady shear flow, 20 °C

q sec^{-1}	$2\, p_{12}\, \gamma_r$ $dyne/cm^2$
3.1×10^{-2}	6.9×10^2
3.6×10^{-2}	6.0×10^2
5.5×10^{-2}	7.5×10^2
6.7×10^{-2}	2.0×10^3
8.2×10^{-2}	1.5×10^3
0.118	2.7×10^3
0.17	6.0×10^3
0.24	6.5×10^3
0.55	2.0×10^4

The measurements were performed in a cone-and-plate viscometer, the angle over which the cone turned back after steady shear flow, was measured. The results will be compared with flow birefringence and dynamic measurements on the same material in Chapter VIII. 2.

The total force trying to separate the cone and plate during steady shear flow can also be used to estimate normal stress differences. As shown by Lodge[7], this measurement gives $p_{11} - p_{22}$. This method was not used in this investigation.

6. Rim pressures

The experimental values of p_{22} are positive at the rim for both parallel plate and cone-and-plate measurements. It was demonstrated in Secs 2 and 3 that this is not caused by inertial forces or by the surrounding liquid at the low speeds of rotation used. If it is assumed that p_{33} at the rim is zero (the pressure is equal to atmospheric pressure), then it follows that:

$$p_{22}\,(\text{rim}) = p_{22} - p_{33} \qquad (V.9)$$

This implies that the hydrostatic pressure $\bar{p}$ is independent of shear rate. Very few rim pressure measurements are given in the literature[1)8)]. In one case it was stated that rim pressures in the parallel plate system were zero[8)]. Inspection of the results given shows, however, that the small rim pressures reported in this chapter would not have been detected with those experiments, because no pressures near to the rim were actually measured.

All results are given in Figs 11 to 14. Rim pressures determined by cone-and-plate or by parallel plate measurements are in reasonable agreement. The large scatter is due to the low pressures involved, compared to an estimated overall accuracy of individual pressure measurements, about 10 dyne/cm^2. The extrapolation procedure is also a source of errors, the magnitude of which is difficult to estimate. Extrapolation of a straight line, for cone-and-plate measurements, is more accurate than extrapolation of a curve, for parallel plate measurements. For this reason, rim pressures determined by the cone-and-plate method are more reliable than those determined by the parallel plate method, which show larger scatter.

Especially parallel plate measurements for the 1.03 % B 200 solution, show a systematic shift to lower rim pressures as the distance between plates increases (Fig. 12). It seems likely that the flow at the rim will become more disturbed as the distance between plates increases. Measurements performed with the smallest distance between plates are in good agreement with cone-and-plate results, as expected. This is a strong indication that the assumptions used in Eq. (V.9) are justified.

7. Comparison of parallel plate and cone-and-plate results

In Figs 11- 14 all experimental values of Δ_{cp}, Δ_{pp} and rim pressures, Δ_{rim}, are combined. Δ_{pp} was obtained from Eqs (V.3) and (V.4) or (for the 0.2 % solution and for some results of the 1.03 % solution) Eq. (V.5). Measurements of Δ_{pp} at different distances between plates are in good agreement; use of Eq. (V.4) or (V.5) gave no noticeable difference. Values of Δ_{cp} from

cone-and-plate measurements, with gaps of different angles, are also in good agreement. All results in Figs 11 to 14 are well represented by straight lines on the log-log plot with slopes of 1.6-2.0 (0.2 % solution), 1.2 (1.03 % solution), 0.9 (2 % solution) and 1.6 (15 % solution). (The 0.2 % solution shows a change in slope from 1.6 to 2.0 at shear rates above 150 sec^{-1}.)

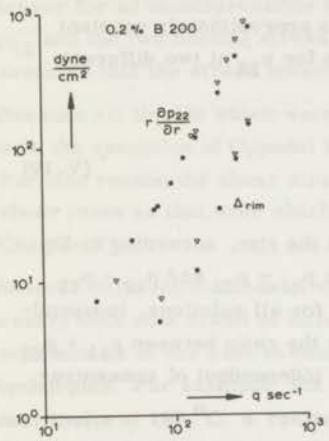

Fig. 11

• cone-and-plate, θ_c = 0.0565 rad
▽ par. plate at 0.0792 cm

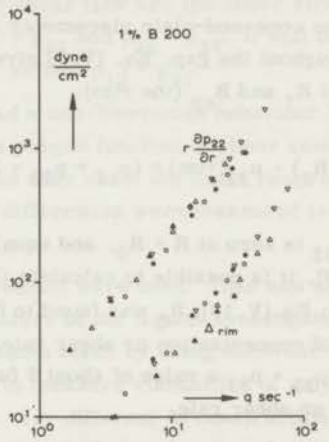

Fig. 12

cone-and-plate, ∘ θ_c = 0.0912 rad
• θ_c = 0.0565 rad
par. plate at 0.237 cm ▽
0.317 cm Δ
0.476 cm ▲

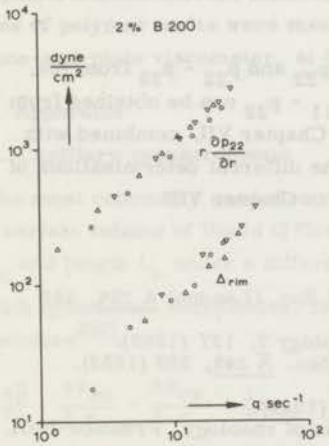

Fig. 13.

Meaning of symbols as in Fig. 12

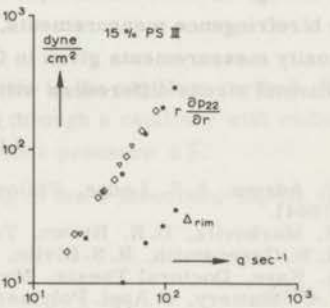

Fig. 14

Meaning of symbols as in Fig. 12
◇ par. plate at 0.1577 cm

As already shown in Sec. 6, the lines giving p_{22} as a function of log r for cone-and-plate measurements cross in one point, at r = 3.9 cm, with p_{22} zero. As the rim pressure is equal to $p_{22} - p_{33}$, and the slope Δ_{cp} is equal to $p_{11} - p_{22} + 2(p_{22} - p_{33})$, from Eq. (V.7), this concurrency gives a constant ratio between $p_{11} - p_{22}$ and $p_{22} - p_{33}$.

In the cone-and-plate viscometer the shear rate is approximately constant throughout the gap. Eq. (V.7) gives on integration for p_{22} at two different radii R_1 and R_{cp} (the rim):

$$p_{22}(R_1) - p_{22}(\text{rim}) = (p_{11} + p_{22} - 2\,p_{33}) \ln \frac{R_1}{R_{cp}} \qquad (V.10)$$

If p_{22} is zero at $R = R_0$, and equal to $p_{22} - p_{33}$ at the rim, according to Eq. (V.9), it is possible to calculate the ratio between $p_{11} - p_{22}$ and $p_{22} - p_{33}$ from Eq. (V.10); R_0 was found to be 3.8 - 3.9 cm for all solutions, independent of concentration or shear rate. This gives for the ratio between $p_{11} - p_{22}$ and $p_{22} - p_{33}$ a value of about 6 for all solutions, independent of concentration or shear rate.

Inertial corrections for the 0.2 % and 15 % solutions were very large, so that at the highest shear rates corrections to p_{22} near the axis of rotation were up to 50 % of the total value. As a result these measurements are less accurate than those for the 1 % and 2 % solutions, where inertial corrections were always smaller than 1 %.

It is possible to obtain other estimates of $p_{11} - p_{22}$ and $p_{22} - p_{33}$ from the data in Figs 11 to 14. An independent value of $p_{11} - p_{22}$ can be obtained from flow birefringence measurements, described in Chapter VII, combined with viscosity measurements given in Chapter VI. The different determinations of the normal stress differences will be discussed in Chapter VIII.

Literature

1. N. Adams, A.S. Lodge, Philos. Trans. Royal Soc. (London) A 256, 149 (1964).
2. H. Markovitz, D.R. Brown, Trans. Soc. Rheology 7, 137 (1963).
3. H.W. Greensmith, R.S. Rivlin, Trans. Royal Soc. A 245, 399 (1953).
4. A. Kaye, Doctoral Thesis, Manchester 1965.
5. J.C. Slattery, J. Appl. Polymer Sci. 8, 2631 (1964).
6. A.G. Fredrickson, Principles and applications of rheology, Prentice-Hall, Englewood Cliffs, 1964.
7. A.S. Lodge, Elastic liquids, Academic Press, London 1964.
8. T. Kotaka, M. Kurata, M. Tamura, J. Appl. Phys. 30, 1705 (1959).
9. B.D. Coleman, H. Markovitz, W. Noll, Viscometric flows of non-Newtonian fluids, Springer, Berlin 1966.

VI VISCOSITY MEASUREMENTS

1. Methods

As was pointed out in Chapter II, the interesting components of the stress tensor for an incompressible liquid in laminar shear flow are the shear stress p_{12} and the two normal stress differences $p_{11} - p_{22}$ and $p_{22} - p_{33}$. It will be assumed that the stress tensor is symmetric, so that $p_{12} = p_{21}$.

Because all liquids which were investigated had a non-Newtonian behaviour, with the exception of Oppanol B 1, p_{12} is not a simple function of shear rate. For this reason the shear stress was measured over about the same range of shear rates as that,over which normal stress differences were measured (see Chapter V).

Several different methods of viscosity measurement were used. This was necessary both as a result of differences in the nature of the liquids investigated, and because of the wish to compare measurements made by using different techniques. For example, the apparatus used to measure viscosities of polymer melts at 190 °C, a rectangular slit, was very different in construction from the apparatus used to measure the viscosity of dilute polymer solutions at 25 °C, a glass capillary. In the second case the forces can be a factor 10^6 smaller than in the first case. Often it is even necessary to use different types of viscometer for different shear rate ranges. For this reason viscosities of polymer melts were measured at low ($< 1\ \text{sec}^{-1}$) shear rates with a cone-and-plate viscometer, at higher shear rates rectangular slits were used.

2. Apparatus

A. Capillary measurements

The most commonly used viscosity measurement is the capillary method. Here a certain volume of liquid Q flows per second through a capillary with radius R_c and length L_c under a difference in hydrostatic pressure $\Delta \bar{p}$.

With cylindrical coordinates, the liquid flowing in the z-direction, Eq. (II. 4b) becomes[2)9)]:

$$-\frac{\partial \bar{p}}{\partial z} + \frac{\partial p_{zz}}{\partial z} + \frac{\partial p_{rz}}{\partial r} + \frac{1}{r} p_{rz} + F_z = 0 \qquad \text{(VI. 1)}$$

where p_{rz} is the shear stress,

r the distance from the z axis and

F_z is the volume force.

The assumption is made, that the flow is stationary along the length of the capillary. In that case $\partial p_{zz}/\partial z$ is zero, so that[2)9)]:

$$p_{rz}(r) = \frac{r}{2} \frac{\partial \bar{p}}{\partial z} \qquad \text{(VI. 2)}$$

For a capillary with zero length a pressure difference, the entrance effect, will still be necessary to maintain the flow. In order to obtain $\frac{\partial \bar{p}}{\partial z}$ from measurements of the change in $\Delta \bar{p}$ with increasing capillary length, the entrance effect must be subtracted. If the capillary is sufficiently long, the entrance effect can be neglected, so that (VI. 2) becomes:

$$p_{rz}(r) = \frac{\Delta \bar{p}\, r}{2 L_c} \qquad \text{(VI. 2')}$$

Shear rates at the capillary wall were calculated by means of the well-known equation[1)2)]:

$$q(R_c) = \frac{Q}{\pi R_c^3} \left[3 + \frac{\partial (\ln Q)}{\partial (\ln \Delta \bar{p})} \right] \qquad \text{(VI. 3)}$$

All measurements on solutions were performed with an Ubbelohde viscometer, where a constant volume of liquid (3.030 ml) flowed under an adjustable gas pressure through a capillary with a length of 6.3 cm and radius 0.052 cm, in a measured time of t seconds. Inertial and entrance effects were neglected. The viscometer has been described in detail by Selier[3)]. All measurements were performed at a temperature of 25 $\pm$ 0.02 °C.

For the polymer melt pdms RS, measurements were performed with capillaries of different lengths and diameters of 0.250 cm. Inertial corrections were neglected, but the entrance effect was subtracted. The output of the capillary was measured by weighing the extrudate, $\Delta \bar{p}$ was measured with precision manometers, accurate to better than 5 % of the measured pressure.

B. Cone-and-plate viscometer

The liquid is held between a cone and a plate, which rotate relative to each other around a common axis. The apex of the cone coincides with the plane of the plate. Assuming laminar flow in the liquid, the torsion on the cone or plate is given by[2)9)]:

$$M_{cp} = \frac{2}{3} \pi R_{cp}^3 p_{12} \qquad \text{(VI. 4)}$$

If the gap angle is small (less than about 10°), the shear rate in the gap is constant (see the discussion in Chapters II and V) and given by:

$$q = \frac{\omega}{\theta_c} \qquad \text{(VI. 5)}$$

ω is the angular velocity of the cone relative to the plate.
θ_c is the gap angle.

The cone-and-plate viscometer used for viscosity measurements was a modified commercial apparatus, supplied by Farol Research Engineers, Bognor Regis, England. All measurements were performed at 25 $\pm$ 0.5 °C. The cone angle θ_c was 2°6', R_{cp} was 3.00 cm.

C. Slit measurements

Viscosities of all polymer melts were measured by means of rectangular slits. The procedure has been described in the literature[5], where it was shown that viscosities obtained this way are in good agreement with those obtained by using capillaries. The velocity profiles of polymer melts flowing through a slit, were also found to be in good agreement with those calculated from the flow curve[10]:

If b is the width of the slit, d the depth and L_s the length, the following equations were obtained, with the same assumptions as for capillary measurements[5)8)], if b >> d:

$$p_{12}(w) = \frac{\Delta \bar{p}}{2 L_s d} \qquad \text{(VI. 6)}$$

$$q(w) = \frac{2Q}{bd^2} \left[2 + \frac{\partial(\ln Q)}{\partial(\ln \Delta \bar{p})}\right] \qquad \text{(VI. 7)}$$

Q and $\Delta \bar{p}$ have the same meaning as for the capillary measurements; $p_{12}(w)$ and $q(w)$ indicate shear stress and shear rate at the wall along the long side of the slit. The slit consists of a rectangular channel, with a length of 10 cm, width of 1 cm and depth of 0.1 cm, with a width-depth ratio of 10. In the long side of the slit electronic pressure gauges were mounted at two different distances from the entrance.

Measurements were performed at temperatures up to 220 °C, the temperature was kept constant to $\pm$ 1 °C.

3. Measurements

A typical example of a measurement of the output of a capillary as a function of the shear stress at the wall is given in Fig. 1 for a 15 % solution of polystyrene III in bromobenzene. The shear stress at the wall was calculated from Eq. (VI. 2'). The slope of the curve through the experimental points was then determined. From this the shear rate at the wall could be determined, using Eq. (VI. 3).

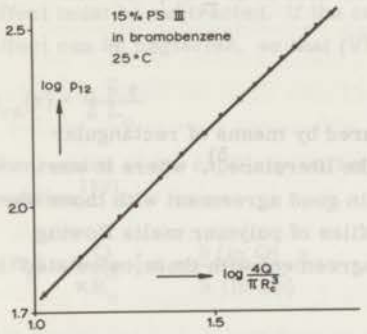

Fig. 1

Fig. 2 gives a typical example of the pressures measured along the length of a rectangular slit, b = 1.0 cm, d = 0.10 cm, for the molten high density polyethylene HDPE-NMWD at 146 °C and 190 °C, at the output indicated in the figure. The shear stress was calculated from Eq. (VI. 6). By plotting the output against shear stress as in Fig. 1, and measuring the slope, the shear rate at the wall was calculated according to Eq. (VI. 7).

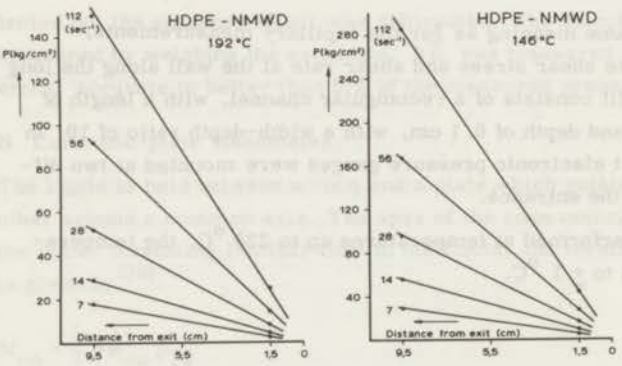

Fig. 2

In Figs 3 to 11 viscosity measurements are given for the materials investigated. In Fig. 3, $\eta(q) = p_{12}/q$, as a function of shear rate, is given for the solutions of polyisobutene B 200 in B 1 at 25 °C. Comparison of capillary and cone-and-plate measurements for the 2 % solution shows, that they are in excellent agreement.

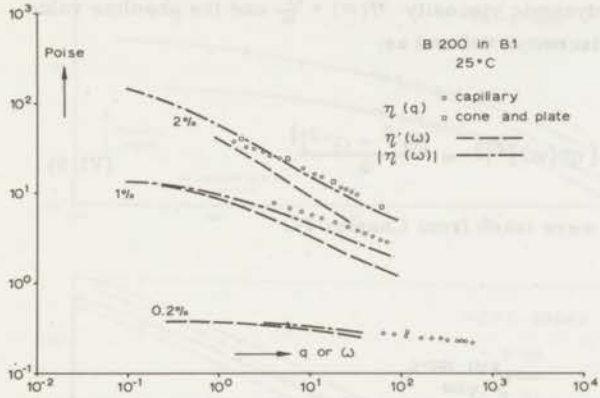

Fig. 3

In Fig. 4 the viscosity at 25 °C is given for the solutions of polystyrene III in bromobenzene, all measurements were performed with a capillary of length/radius ratio 121. Measurements on polymer melts are given in Figs 5 to 11.

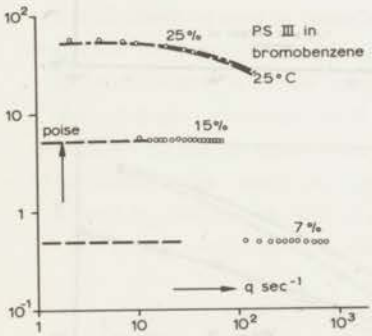

Fig. 4

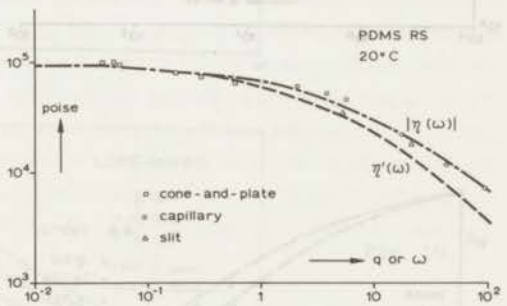

Fig. 5

All measurements were performed with rectangular slits, except for polydimethylsiloxane RS, in Fig. 5, where capillary measurements are indicated by circles, and cone-and-plate measurements by squares. The measurements are in fair agreement with slit measurements, triangles on the same material.

In Figs 3 to 11, also the dynamic viscosity $\eta'(\omega) = \frac{G''}{\omega}$ and the absolute value of the complex dynamic viscosity, defined as:

$$|\eta(\omega)| = \{[\eta'(\omega)]^2 + [\eta''(\omega)]^2\}^{\frac{1}{2}} = \frac{[G'^2 + G''^2]^{\frac{1}{2}}}{\omega} \qquad \text{(VI. 9)}$$

are given. These results were taken from Chapter IV.

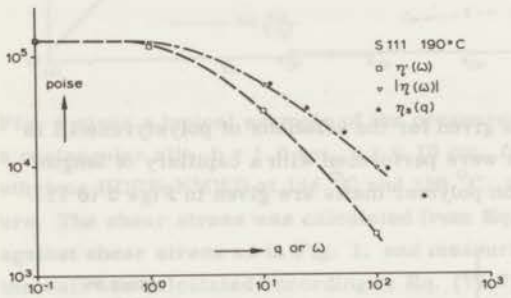

Fig. 6

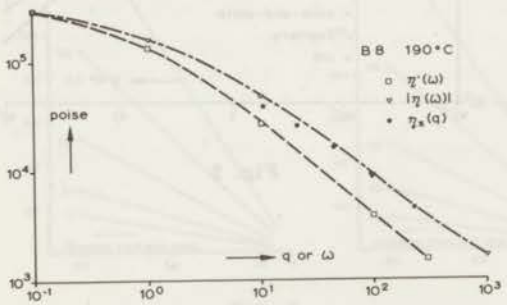

Fig. 7

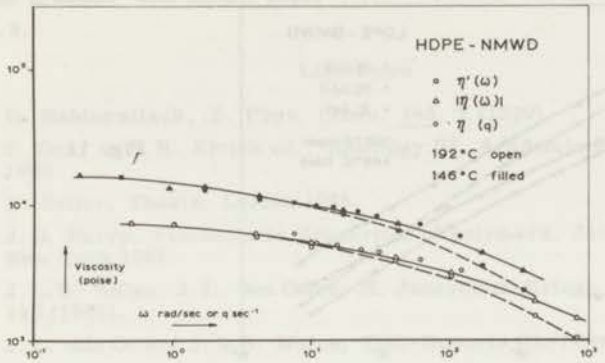

Fig. 8

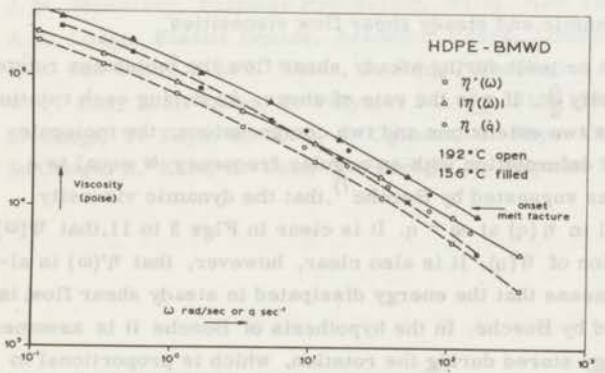

Fig. 9

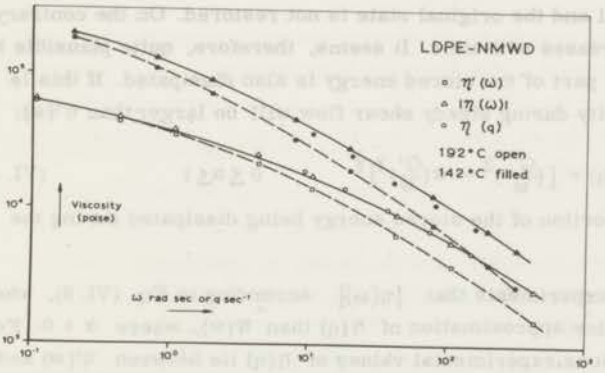

Fig. 10

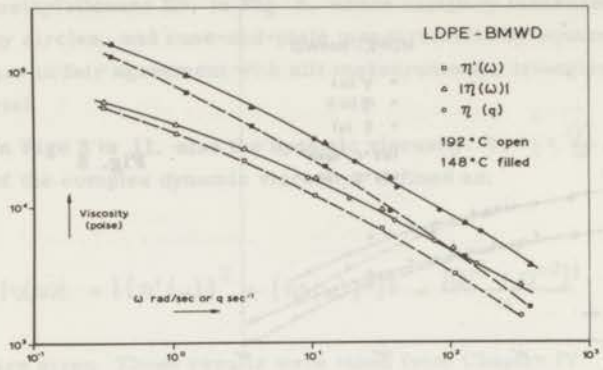

Fig. 11

4. Comparison of dynamic and steady shear flow viscosities

In a polymer solution or melt during steady shear flow, the molecules rotate with an angular velocity $\frac{q}{2}$, if q is the rate of shear. As during each rotation a molecule undergoes two extensions and two compressions, the molecule undergoes a periodic deformation with an angular frequency ω equal to q. For this reason it was suggested by Bueche[7], that the dynamic viscosity $\eta'(\omega)$ should be equal to $\eta(q)$ at $\omega = q$. It is clear in Figs 3 to 11, that $\eta'(\omega)$ is a fair approximation of $\eta(q)$. It is also clear, however, that $\eta'(\omega)$ is always too low. This means that the energy dissipated in steady shear flow, is larger than estimated by Bueche. In the hypothesis of Bueche it is assumed that the elastic energy stored during the rotation, which is proportional to $G'(\omega)$, is not dissipated. During steady shear flow, however, the deformation is not sinusoidal and the original state is not restored. On the contrary, the deformation increases with time. It seems, therefore, quite plausible to assume that at least part of the stored energy is also dissipated. If this is the case, the viscosity during steady shear flow will be larger than $\eta'(\omega)$:

$$\eta(q) = \left[\left(\frac{G''}{\omega}\right)^2 + \alpha\left(\frac{G'}{\omega}\right)^2\right]^{\frac{1}{2}} \qquad 0 \leq \alpha \leq 1 \qquad \text{(VI. 10)}$$

where α is the proportion of the stored energy being dissipated during the flow.

It is clear from the experiments that $|\eta(\omega)|$ according to Eq. (VI. 9), where $\alpha = 1$, is a much better approximation of $\eta(q)$ than $\eta'(\omega)$, where $\alpha = 0$. For both melts and solutions, experimental values of $\eta(q)$ lie between $\eta'(\omega)$ and $|\eta(\omega)|$, but are nearer the latter, as was also found by several authors (Cox

Merz[11], Onogi et al[12)13)]). An alternative explanation of the agreement between dynamic and steady shear viscosities will be discussed in Chapter VIII. 3.

Literature

1. B. Rabinowitsch, Z. Phys. Chem. 145, 1 (1929).
2. S. Oka, in F.R. Eirich ed., Rheology III, Academic Press, New York 1960.
3. P. Selier, Thesis, Leiden 1965.
4. J.D. Ferry, Viscoelastic properties of polymers, John Wiley and Sons, New York 1961.
5. J.L.S. Wales, J.L. den Otter, H. Janeschitz-Kriegl, Rheologica Acta 4, 146 (1965).
6. J.L. den Otter, J.L.S. Wales, TNO-Reports CL/66/11 and CL/65/57.
7. F. Bueche, Physical properties of polymers, Interscience, New York 1962.
8. J.M. McKelvey, Polymer Processing, Wiley, New York 1962.
9. A.S. Lodge, Elastic liquids, Academic Press, London 1964.
10. J.L. den Otter, J.L.S. Wales, J. Schijf, Rheologica Acta 6, 205 (1967).
11. W.P. Cox, E.H. Merz, J. Polymer Sci. 28, 619 (1958).
12. S. Onogi, T. Fujii, H. Kato, S. Ogihara, J. Phys. Chem. 68, 1598 (1964).
13. S. Onogi, H. Kato, S. Ueki, T. Ibaragi, J. Polymer Sci. C 15, 481 (1966).

VII FLOW BIREFRINGENCE

1. General remarks

A polymer molecule in a velocity field will in general be both oriented and deformed. If the average polarizability of a segment parallel to the chain α_1 is different from that perpendicular to the chain α_2, the polymers will cause optical anisotropy during flow, flow birefringence. This provides a very important means to study the shape and the orientation of polymer molecules in steady shear flow. In Chapter II it was shown that according to the theory of rubber-elasticity, a simple relationship exists between the difference of the two main axes of the index of refraction ellipse Δn, the sharp orientation angle χ of one of the main axes with the flow lines, and components of the stress tensor. The proportionality factor, C, was defined by Eq. (II.22). In this chapter only the case where the average polarizability of the chain is equal to that of the solvent, will be considered. It is customary to call birefringence positive, when $\alpha_1 > \alpha_2$, and negative in the other case. The stress optical coefficient C can in principle be obtained from Eq. (II.22), if $\alpha_1 - \alpha_2$ is known for the polymer. In this investigation C was obtained from:

$$C = \frac{\Delta n \sin 2\chi}{2 p_{12}} \qquad \text{(VII. 1)}$$

where p_{12} is the contribution of the polymer to the shear stress. Eq. (VII. 1) follows directly from (II. 74), (II. 77) and (II. 78).

Using Eq. (II. 75), (II. 77) and (II. 78) it can be shown that:

$$p_{11} - p_{12} = \frac{\Delta n}{C} \cos 2\chi \qquad \text{(VII. 2)}$$

The last equation is the reason of our interest in flow birefringence, because it gives an independent method for the determination of $p_{11} - p_{22}$. A very important point when using Eq. (VII. 2) is, that C must be independent of shear rate q. This was investigated in each case, by plotting C as obtained from (VII. 1) as a function of q (see Sec. 3).

2. Apparatus

The apparatus used for solutions was a concentric cylinder viscometer, which has been developed by Dr. H. Janeschitz-Kriegl[1]. Only the main points will be repeated here.

The liquid is sheared in a narrow gap of 0.025 cm between two concentric cylinders. The inner cylinder has a radius R_i of 2.50 cm, and is rotated with

an angular velocity of ω rad/sec. The shear rate in the liquid q is given by:

$$q = \frac{\omega R_i}{R_u - R_i} \qquad \text{(VII. 3)}$$

where R_u is the radius of the outer cylinder, and $R_u - R_i$ is small compared to R_i. The lower limit in shear rate at which flow birefringence can be investigated is given by the accuracy of the optical measurement, for this apparatus $\Delta n = 1.5 \times 10^{-8}$. The upper limit of q is given by the onset of turbulence for dilute solutions.

At low values of Δn a de Sénarmont compensator was used, at higher values, ($\Delta n > 2 \times 10^{-7}$) an Ehringhaus compensator[1]. The orientation angle χ was measured by determining the position of maximum extinction between crossed nicols. All measurements were performed with the inner cylinder rotating both clockwise and anti-clockwise. The average of the two values, obtained in this way, was used. All measurements were performed at $25 \pm 0.1\ ^{\circ}C$.

Measurements on melts were performed in a cone-and-plate apparatus especially designed for this purpose by Dr. H. Janeschitz-Kriegl. The apparatus will be described elsewhere[10]. In this apparatus the material is held between a cone with a diameter of 5.0 cm and a flat plate, which are in relative rotation with an angular velocity of ω rad/sec. Subject to the same conditions as given in Chapter V (Eq. (V. 6)) the shear rate in the material is given by:

$$q = \frac{\omega}{\theta_c} \qquad \text{(VII. 4)}$$

where θ_c is the gap angle, here 0.0200 rad.

The light path is along the radial direction through the gap, and then, after reflection by a mirror, along the axis of rotation. Measurements of Δn and χ are performed in the same way as above. The range of shear rates is from 10^{-3} to 10^{2} sec^{-1}.

The wavelength of the light used in all measurements was 548 mμ.

In the concentric cylinder apparatus the light path is through the gap between the cylinders, parallel to the common axis of the cylinders. We set up a local cartesian coordinate system in the gap, according to the convention given in Chapter I. Then the flow lines are in the 1-direction, the radial direction is the 2-axis, and the light beam proceeds along the 3-axis. As a result, the index of refraction ellipse lies in the 1-2 plane.

In the cone-and-plate apparatus the light path is in radial direction. For a

local cartesian coordinate system the flow lines are in the 1-direction, the shear gradient is in the 2-direction, the light path is along the 3-direction. As before, the index of refraction ellipse lies in the 1-2 plane.

3. Measurements

In Fig. 1 the flow birefringence Δn as a function of shear rate q is given for solutions of polyisobutene B 200 and B 1 at 25 °C. Fig. 2 gives the same for the solutions of polystyrene III in bromobenzene at 25 °C, while data for the polymer melts polystyrene S 111, and B 8, polydimethylsiloxane RS, two high density polyethylenes and two low density polyethylenes are given in Fig. 3 at the temperatures indicated.

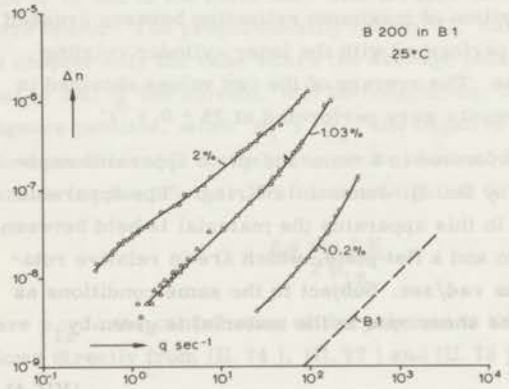

Fig. 1.

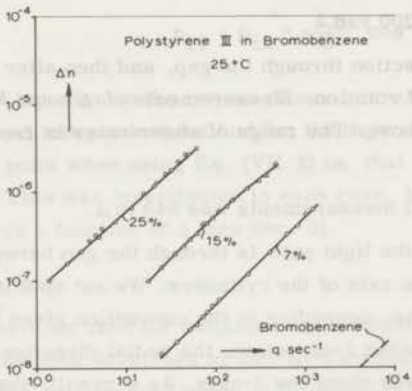

Fig. 2.

The extinction angle χ as a function of shear rate for the materials in Figs 1 to 3 with the same meaning for the symbols, is given in Figs 4 to 6.

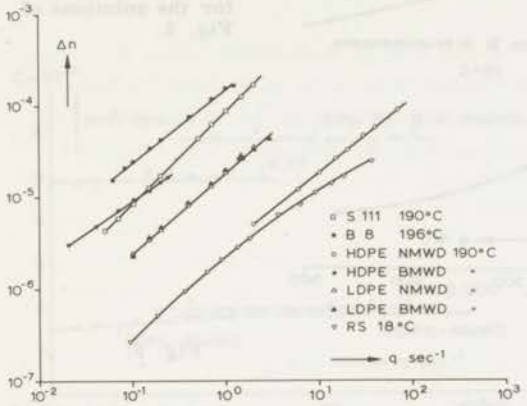

Fig. 3.

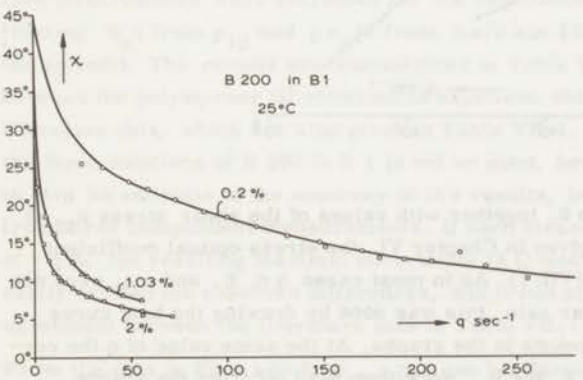

Fig. 4.

χ as a function of q for the solutions of Fig. 1.

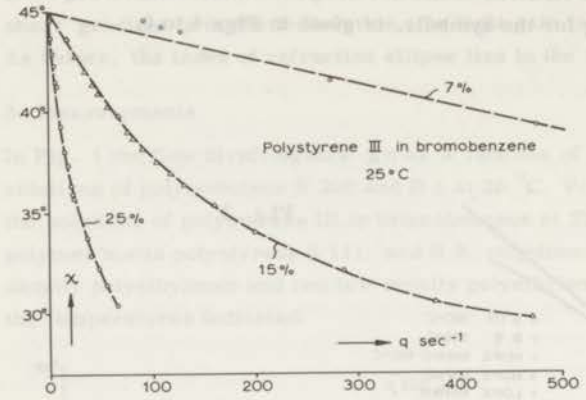

Fig. 5.

χ as a funtion of q for the solutions of Fig. 2.

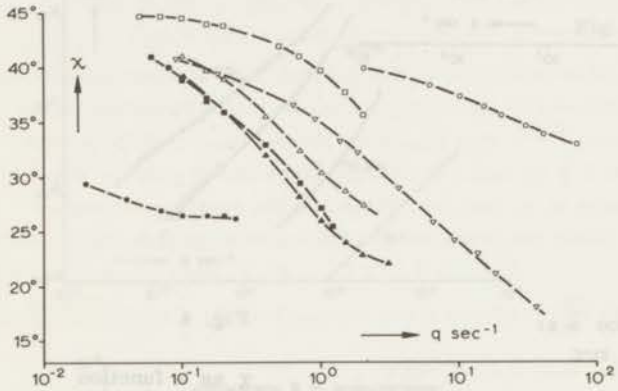

Fig. 6.

χ as a function of q for the melts of Fig. 3, the symbols have the same meaning as in Fig. 3.

From the data in Figs 1 to 6, together with values of the shear stress p_{12} at the same shear rate, as given in Chapter VI, the stress optical coefficient can be obtained from Eq. (VII. 1). As in most cases Δn, χ, and p_{12} were not measured at the same shear rate, this was done by drawing the best curve through the experimental points in the graphs. At the same value of q the corresponding results of Δn, χ and p_{12} were then read off from the graphs.

Some typical results are given in Fig. 7. According to the molecular theories discussed in Chapter II, the stress optical coefficient C should be independent of concentration and shear stress. Moreover, C must be inversely proportional to the absolute temperature according to Eq. (II. 22).

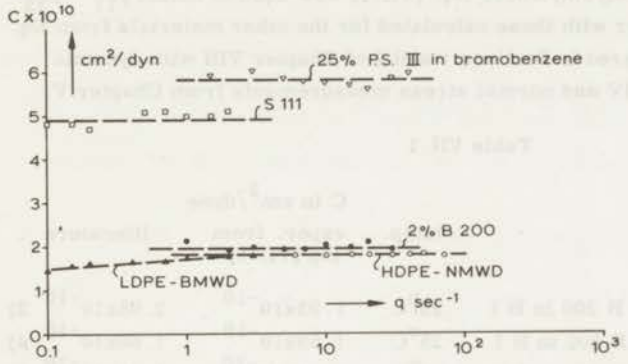

Fig. 7.

As shown in Fig. 7, C is independent of q for the polymers investigated, except for the low density polyethylenes. Where necessary, shear stress and flow birefringence were corrected for the contribution of the solvent, by subtracting $\eta_s q$ from p_{12} and $\Delta n_s/2$ from $\Delta n/2 \sin 2\chi$ (the index s indicates the solvent). The results are summarized in Table VII. 1. The agreement between the polystyrene III solutions is excellent; the results agree well with literature data, which are also given in Table VII. 1. The agreement between the three solutions of B 200 in B 1 is not so good, however. It is very difficult to give an estimate of the accuracy of the results, because C is calculated from three independent measurements. If each measurement has an accuracy of $\pm$ 5 %, the resulting maximal uncertainty in C would be $\pm$ 15 %. This can easily explain the observed differences, and it can also explain the very bad agreement between the literature data in Table VII. 1.

From the data in Figs 1 to 6, $p_{11} - p_{22}$ can be obtained by using Eq. (VII. 2). The solvent gives no contribution to $\Delta n \cos 2\chi$, so that Eq. (VII. 2) can be used without correction.

As the stress-optical coefficient for low density polyethylenes was found to increase with increasing shear rate (Fig. 7), Eq. (VII. 2) could not be used for these materials. However, if the assumption is made, that the orientation

of the stress tensor and the index of refraction ellipse remain the same, Eqs (VII. 1) and (VII. 2) give:

$$p_{11} - p_{22} = 2\, p_{12} \operatorname{ctn} 2\chi \qquad \text{(VII. 5)}$$

For the low density polyethylenes, Eq. (VII. 5) was used to obtain $p_{11} - p_{22}$. These values, together with those calculated for the other materials from Eq. (VII. 2), will be compared in Sections 1 and 2 of Chapter VIII with dynamic moduli from Chapter IV and normal stress measurements from Chapter V.

Table VII. 1

polymer	temp.	C in cm^2/dyne exper. from Eq. (VII. 1)	literature	
polyisobutene 0.2 % B 200 in B 1	25°C	1.93×10^{-10}	2.05×10^{-10}	2)
polyisobutene 1.03 % B 200 in B 1	25°C	1.59×10^{-10}	1.60×10^{-10}	4)
polyisobutene 2 % B 200 in B 1	25°C	1.97×10^{-10}	1.61×10^{-10}	6)
			1.55×10^{-10}	8)
polystyrene III 7 % in bromobenzene	25°C	-5.62×10^{-10}	-6.1×10^{-10}	2)
polystyrene III 15 % in bromobenzene	25°C	-5.41×10^{-10}	-6.80×10^{-10}	4)
polystyrene III 25 % in bromobenzene	25°C	-5.83×10^{-10}	-5.85×10^{-10}	5)
			-5.5×10^{-10}	6)
polystyrene S111	196°C	-4.89×10^{-10}	-3.95×10^{-10}	2)
polystyrene B 8	190°C	-3.63×10^{-10}	-3.99×10^{-10}	2)
polydimethylsiloxane RS	18°C	1.6×10^{-11}	1.96×10^{-11}	2)
polyethylene HDPE-NMWD	190°C	1.81×10^{-10}	1.31×10^{-10}	2)
			2×10^{-10}	7)

Literature

1. H. Janeschitz-Kriegl, Physica 22, 1197 (1956); J. Polymer Sci. 23, 181 (1957); Physica 24, 913 (1958); Rev. Sci. Instr. 31, 119 (1960); Laboratory Practice 10, 802 (1961).
2. V. N. Tsvetkov, Chapter XIV in B. Ke, ed., Newer methods of polymer characterization, Interscience, New York 1964.
3. A. Peterlin, Chapter XII in H. A. Stuart, ed., Die Physik der Hochpolymeren II, Springer, Berlin 1953.
4. W. Philippoff, J. Polymer Sci. C 5, 1 (1964).
5. H. Janeschitz-Kriegl, Makromol. Chem. 33, 55 (1959).
6. D. M. Bancroft, to be published.
7. D. W. Saunders, Trans. Faraday Soc. 52, 1414 (1956).

8. A. Kaye, D. W. Saunders, J. Sci. Instr. 41, 139 (1964).
9. J. L. S. Wales, H. Janeschitz-Kriegl, TNO-Report CL/66/43, 21st April 1966.
10. J. L. S. Wales, H. Janeschitz-Kriegl, to be published.

VIII CONCLUSIONS

1. Comparison between different determinations of the normal stress differences

Normal stress gradients and rim pressures were measured on four liquids: 0.2 %, 1 % and 2 % solutions of Oppanol B 200 in Oppanol B 1, and a 15 % solution of polystyrene III in bromobenzene (Chapter V). Viscosity (Chapter VI) and flow birefringence (Chapter VII) measurements were also performed on these liquids. The discussion in Sec. VIII. 1 will be limited to these four solutions, which will be indicated in the following by their concentrations only.

As discussed in Chapters II, V, and VII, the interpretation of the measurements is as follows[1)2)]:

cone-and-plate measurements (Eq. (V. 7))

$$\Delta_{cp} = r \frac{\partial p_{22}}{\partial r} = p_{11} - p_{22} + 2(p_{22} - p_{33}) \qquad \text{(VIII. 1)}$$

parallel plate (Eq. (V. 4))

$$\Delta_{pp} = r \frac{\partial p_{22}}{\partial r} = (p_{11} - p_{22}) + (p_{22} - p_{33}) + q \frac{\partial}{\partial q}(p_{22} - p_{33}) \qquad \text{(VIII. 2)}$$

both cone-and-plate and parallel plate rim pressures (Eq. (V. 9))

$$\Delta_{rim} = p_{22}(rim) = (p_{22} - p_{33}) \qquad \text{(VIII. 3)}$$

flow birefringence (Eq. (VII. 2))

$$\Delta_{opt} = \frac{\Delta n}{C} \cos 2\chi = (p_{11} - p_{22}) \qquad \text{(VIII. 4)}$$

recovery (Eq. (V. 8))

$$2 \gamma_r p_{12} = (p_{11} - p_{22}) \qquad \text{(VIII. 5)}$$

As recovery is very difficult to measure on dilute solutions, and, moreover, its interpretation is uncertain, these measurements were not performed on the four solutions discussed in this section, so that we have four equations to determine $p_{11} - p_{22}$ and $p_{22} - p_{33}$. A few measurements on the melt PDMS RS will be discussed in Sec. VIII. 2.

Eqs (VIII. 1) to (VIII. 5) have been obtained, subject to the following conditions 1)2):

A. the flow is steady shear flow, secondary flow is neglected (see Chapters

II and V);

B. the normal stress differences at a point in the liquid depend on the local shear rate only (so that the rheological equation of state does not contain spatial derivatives of the metric tensor[1]);

C. the stress tensor is symmetric (see Chapter II).

For (VIII. 4) only, an additional condition is that the stress optical coefficient C is a constant. For a discussion on (VIII. 3) and (VIII. 5) see Chapter V.

In Fig. 1 experimental results from Chapters V, VI and VII are combined for all four solutions.

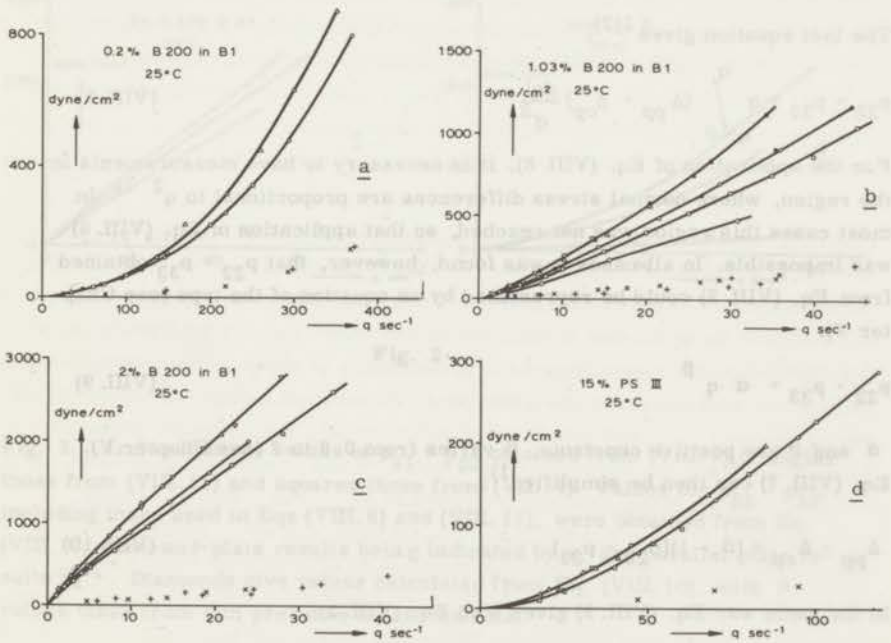

Fig. 1

Circles indicate Δ_{cp}, squares Δ_{opt} and triangles Δ_{pp}. Rim pressures from cone-and-plate measurements are indicated by x, from parallel plate measurements by +.

As discussed in Chapter V, it is clear that Δ_{cp} obtained with different cones and Δ_{pp} obtained with different distances between plates are each in excellent agreement. Measurements of $p_{22} - p_{33}$ obtained from rim pressures show a rather large scatter, due to the very small pressures that had to be measured, but they are in fair agreement.

In principle, any normal stress difference can be obtained from the experiments, using different combinations of Eqs (VIII. 1) to (VIII. 4), for example:

$$p_{11} - p_{22} = \Delta_{cp} - 2\,\Delta_{rim} \qquad \text{(VIII. 6)}$$

$$\Delta_{pp} - \Delta_{cp} = (-1 + q\,\frac{\partial}{\partial q})(p_{22} - p_{33}) \qquad \text{(VIII. 7)}$$

The last equation gives [1)2)]:

$$p_{22} - p_{33} = q \int_{q'=0}^{q} (\Delta_{pp} - \Delta_{cp})\,\frac{dq'}{q'^2} \qquad \text{(VIII. 8)}$$

For the application of Eq. (VIII. 8), it is necessary to have measurements in the region, where normal stress differences are proportional to q^2 [1)]. In most cases this region was not reached, so that application of Eq. (VIII. 8) was impossible. In all cases it was found, however, that $p_{22} - p_{33}$ obtained from Eq. (VIII. 3) could be represented by an equation of the type (see Chapter V):

$$p_{22} - p_{33} = \alpha\, q^{\beta} \qquad \text{(VIII. 9)}$$

α and β are positive constants, β varies from 0.8 to 2 (see Chapter V). Eq. (VIII. 7) can then be simplified [1)]:

$$\Delta_{pp} - \Delta_{cp} = (\beta - 1)(p_{22} - p_{33}) \qquad \text{(VIII. 10)}$$

In the same way Eq. (VIII. 9) gives with Eq. (VIII. 2):

$$p_{11} - p_{22} = \Delta_{pp} - (\beta + 1)(p_{22} - p_{33}) \qquad \text{(VIII. 11)}$$

Fig. 2 gives $p_{11} - p_{22}$ and $p_{22} - p_{33}$ obtained by means of Eqs (VIII. 3), (VIII. 4), (VIII. 6), (VIII. 10) and (VIII. 11).

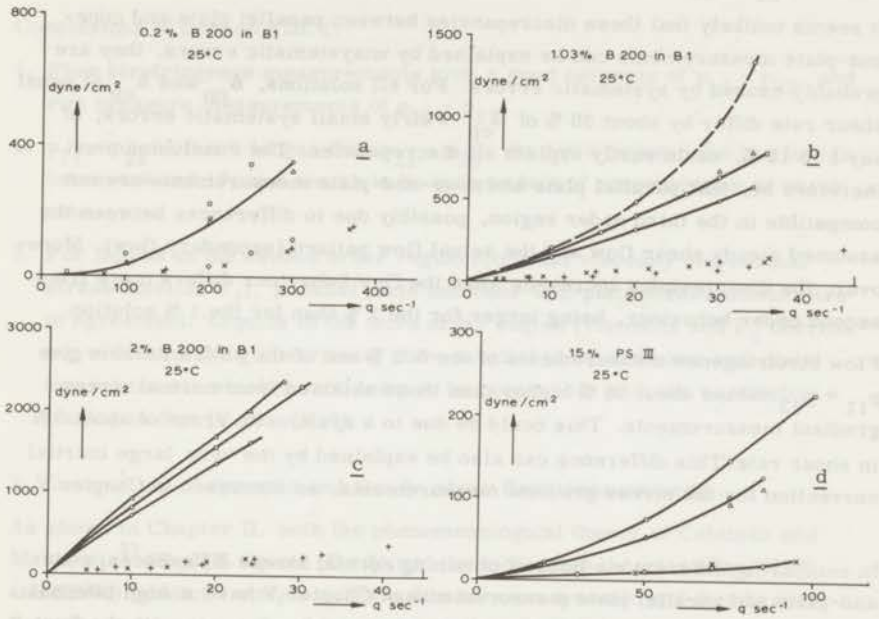

Fig. 2

Fig. 2. Circles indicate values of $p_{11} - p_{22}$ obtained from (VIII. 6), triangles those from (VIII. 11) and squares those from (VIII. 4). Values for $p_{22} - p_{33}$, including those used in Eqs (VIII. 6) and (VIII. 11), were obtained from Eq. (VIII. 3), cone-and-plate results being indicated by x, and parallel plate results by +. Diamonds give values calculated from Eq. (VIII. 10), with β-values taken from rim pressure measurements.

Especially for $p_{22} - p_{33}$, different methods of obtaining the results in Fig. 2 give different results. For those liquids, the 0.2 % and the 15 % solutions, where measurements were taken in or not far above the second order region, $p_{22} - p_{33}$ values obtained from (VIII. 3) are in good agreement with those obtained from Eq. (VIII. 10). The two liquids with a pronounced third order behaviour, the 1 % and 2 % solutions, show very bad agreement between different methods of obtaining $p_{22} - p_{33}$. With Eq. (VIII. 10), the 1 % solution gives values for $p_{22} - p_{33}$ larger than $p_{11} - p_{22}$ (diamonds in Fig. 2 b), for the 2 %

solution $p_{22} - p_{33}$ would even become negative.

It seems unlikely that these discrepancies between parallel plate and cone-and-plate measurements can be explained by unsystematic errors, they are probably caused by systematic errors. For all solutions, Δ_{pp} and Δ_{cp} at equal shear rate differ by about 20 % of Δ_{cp}. Fairly small systematic errors, of say 5 to 10 %, could easily explain all discrepancies. The conclusion must therefore be, that parallel plate and cone-and-plate measurements are not compatible in the third order region, possibly due to differences between the assumed steady shear flow and the actual flow pattern (secondary flow). Moreover, the disagreement increases when the flow behaviour differs more from second order behaviour, being larger for the 2 % than for the 1 % solution.

Flow birefringence measurements of the 0.2 % and of the 15 % solutions give $p_{11} - p_{22}$ values about 20 % higher than those obtained from normal stress gradient measurements. This could be due to a systematic error of about 5 % in shear rate. This difference can also be explained by the very large inertial correction for the stress gradient measurements, as discussed in Chapter V.

In comparing different methods of obtaining normal stress differences, cone-and-plate and parallel plate measurements of Chapter V have a high internal consistency as compared with flow birefringence data, because with the first two methods the apparatus is very nearly the same. For the interpretation of flow birefringence measurements, it is necessary to measure the viscosity on yet another apparatus. On the other hand, all methods except the rim pressure method for $p_{22} - p_{33}$ and flow birefringence for $p_{11} - p_{22}$ involve taking differences between two separately determined values of similar magnitude. As explained above, small systematic errors in Δ_{cp} or Δ_{pp} will give much larger errors in $p_{11} - p_{22}$ and $p_{22} - p_{33}$. Similar errors in rim pressure or flow birefringence measurements will only give proportional errors in $p_{22} - p_{33}$ or $p_{11} - p_{22}$, so that these two methods seem to be more reliable.

From the experimental results the ratio of $p_{11} - p_{22}$ and $p_{22} - p_{33}$ can be calculated. In order to simplify comparison with literature data, these results will be expressed as the ratio

$p_{11} - p_{33}/p_{22} - p_{33} = 1 + (p_{11} - p_{22})/(p_{22} - p_{33})$. For this ratio we get:

this work	Huppler[3]	Markovitz et al[2)4)]
5 - 11	5 - 16	2 - 4

The agreement, especially with the results of Huppler, is fair. All investigations agree in that they give positive values for $p_{22} - p_{33}$, with $p_{11} - p_{33}$

considerably larger than $p_{22} - p_{33}$.

Conclusions of Section VIII. 1:

1. Flow birefringence measurements give a good estimate of $p_{11} - p_{22}$, and rim pressure measurements of $p_{22} - p_{33}$.
2. $p_{11} - p_{22}$ is much larger than $p_{22} - p_{33}$, the ratio between the two lies in between 4 and 10, and seems to be independent of concentration or shear rate.
3. For liquids in the second order region (constant viscosity and normal stress function F_1), parallel plate and cone-and-plate measurements are in agreement. Liquids in the third order region (viscosity and F_1 decreasing with increasing shear rate) show parallel plate and cone-and-plate measurements which do not seem to be compatible with the assumptions leading to Eqs (V. 3) - (V. 7).

2. Comparison of dynamic and steady shear flow measurements.

As shown in Chapter II, both the phenomenological theory of Coleman and Markovitz[5] (Eqs (II. 9) and (II.10)),and the molecular theories (Eqs (II.74) and (II.75)) predict a simple relationship between dynamic and steady shear flow measurements at low frequencies and shear rates:

$$2 \lim_{\omega \to 0} \frac{G'}{\omega^2} = \lim_{q \to 0} \frac{p_{11} - p_{22}}{q^2} \qquad \text{(VIII. 12)}$$

$$\lim_{\omega \to 0} \left(\eta' = \frac{G''}{\omega}\right) = \lim_{q \to 0} \left(\eta = \frac{p_{12}}{q}\right) \qquad \text{(VIII. 13)}$$

In Chapter VI,dynamic and steady shear flow viscosities were compared. In agreement with theory it was found that in all cases Eq. (VIII. 13) was satisfied. Moreover, $\eta(q)$ at high shear rates was found to be in good agreement with the absolute value of the complex dynamic viscosity as defined in Sec. VI. 3.

In Figs 3 - 9, $p_{11} - p_{22}$ is plotted against q and 2 G' is plotted against ω, for all liquids where those measurements were available. In Fig. 3 this is done for dilute solutions of B 200 in B 1, in Fig. 4 and 5 for moderately to highly concentrated solutions. The normal stress gradients of Fig. 4 were taken from the literature[4], for the polystyrene solutions of Fig. 5 flow birefringence data of Chapter VII were used. Figs 6 to 9 give results for the polymer melts, polydimethylsiloxane PDMS RS in Fig. 6, two high density polyethylenes in Fig. 8, two low density polyethylenes in Fig. 7, and two

polystyrenes in Fig. 9. Squares indicate $p_{11} - p_{22}$ values obtained from flow birefringence. In Fig. 6, $p_{11} - p_{22}$ values calculated from recovery measurements are given by diamonds, using Eq. (VIII. 5) and data from Table V. 1., in good agreement with other determinations of $p_{11} - p_{22}$. This is an important result, because of an uncertainty of a factor 2 in the numerical constant in Eq. (VIII. 5). The agreement is fair if the factor is 2, which agrees with earlier results (see the discussion in ref. [1]).

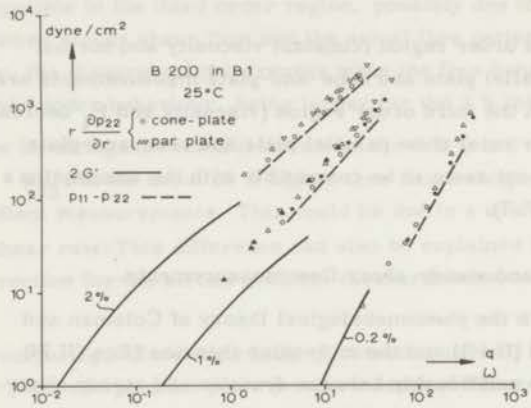

Fig. 3

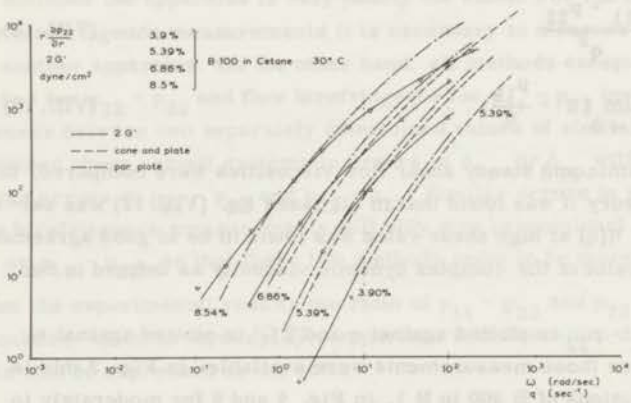

Fig. 4

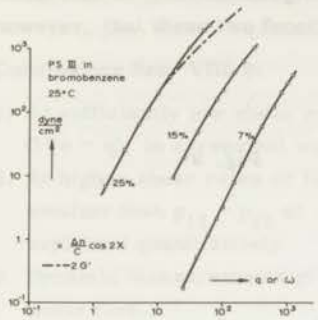

Fig. 5

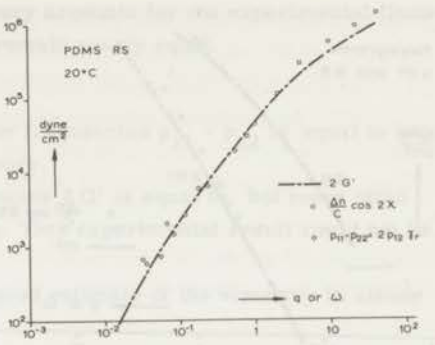

Fig. 6

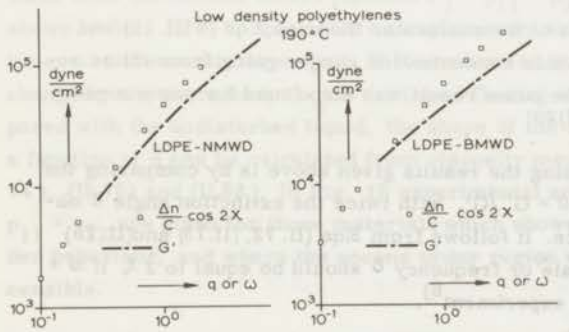

Fig. 7

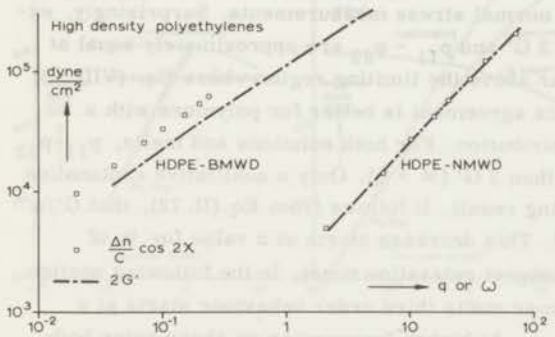

Fig. 8

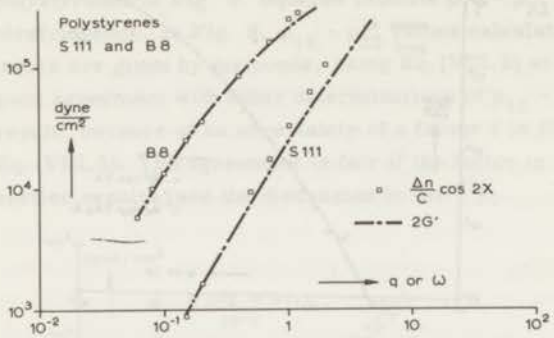

Fig. 9

The experimental difficulties in checking Eq. (VIII. 12) are considerable, because two small quantities must be measured. For this reason the agreement is satisfactory for the solutions, and good for the melts.

In agreement with predictions of the molecular theories, Eqs (VIII. 12) and (VIII. 13) are valid over the whole concentration range, going from dilute solutions to melts. Recently, the same result was also found for some moderately concentrated solutions[8)20)]

An alternative way of expressing the results given above is by comparing the loss angle δ, defined by $\tan \delta = G''/G'$, with twice the extinction angle χ obtained from flow birefringence. It follows from Eqs (II. 72, (II.73) and(II. 78) that at low values of shear rate or frequency δ should be equal to 2χ if $\omega = q$. This is in agreement with experiment[6)].

All experiments in Figs 3 to 9 show, that 2 G' gives a fair estimate of $p_{11}-p_{22}$ in steady shear flow. This is of interest, because dynamic measurements are much easier to perform than normal stress measurements. Surprisingly, experimental results show that 2 G' and $p_{11} - p_{22}$ are approximately equal at shear rates or frequencies far above the limiting region, where Eq. (VIII. 12) should hold. It seems, that this agreement is better for polymers with a broader molecular weight distribution. For both solutions and melts, $p_{11}-p_{22}$ is either equal to or greater than 2 G' ($\omega = q$). Only a qualitative explanation can be given for this surprising result. It follows from Eq. (II. 72), that G'/ω^2 decreases with increasing ω. This decrease starts at a value for ω of about $1/\tau_{max}$ (τ_{max} is the longest relaxation time). In the following section it will be shown, that for polymer melts third order behaviour starts at a value of q also equal to $1/\tau_{max}$. At higher frequencies or shear rates, both G'/ω^2 and $F_1 = p_{11} - p_{22}/q^2$ decrease with increasing ω or q. No existing

molecular or phenomenological theory accounts for the experimental finding, however, that these two functions remain nearly equal.

Conclusions Sec. VIII. 2:

1. At sufficiently low shear rates or frequencies $p_{11} - p_{22}$ is equal to twice $G'(\omega = q)$, in agreement with theory.
2. At higher shear rates or frequencies 2 G' is equal to, but more often smaller than $p_{11} - p_{22}$ at $\omega = q$. This experimental result could not be explained quantitatively.
3. Dynamic measurements give a good estimate of the viscosity in steady shear flow.

3. Third order behaviour

All polymer solutions and melts, with the exception of B 1, had viscosities diminishing with increasing shear rate at sufficiently high shear rate. At the same time the normal stress function $F_1 = p_{11} - p_{22}/q^2$ also decreases. As shown in Sec. II. B. 7, this could be explained by assuming that the relaxation times are shear rate dependent. If it is assumed that all relaxation times change by the same factor a_q in the liquid flowing with shear rate q, as compared with the undisturbed liquid, the shape of the curve giving $p_{11} - p_{22}$ as a function of q can be calculated from viscosity measurements, using Eqs (II. 74), (II. 75) and (II.82). In Fig. 10 experimental and calculated values of $p_{11} - p_{22}$ are given for those materials which showed a pronounced third order behaviour, and where the second order region was experimentally accessible.

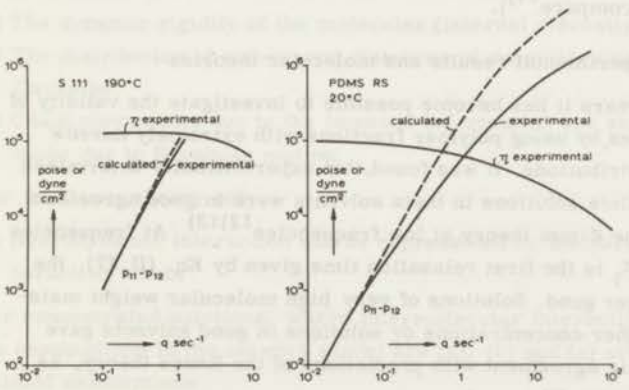

Fig. 10
$p_{11}-p_{22}$ calculated from Eqs(II. 74), (II. 75) and (II. 82)

At high shear rates, experimental values of $p_{11} - p_{22}$ are lower than calculated ones. This would mean that $a_{q'}$ as defined above, is smaller for longer relaxation times than for shorter ones. A more sensitive method, in principle, of investigating this phenomenon consists of measuring dynamic moduli during steady shear flow. A few experiments of this kind were published recently[7)8)20)]. These results are in qualitative agreement with the conclusions given above.

The network model gives a simple explanation of third order behaviour if it is assumed, that an extension of the polymer chain between two neighbouring crosslinks influences crosslink lifetime[9)10)11)12)]. If the crosslink lifetime is τ sec, the maximum relative chain extension will be proportional to $q\tau$. An analogous result can be obtained for sinusoidal shear with amplitude γ_o and angular frequency ω. Maximum relative chain extension in this case is equal to $\gamma_o [\sin \omega t - \sin \omega (t - \tau)$ (See Sec. II. B. 5). This expression has a maximum of $2\ \gamma_o$ if $\omega \geq \pi/\tau$. Both for steady shear and for sinusoidal shear, affine deformation is assumed (see discussion in Sec. VIII. 4). For the liquids in Fig. 10, the maximum relative chain deformation is about one at the onset of third order behaviour, if τ is taken from the relaxation spectra in Chapter IV. These values can be compared with dynamic measurements given in Sec. IV. 2, where PDMS RS was found to be still in the linear region at an amplitude γ_o of 0.28, the largest deformation possible with the apparatus. This result is not in contradiction with steady shear flow results, as a non-linear effect would be expected to start at an amplitude of 0.5 to 1 only. Further experiments to investigate non-linear effects in dynamic shear are still in preparation (compare[17)]).

4. Comparison of experimental results and molecular theories

During the last few years it has become possible to investigate the validity of the molecular theories, by using polymer fractions with extremely narrow molecular weight distributions. It was found, that experimentally determined dynamic moduli of dilute solutions in theta solvents were in good agreement with predictions of the Zimm theory at low frequencies[12)13)]. At frequencies above $1/\tau_1$, where τ_1 is the first relaxation time given by Eq. (II. 37), the agreement is no longer good. Solutions of very high molecular weight material, solutions of higher concentrations or solutions in good solvents gave dynamic moduli in fair agreement with predictions of the Rouse theory, as was also found in Chapter IV.

Recently it was found that flow birefringence measurements on polymers with

a narrow molecular weight distribution also gave results in good agreement with the Zimm theory at low shear rates ($q < 1/\tau_1$).[14] As for these solutions the stress optical coefficient was found to be independent of shear rate, the results of Sec. VIII. 1 show that $p_{11} - p_{22}$ is in agreement with predictions of the Zimm theory. No measurements of $p_{22} - p_{33}$ have been performed as yet on these solutions, but the results in Sec. VIII. 1 indicate that $p_{22} - p_{33}$ will be different from zero, in disagreement with theory.

As shown in Chapter IV, dynamic moduli calculated from the extension of the Rouse theory, with an adapted zero shear viscosity, are in good agreement with experimental values for a polystyrene melt.

Summarizing, it appears that the molecular theories, discussed in Chapter II, give a fair description of the flow behaviour of dilute polymer solutions and polymer melts. The three main discrepancies between experiment and the molecular theories are:

I $p_{22} \neq p_{33}$, both in the second and in the third order region during steady shear flow.

II Non-linear behaviour in the third order region during steady shear flow, is not predicted by the molecular theories.

III The dynamic moduli differ from predictions of the molecular theories at high frequencies, in particular $\eta'(\omega)$ has a non-zero limiting value at high frequencies, η'_∞.

The most important simplifying assumptions used in deriving the dilute solution theories of Chapter II (Rouse and Zimm theories) are:

(a) The dynamic rigidity of the molecules (internal viscosity) can be neglected.

(b) The distribution of end-to-end distances of submolecules and chains is Gaussian.

(c) Chain movements due to the imposed deformation are slow compared to those due to Brownian motion.

For the Zimm theory only:

(d) Hydrodynamic interaction can be represented by the Kirkwood-Riseman interaction tensor.

For concentrated solutions, where intermolecular interactions are dominant, the assumptions in the network model are (a), (b) and (c) above, with two additional assumptions:

(e) Crosslink lifetimes are independent of deformation, as discussed in Chapter II and in Sec. VIII. 3.

(f) Network deformation is equal to macroscopic deformation. This last assumption is doubtful, as shown by Duiser and Staverman[19].

It is not easy to see how these assumptions affect discrepancy I. However, Giesekus[18] has shown that a more detailed calculation of the hydrodynamic interaction in the dumbbell model gives $p_{22} \neq p_{33}$, whereas Lodge[9] has shown that a non-Gaussian distribution of end-to-end distances, the Langevin function (compare ref. [16]) gives the same result for the network model. An interesting comparison can be made with the behaviour of permanently crosslinked rubber networks. Here Treloar[16] has shown that, if the elastic energy of deformation is a function of not only the first invariant of the deformation tensor, but also of the second invariant, p_{22} will also be different from p_{33} in shear.

Internal viscosity has been given as an explanation for discrepancy II[15)22] and for discrepancy III[22]. Predictions of theories incorporating internal viscosity are not in agreement with flow birefringence experiments on dilute solutions, however[14]. The constancy of the stress optical coefficient, as found for solutions and melts of linear polymers, also would seem to exclude an appreciable influence of internal viscosity. Moreover, discrepancy III could also be explained qualitatively by assumption (d). A conclusive check on the influence of internal viscosity would be obtained by measuring limiting values of the dynamic viscosity for one polymer fraction dissolved in solvents of widely varying viscosities.

For concentrated solutions and melts, the network model gives a satisfactory qualitative explanation of discrepancy II, if crosslink lifetimes are assumed to be shear rate dependent[1)9)10)11]. No such single plausible explanation of third order behaviour exists for dilute solutions, so that this very important question is still not solved, as pointed out by Zimm[21].

Literature

1. A.S. Lodge, Elastic liquids, Academic Press, London 1964.
2. B.D. Coleman, H. Markovitz, W. Noll, Viscometric flows of non-Newtonian fluids, Springer, Berlin 1966.
3. J. Huppler, Trans. Soc. Rheology 9/2, 273 (1965).
4. H. Markovitz, D.R. Brown, Trans. Soc. Rheology 7, 137 (1963).
5. B.D. Coleman, H. Markovitz, J. Appl. Phys. 35, 1 (1964).
6. J.W.C. Adamse, H. Janeschitz-Kriegl, J.L. den Otter, J.L.S. Wales, to be published.
7. H.C. Booij, Rheologica Acta 5, 215 (1966).
8. K. Osaki, M. Tamura, T. Kotaka, M. Kurata, J. Chem. Phys. 69, 3642 (1965).

9. A. S. Lodge, M. C. R. Technical summary report 708, Wisconsin 1966.

10. A. Kaye, Doctoral Thesis, Manchester 1965.

11. M. Yamamoto, J. Phys. Soc. Japan 11, 413 (1956); 12, 1148 (1957); 13, 1200 (1958).

12. N. W. Tschoegl, J. D. Ferry, J. Phys. Chem. 68, 867 (1964); J. E. Frederick, N. W. Tschoegl, J. D. Ferry, J. Phys. Chem. 68, 1974 (1964).

13. G. Harrison, J. Lamb, H. J. Matheson, J. Phys. Chem. 68, 1072 (1964); W. Philippoff, Trans. Soc. Rheology 8, 117 (1964).

14. H. Janeschitz-Kriegl, Kolloid Z. 203, 119 (1965).

15. R. Cerf, Fortschr. Hochpolym.-Forsch. 1, 382 (1959).

16. L. R. G. Treloar, The physics of rubber elasticity, Oxford University Press, Oxford 1958.

17. W. Philippoff, Trans. Soc. Rheology 10/1, 317 (1966).

18. H. Giesekus, p 553 in Proceed. Int. Symp. on second order effects in elasticity, Haifa 1962.

19. J. A. Duiser, Doctoral Thesis, Leiden 1965; J. A. Duiser, A. J. Staverman, Physics of non-crystalline solids, ed. J. A. Prins; North-Holland Publ. Co. Amsterdam (1965), p 376.

20. T. Kotaka, K. Osaki, J. Polymer Sci. C 15, 453 (1966).

21. B. H. Zimm, p D 91 in Unsolved problems in polymer physics, National Academy of Sciences, Publication 995, Washington 1962.

22. A. Peterlin, Kolloid Z. 209, 181 (1966); J. Polymer Sci. A-2, 5, 179 (1967).

SUMMARY

In the present thesis, the relation between molecular parameters and viscoelastic behaviour of polymer solutions and melts is investigated. It could be shown, that a number of molecular theories, describing mechanical and optical behaviour of polymeric systems, the Rouse and Zimm theories for dilute solutions, and the network theory of Lodge for concentrated systems, gave identical results if expressed in the relaxation spectrum. It proved possible to obtain equations, expressing the normal stress difference $p_{11} - p_{22}$ (flow lines in 1-direction, shear gradient in 2-direction) and flow birefringence, as a function of the relaxation spectrum. The molecular theories predict a zero value for the second normal stress difference, $p_{22} - p_{33}$.

The theories given above, describe only the shear rate range where normal stress differences are proportional to q^2 or γ_o^2 (q shear rate, γ_o amplitude of sinusoidal deformation). In dynamic measurements of the shear stress, only the linear region is described. This was called second order behaviour.

The molecular theories should be valid over the complete concentration range, for that reason measurements were performed on polymeric systems, ranging from dilute (0.2 volume %) to the highest concentration possible, the melt.

The measurements performed were:

(a) dynamic shear moduli in the frequency range going from 10^{-3} to 300 rad/sec;

(b) flow birefringence in steady shear flow;

(c) viscosity as a function of shear rate;

(d) for some solutions only: normal stress gradients and rim pressures in parallel plate and cone-and-plate viscometers.

From these measurements, the normal stress differences $p_{11} - p_{22}$ and $p_{22} - p_{33}$ were obtained. It was found that flow birefringence measurements give a good estimate of $p_{11} - p_{22}$, and rim pressures of $p_{22} - p_{33}$. In disagreement with theory, $p_{22} - p_{33}$ was found to be different from zero. In agreement with other investigations, $p_{22} - p_{33}$ was found to be considerably smaller than $p_{11} - p_{22}$. For the same material at equal shear rate, $p_{22} - p_{33}$ was estimated to be 10 - 25 % of $p_{11} - p_{22}$.

For liquids in or near the second order region (constant viscosity, normal stresses proportional to q^2), parallel plate and cone-and-plate measurements gave good agreement in the determination of the two normal stress differences. If the flow behaviour differed appreciably from second order behaviour, parallel plate and cone-and-plate measurements did no longer seem to be compatible

with the assumptions necessary for their interpretation.

It could be shown, that for two polyisobutene solutions of equal concentration in two chemically similar solvents, all relaxation times were proportional to the viscosities of the solvents, in agreement with predictions of the Rouse and Zimm theories. This was also shown by the experimental finding, that the maximum relaxation time of a number of polyisobutene solutions was directly proportional to the zero shear viscosities of those solutions.

The linearity of the dynamic behaviour was investigated for a polydimethylsiloxane melt of 10^5 poise at 25 °C. The dynamic shear moduli were found to be independent of the amplitude of the deformation, even at deformations (in shear) of 0.28.

From the maximum in the dynamic loss modulus as a function of frequency, an estimate could be made of the molecular weight between entanglements for polymer melts. This maximum gave, according to a theory of Marvin, for a polystyrene melt 29.600, and for a polydimethylsiloxane melt 30.000. These values are in good agreement with literature data, obtained from viscosity measurements, of 32.000 for polystyrene, and 29.000 for polydimethylsiloxane.

Experimental values of the dynamic moduli as a function of frequency were compared with values calculated from the molecular weight distribution. The Rouse theory was found to give a good description for a dilute solution (0.2 % of a high molecular weight polyisobutene). The extension given by Ferry, Landel and Williams of the Rouse theory, gave a good description for a polystyrene melt (S 111) with a narrow molecular weight distribution.

In agreement with the results of Cox and Merz, polymer solutions were found to have a viscosity in steady shear flow, $\eta(q)$, larger than the dynamic viscosity, if $\omega = q$, but in very good agreement with the absolute value of the complex dynamic viscosity. This was also found to be true for polymer melts.

According to the molecular theories, and according to a phenomenological theory of Coleman and Markovitz, $p_{11} - p_{22}$ in the second order region must be equal to twice the dynamic storage modulus, $G'(\omega)$, if $\omega = q$. This could be experimentally verified for all polymeric systems, going from dilute solutions to melts. This is in agreement with earlier results, obtained for concentrated solutions. In particular for polymer melts, this description is very good, even in the shear rate range, where normal stress differences are no longer proportional to q^2, the third order region. In this region, $p_{11} - p_{22}$ was found to be equal too, but more often larger than $2\,G'(\omega)$, at $\omega = q$. No satisfactory theoretical explanation could be given for this experimental result.

Evidently, the dynamic moduli give a good estimate of the components of the stress tensor in steady shear flow. Because it was also found, that for melts the dynamic moduli can be calculated with fair accuracy from the molecular weight distribution, flow behaviour in steady shear flow can also be predicted from the molecular weight distribution.

SAMENVATTING

In dit proefschrift wordt een onderzoek beschreven van het verband tussen de moleculaire parameters, en het viscoelastisch gedrag van polymere oplossingen en smelten. Aangetoond kon worden, dat een aantal moleculaire theorieën die het mechanisch en optisch gedrag van polymere systemen beschrijven, de Rouse- en Zimm-theorieën voor verdunde oplossingen, en de netwerktheorie van Lodge voor geconcentreerde systemen, identieke resultaten geven als ze worden uitgedrukt in het relaxatiespectrum. Het bleek mogelijk te zijn om vergelijkingen te geven, die het verband beschrijven tussen het normaalspanningsverschil $p_{11} - p_{22}$ (stroomlijnen in 1-richting, snelheidsgradiënt in 2-richting), de stromingsdubbelebreking, en het relaxatiespectrum. De moleculaire theorieën voorspellen, dat $p_{22} - p_{33}$, het tweede normaalspanningsverschil, nul zal zijn.

De bovengenoemde moleculaire theorieën beschrijven alleen het gebied van afschuifsnelheden, waar de normaalspanningen kwadratisch in q en γ_o zijn (q is de afschuifsnelheid, γ_o de amplitude van de deformatie). Bij dynamische meting van de afschuifspanning wordt alleen het lineaire gebied beschreven. Dit werd het tweedeordegebied genoemd.

De moleculaire theorieën zijn geldig voor het gehele concentratiegebied, daarom werden metingen verricht aan polymeersystemen, variërend in concentratie van verdund (0, 2 volume % polyisobuteen) tot de hoogst mogelijke concentratie, de smelt.

Gemeten werden:

a) de dynamische glijdingsmodulus in het frequentiegebied van 10^{-3} tot 300 rad/sec;
b) stromingsdubbelebreking bij stationaire stroming;
c) viscositeit als functie van de afschuifsnelheid;
d) alleen voor enkele oplossingen: de normaalspanningsgradiënt en rand-druk in parallelle plaat en kegelplaatviscosimeters.

Uit deze metingen werden de normaalspanningsverschillen $p_{11} - p_{22}$ en $p_{22} - p_{33}$ bepaald. Het bleek dat de stromingsdubbelebrekingsmetingen een goede waarde voor $p_{11} - p_{22}$ opleverden, terwijl de rand-druk $p_{22} - p_{33}$ gaf. In tegenstelling tot de voorspellingen van de moleculaire theorieën bleek $p_{22} - p_{33}$ ongelijk nul te zijn. In overeenstemming met eerder verrichte metingen, bleek $p_{22} - p_{33}$ veel kleiner te zijn dan $p_{11} - p_{22}$. Voor hetzelfde materiaal bij gelijke afschuifsnelheid, bleek $p_{22} - p_{33}$ 10 tot 25 % te bedragen van $p_{11} - p_{22}$.

Voor vloeistoffen in of nabij het tweedeordegebied (constante viscositeit, normaalspanningen evenredig met q^2), gaven de parallelle plaat en de kegelplaatmetingen goede overeenstemming bij de bepaling van de twee normaalspanningsverschillen. Wanneer het stromingsgedrag aanmerkelijk afweek van het tweedeordegedrag, leken de parallelle plaat- en kegelplaatmetingen niet meer in overeenstemming te zijn met de noodzakelijke veronderstellingen voor de interpretatie van deze metingen.

Aangetoond kon worden, dat voor twee oplossingen van dezelfde concentratie van een polyisobuteen in twee chemisch verwante oplosmiddelen, alle relaxatietijden evenredig waren met de viscositeit van het oplosmiddel, in overeenstemming met de voorspellingen van de theorieën van Rouse en Zimm. Dit bleek ook uit het feit, dat de langste relaxatietijden van een aantal polyisobuteenoplossingen recht evenredig waren met de viscositeit bij afschuifsnelheid nul van deze oplossingen.

De lineariteit bij dynamische metingen werd onderzocht aan een polydimethylsiloxaansmelt, met een viscositeit van 10^5 poise bij 25 °C. Aangetoond werd, dat de dynamische glijdingsmoduli onafhankelijk waren van de amplitude van de deformatie, zelfs bij een deformatie (afschuiving) van 0, 28.

Uit het maximum in de verliesmodulus als functie van de frequentie, kon een schatting worden gemaakt van het molecuulgewicht tussen de verstrengelingen voor polymere smelten. Dit maximum gaf volgens een theorie van Marvin voor een polystyreensmelt 29. 600, en voor een polydimethylsiloxaansmelt 30. 000. Deze waarden zijn in goede overeenstemming met waarden uit de literatuur, verkregen uit viscositeitsmetingen, 32. 000 voor polystyreen, en 29. 000 voor polydimethylsiloxaan.

Gemeten waarden van de dynamische moduli als functie van de frequentie werden vergeleken met waarden berekend uit de molecuulgewichtverdeling. Het bleek dat de theorie van Rouse een goede beschrijving gaf van het gedrag van een verdunde oplossing (0, 2 % van een hoogmoleculair polyisobuteen). De uitbreiding van de theorie van Rouse (gegeven door Ferry, Landel en Williams) gaf een goede beschrijving van het gedrag van een polystyreensmelt (S 111), met een nauwe molecuulgewichtverdeling.

In overeenstemming met onderzoekingen van Cox en Merz werd voor polymeeroplossingen gevonden, dat bij gelijke hoeksnelheid en snelheidsgradiënt, de viscositeit bij stationaire stroming (η (q)) groter was dan de dynamische viscositeit, maar zeer goed werd benaderd door de absolute waarde van de complexe dynamische viscositeit. Dit bleek ook het geval te zijn bij polymere

smelten.

Volgens de moleculaire theorieën, en volgens een phenomenologische theorie van Coleman en Markovitz, moet $p_{11} - p_{22}$ in het tweedeordegebied gelijk zijn aan tweemaal de opslagmodulus, $G'(\omega)$, als $\omega = q$. Dit kon experimenteel worden bevestigd voor alle polymere systemen, gaande van verdunde oplossingen tot smelten. Dit is in overeenstemming met vroegere resultaten, verkregen aan geconcentreerde oplossingen. In het bijzonder voor polymere smelten bleek dit zelfs het geval te zijn in het gebied van afschuifsnelheden, waar de normaalspanningsverschillen niet meer evenredig zijn met q^2, het derdeordegebied. In dit gebied bleek $p_{11} - p_{22}$ gelijk aan of (vaker) groter te zijn dan $2\,G'(\omega = q)$. Voor dit experimentele resultaat kon geen bevredigende theoretische verklaring worden gegeven. Blijkbaar geven de dynamische moduli een goede indruk van de componenten van de spanningstensor bij stationaire stroming. Omdat ook bleek, dat voor smelten de dynamische moduli bij goede benadering met behulp van de molecuulgewichtverdeling kunnen worden berekend, volgt hieruit dat het stromingsgedrag bij stationaire stroming ook uit de molecuulgewichtverdeling kan worden voorspeld.

ACKNOWLEDGEMENTS

The author wishes to thank the management of the Centraal Laboratorium TNO, for the opportunity of publishing the investigations described in this thesis.

Stimulating discussions with Drs H. Janeschitz-Kriegl, F.R. Schwarzl and J.A. Duiser, Mr. J.L.S. Wales, Ir. J. Heijboer and Drs. U. Daum are gratefully acknowledged.

Many collaborators of the laboratory assisted in the performance of the experiments, I want to thank especially Miss P.M.J. de Haan and Mr. E. de Boer for their help in the dynamic measurements.

Mr. R. Nauta and Mr. J. Schijf took part in the design of the experimental equipment.

The manuscript was carefully typed by Mrs. H.E. Koot.

Many thanks are due to Dr. A.S. Lodge, University of Manchester College of Science and Technology, for allowing me to use the apparatus in Manchester for measuring normal stresses, and for many helpful discussions.

LEVENSLOOP

De schrijver werd in 1932 te 's-Gravenhage geboren. Hij bezocht de Stevin-H.B.S. te Den Haag van 1944 tot 1949, en de H.T.S. te Dordrecht, Afdeling Chemische Techniek, van 1949 tot 1952. Na vervulling van militaire dienstplicht, en een korte werkperiode in de industrie, werd de studie aan de Universiteit te Leiden aangevangen in 1957. Deze werd in 1961 afgesloten met het doctoraal examen. Sindsdien is hij werkzaam op het Centraal Laboratorium van de Nijverheidsorganisatie TNO te Delft, waar het grootste deel van het hier beschreven onderzoek is uitgevoerd.

STELLINGEN

1. Het vermelden van de coefficiënten der "beste vlakken" door een aantal atomen levert slechts dan nuttige en toegankelijke informatie, indien tevens de cartesische coordinaten der atomen, betrokken op dezelfde oorsprong, vermeld zijn.

   D.A. Norton, G. Kartha, C.T. Lu, Acta Cryst. 17, 77 (1964)

2. Bij de door Laufer uitgevoerde alkyleringen van thiophenol is de katalysator niet eenduidig te defieëren.

   G.A Olah, ed., Friedel Crafts and related reactions, Vol. IIa, Interscience, New York 1964, p. 97

3. Segalova en medewerkers menen ten onrechte uit hun meetresultaten te mogen concluderen, dat zij de metastabiele oplosbaarheid van tri-Calcium silicaat en β- di-Calcium silicaat bepaald hebben.

   E.E. Segalova, O.I. Luk'yanova, Chou P'ing-i, Kolloidn. Zh. 26, 341 (Eng. 288), (1964). H.N. Stein, J.M. Stevels, J.Phys. Chem. 69, 2489 (1965)

4. Het mechanisme dat Chatterjee en Bhadra voorstellen om de hoge waarde van de diëlectrische constante in electreten te verklaren, is onwaarschijnlijk.

   S.D. Chatterjee, T.C. Bhadra. Phys. Rev. 98, 1728 (1955).

5. Matsuda en medewerkers hebben alternatieve snelheidsbepalende processen in hun membraanbrandstofcel onvoldoende overwogen.

   Y. Matsuda, J. Shiokawa, H. Tamura, T. Ishino, Electrochim. Acta 12, 1435 (1967)

6. De methode, waarmede Barlow, Harrison en Lamb de dynamische moduli berekenen, gebruikmakend van de molecuulgewichtsverdeling, leidt tot onderschatting van het aandeel van de hoogmoleculaire fracties.

A.J. Barlow, G. Harrison, J. Lamb, Proc. Roy.Soc. (London) Ser. A 282, 228 (1964)

7. De conclusie van Maxwell en Galt, dat bij laminaire stroming van polymere smelten de snelheid aan de wand ongelijk nul is, wordt door hun experimenten niet bewezen.

B. Maxwell, J.C. Galt, J. Polymer Sci. 62, S50 (1962) J.L. den Otter, J.L.S. Wales, J. Schijf, Rheologica Acta 6, 205, (1967)

8. De experimenten van Schreiber, Bagley en West geven onvoldoende steun aan hun bewering, dat het verband tussen viscositeit en molecuulgewicht voor polyethenen afwijkt van dat voor andere polymere smelten.

H.P. Schreiber, E.B. Bagley, D.C. West, Polymer, 4,355 (1963)

9. Het gebruik door Peterlin van het Zimm- model met inwendige stijfheid, om het niet naar nul gaan van de dynamische viscositeit bij hoge frequenties te verklaren, is aanvechtbaar.

A. Peterlin, Kolloid Z. 209, 181 (1966) J. Polymer Sci. A2 5, 179 (1967)

10. De verkeersveiligheid bij nacht zou aanzienlijk verhoogd worden, wanneer bromfietsen enerzijds, en motoren en scooters anderzijds, duidelijk onderscheidbaar zouden zijn, bijvoorbeeld door een verschillende kleur van het licht van de koplampen.